

Theory of Liquid-Liquid Phase Separation in Model Lipid Bilayers

Gregory Garbès Putzel

A dissertation submitted in partial fulfillment of
the requirements for the degree of

Doctor of Philosophy

University of Washington

2010

Program Authorized to Offer Degree: Department of Physics

University of Washington
Graduate School

This is to certify that I have examined this copy of a doctoral dissertation by

Gregory Garbès Putzel

and have found that it is complete and satisfactory in all respects,
and that any and all revisions required by the final
examining committee have been made.

Chair of the Supervisory Committee:

Michael Schick

Reading Committee:

Michael Schick

Sarah Keller

Marcel den Nijs

Date: _____

In presenting this dissertation in partial fulfillment of the requirements for the doctoral degree at the University of Washington, I agree that the Library shall make its copies freely available for inspection. I further agree that extensive copying of the dissertation is allowable only for scholarly purposes, consistent with fair use as prescribed in the U.S. Copyright Law. Requests for copying or reproduction of this dissertation may be referred to ProQuest Information and Learning, 300 North Zeeb Road, Ann Arbor, MI 48106-1346, 1-800-521-0600, to whom the author has granted "the right to reproduce and sell (a) copies of the manuscript in microform and/or (b) printed copies of the manuscript made from microform."

Signature_____

Date_____

University of Washington

Abstract

Theory of Liquid-Liquid Phase Separation in Model Lipid Bilayers

Gregory Garbès Putzel

Chair of the Supervisory Committee:
Professor Michael Schick
Department of Physics

This thesis presents phenomenological and theoretical work related to phase separation in fluid lipid bilayers. We describe a phenomenological model which explains the liquid-liquid phase behavior of the ternary mixture DPPC/diphytanoylPC/cholesterol on the basis of interactions between these components, which depend on the extent of orientational order of the saturated lipid acyl chains. An extension of this model to include complexes of lipids illustrates the effect on phase behavior of chemical crosslinking via a reduction of mixing entropy, which could explain the experimentally observed phenomenon of crosslinking-induced phase separation. We also present a phenomenological model of lipid bilayers with coupled leaflets that describes the conditions under which compositionally asymmetric bilayers undergo phase separation. This model reproduces several experimental observations. We also analyze the fluctuations of phase domain boundaries in phase-separated bilayers with coupled leaflets, showing how the interleaflet coupling energy relates to the spatial extent of areas of mismatch between the states of the apposing leaflets. We estimate the magnitude of this interleaflet coupling on the basis of the molecular mean-field model developed by Elliott et al. Finally, we examine the possibility that the presence of lipids with electrically charged head groups in the inner leaflet of the cell plasma membrane leads to compositional fluctuations with a characteristic spatial extent. By calculating the effect of electrostatic interactions on the spectrum of compositional fluctuations, we derive a criterion by which this characteristic length is manifest in the structure function.

TABLE OF CONTENTS

	Page
List of Figures	iii
List of Tables	v
Chapter 1: Introduction	1
1.1 Lipids and their Interactions	2
1.2 Cholesterol and the Liquid-Ordered Phase	7
1.3 The Lipid Raft Hypothesis	11
1.4 Problems Addressed in this Thesis	14
Chapter 2: Liquid-Liquid Phase Separation in Model Membranes	15
2.1 Phenomenological Modeling of Liquid-Liquid Phase Separation	15
2.2 Microscopic Models of Lipid Bilayers	25
2.3 The Model of Elliott, Szeifer, and Schick	26
Chapter 3: The Interleaflet Coupling	30
3.1 Interleaflet Coupling in Liquid-Liquid Phase-Separated Vesicles	31
3.2 Phenomenological Modeling	32
3.3 Thermodynamic Definition of Interleaflet Coupling: Canonical Ensemble	38
3.4 Thermodynamic Definition of Interleaflet Coupling: Grand Canonical Ensemble	41
3.5 The Nature and Magnitude of the Interleaflet Coupling	43
3.6 Fluctuations of Phase Boundaries in Coupled Leaflets	46
3.7 Microscopic Calculation of Interleaflet Coupling	55
3.8 Calculation of Grand Canonical Interleaflet Coupling	57
Chapter 4: Electrostatic Effects and the Inner Leaflet of the Plasma Membrane	60
4.1 Phase Behavior of Charged Mixtures	60
4.2 Electrostatic Effect on Phase Behavior in Model Membranes	62
4.3 Effect of Charges on Concentration Fluctuations	65
4.4 Effective Electrostatic Potential between Charged Lipids	71

Chapter 5: Questions and Future Research Directions	74
5.1 The Size of Lipid Rafts	74
5.2 The Phase Behavior of Asymmetric Mixed Bilayers	76
Bibliography	78
Appendix A: Thermodynamics of Mixed Bilayers	90
Appendix B: Calculating Phase Diagrams from Phenomenological Free Energies	93
Appendix C: Derivation of Effective Interaction between Charged Lipids	99
Appendix D: Simplified Phenomenological Model of Ternary Mixture of Saturated and Unsaturated Lipids and Cholesterol	104

LIST OF FIGURES

Figure Number	Page
1.1 DPPC and polyethylene	2
1.2 The gel and liquid phases of a lipid bilayer	4
1.3 The lipid POPC	5
1.4 Phase diagram of POPC-DPPC binary mixture	6
1.5 A cholesterol molecule	7
1.6 Phase diagram proposed by Ipsen et al. for mixtures of saturated lipids and cholesterol	9
1.7 Phase diagram with closed-loop miscibility gap	12
2.1 Phase diagram calculated from McConnell's condensed complex theory	18
2.2 Phase diagram calculated from our phenomenological theory	20
2.3 Partial phase diagrams for ternary mixture with cross-linking	24
3.1 Phase diagram of weakly coupled leaves with both c_i and c_o negative.	34
3.2 Phase diagram of strongly coupled leaves with both c_i and c_o negative.	36
3.3 Phase diagram of strongly coupled leaves with $c_i > 0$ and $c_o < 0$	37
3.4 Phase diagram of strongly coupled leaves with $c_i > 0$ and $c_o < 0$	38
3.5 Mismatch process	39
3.6 Fluctuating phase boundaries in coupled leaflets	47
3.7 The histogram of Risselada et al.	51
3.8 Probability distribution of scaled mismatch area	52
3.9 Logarithm of probability distribution of mismatch areas	54
3.10 Ternary phase diagram calculated by Uline et al. from the model of Elliott et al.	56
4.1 Phase diagram of ternary mixture with charged unsaturated lipids	63
4.2 Dimensionless strength of composition fluctuations	69
4.3 Electric charges at the lipid-water interface	71
4.4 Effective electrostatic potential between two charged lipid headgroups	73
4.5 Enhancement of electrostatic repulsion by interface	73
B.1 Free energy of binary mixture	94

B.2 Ternary phase diagram with binary phase separation	95
B.3 Spinodal region of ternary mixture	96
B.4 Convex hull of points on the graph of f	97
B.5 Phase diagram calculated using convex hull method	98

LIST OF TABLES

Table Number	Page
3.1 Statistical mechanics/quantum mechanics correspondence	48
3.2 Calculated values of the canonical interleaflet coupling γ , for four tie-lines labeled in Figure 3.10.	58

ACKNOWLEDGMENTS

It is a pleasure to thank a number of people for their help and encouragement. Most importantly, I thank my advisor Michael Schick for sharing his knowledge and experience, and for our many interesting discussions; I look forward to more of these. I am also grateful to Marcus Müller for including me in his research group in Göttingen during the winter quarter of 2007 when I had little idea of what I was doing. My research would not be what it is without Sarah Keller and the members of her research group. Their thought-provoking experiments have been the inspiration of most of our own research, and due to their weekly group meetings I was kept well-informed (and well-fed). I thank Igal Szleifer and his group for their hospitality during the spring quarter of 2009, and look forward to working with them. I am grateful to Mark Uline for walking me patiently through so much FORTRAN code; to David Andelman and Yoav Tsori for our pleasant trans-Atlantic collaboration; and to David Allender for sharing his insight and for suggesting the hot sauce at Chipotle. I would like to thank my friends in the physics department, especially Wei Chen, Steve Paik, Andrew Lytle, Mat Steuck, and Ethan Thompson, for making my years of graduate school so memorable, and for putting up with my frequent interruption of their own work. Finally, my parents and my sister deserve more thanks than I can give for their encouragement and for keeping my spirits up when necessary.

DEDICATION

This thesis is dedicated to my parents Roger and Georgette and my sister Sonia, with love and appreciation.

Chapter 1

INTRODUCTION

The motivation for the work presented in this thesis is the idea that the principles and methods of physics can help to explain how lipids are organized in the cell membrane. We will discuss phenomenological and theoretical models inspired by *in vitro* experiments on mixed lipid bilayers, themselves partly intended to shed light on the biological phenomenon of “lipid rafts.” According to the lipid raft hypothesis [83], the cell membrane is not a uniform mixture of lipids and proteins, but rather contains domains rich in saturated lipids and cholesterol which diffuse in, but are compositionally distinct from, the surrounding membrane. These rafts have been implicated, via biochemical assays, in a great number of biological processes taking place at the cell plasma membrane [132]. These biochemical experiments do not, however, answer any questions about the physical nature of lipid rafts. What molecular interactions cause the lipids and proteins present in rafts to remain separate from other molecules making up the cell membrane? How large are the rafts, and how long do they last? Biophysicists were motivated by these and other questions to study compositional inhomogeneity in model experimental systems, lipid bilayers composed of a small number of molecular species. These model membranes are much simpler than the cell membranes they are intended to shed light on, and thus lend themselves to a more complete characterization through repeatable experiments. In some lipid mixtures, experimentalists have observed the coexistence of two distinct liquid phases, called the “liquid-ordered” and “liquid-disordered” phases. Because the liquid-ordered phase is rich in ordered, saturated lipids and cholesterol, it has come to be viewed as the biophysical correlate of “lipid rafts” in the context of these simple model systems. A view has emerged according to which lipid rafts in the cell membrane are domains of the liquid-ordered phase in coexistence with, and surrounded by, a continuous region of the liquid-disordered phase. This picture presents a number of difficulties, to be discussed in the concluding chapter, and must be viewed as an

approximate characterization of lipid rafts. Nevertheless, because this view connects the phenomenon of lipid rafts to the thermodynamic phase behavior of simpler and more robust model systems, it brings questions regarding the nature of rafts into the province of Physics.

In this introductory chapter, two concepts are presented which will form the background for the research described in the following chapters. These are the biological phenomenon of lipid rafts and the related concept of liquid-liquid phase coexistence in the model membranes studied *in vitro* by experimentalists. Before introducing these ideas, however, we briefly describe the molecules which will occur throughout this work and how they interact.

1.1 Lipids and their Interactions

The left side of Figure 1.1 shows a saturated lipid molecule known as dipalmitoyl phosphatidylcholine, or DPPC for short. The first part of the name, “dipalmitoyl,” describes

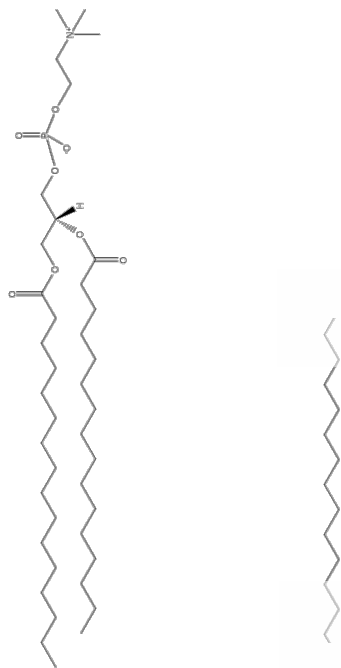


Figure 1.1: Left: A molecule of DPPC (dipalmitoyl phosphatidylcholine). Right: A segment of a polyethylene molecule.

the lipid's two acyl chains, shown as jagged lines in the figure. These consist of 16 carbon atoms linked together covalently. What makes these chains "saturated" is that each carbon atom is bonded to two hydrogen atoms not shown in the figure. The right side of figure 1.1 shows a segment of a molecule of polyethylene, a polymer out of which plastic bags are made. From the figure it is clear that polyethylene has the same basic chemical structure as the acyl chains of DPPC. Like polyethylene, the acyl chains are hydrophobic. When brought together in water, DPPC molecules arrange themselves into bilayers with the hydrophobic chains facing inward. The phosphatidylcholine (PC) head group of DPPC has a dipole moment and thus is hydrophilic. Molecules such as lipids, having hydrophobic and hydrophilic parts, are called "amphiphilic" and often form structures such as bilayers in water. The self-assembly of these structures is driven by the same "hydrophobic effect" responsible for the phase separation of oil and water. It results from the fact that hydrocarbons disrupt the network of hydrogen bonds which water molecules form with each other. This disruption results in a lowering of entropy, and this entropic penalty is responsible for the hydrophobic effect [103].

At a temperature of roughly 140 °C, polyethylene melts, undergoing a phase transition from a solid to a liquid state [100]. A similar phase transition occurs at lower temperatures in bilayers composed of DPPC or other lipids having saturated acyl chains. Below about 41 °C [58] a DPPC bilayer exists in a tightly packed solid state called the "gel phase," in which almost all of the carbon-carbon bonds are as shown in Figure 1.1; the bonds are said to be in the *trans* configuration. The gel phase is further characterized by very slow lateral diffusion of lipids. Above 41 °C the DPPC bilayer is in a fluid state characterized by rapid lateral diffusion of lipids. The acyl chains of the lipids are also more loosely packed in the liquid state, and undergo thermal fluctuations in which the carbon-carbon bonds are in the the so-called *gauche* state, introducing a bend into the regular zig-zag structure shown in Figure 1.1. The gel and liquid phases are depicted schematically in Figure 1.2. The phase transition between the gel and liquid phases of a lipid bilayer is often called the "main-chain transition," or simply the "melting transition." Here we will always refer to it as the gel-liquid transition. Like all phase transitions induced by a change in temperature, the gel-liquid transition is driven by a competition between energy and entropy [100]. In the

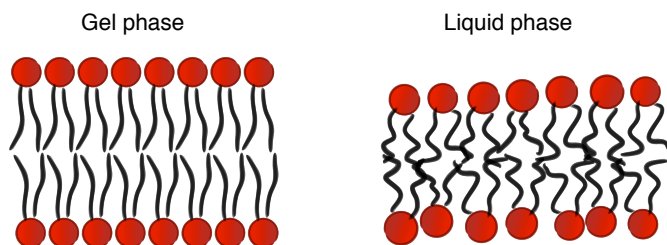


Figure 1.2: The gel and liquid phases of a lipid bilayer

low-temperature gel phase, almost all of the carbon-carbon bonds in the lipid acyl chains are in the *trans* rather than *gauche* state. This configuration gives the chains an overall linear structure and allows them to pack together tightly. This tight packing is favorable in terms of attractive Van der Waals interactions, but has low configurational entropy, since a lipid that is tightly packed among its neighbors can not explore configurations other than the all-*trans* one. These non-*trans* configurations occur more often at higher temperatures, but the restrictive tight packing prevents this change from happening independently in each of the lipids. Instead, as the temperature is increased the lipids undergo a cooperative change to a more disordered, less tightly-packed state, resulting in a first-order gel-liquid transition at a specific temperature T_m . As shown in Figure 1.2, the change in orientational order of the lipid hydrocarbon chains leads to a difference in thickness between the gel and liquid phases which serves as a convenient order parameter for the gel-liquid transition. This transition is closely related to the melting transition of polyethylene; in fact, the gel-liquid transition temperatures of a series of saturated lipids with increasingly longer acyl chains can be extrapolated to the melting transition temperature of polyethylene [101].

The gel phase is of limited interest in biology, since the lipid membranes of living cells are in a fluid state. A rare instance of the biological relevance of the gel phase is in the outermost layer of skin tissue, which is composed of dead cells [95]. In this work we will be concerned only with the liquid state of lipid bilayers, our principle interest being in the coexistence of two or more liquid phases rather than in the gel-liquid transition.

A saturated lipid molecule such as DPPC acquires flexibility due to the thermally excited *gauche* states of its carbon-carbon bonds. In the DPPC molecule's ground state, these bonds are in the *trans* configuration, making the chain zig-zag locally but remain straight overall. In contrast, “unsaturated” lipids have acyl chains with one or more carbons bound to only one hydrogen atom, rather than two. These carbons come in neighboring pairs which share a double bond. Figure 1.3 shows a molecule of palmitoyl-oleoyl phosphatidylcholine (POPC), which has one saturated (palmitoyl) and one unsaturated (oleoyl) acyl chain.

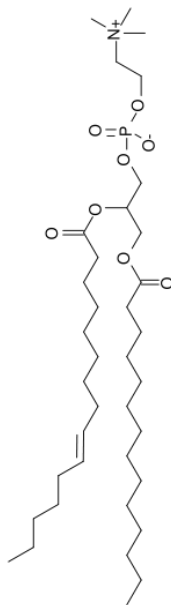


Figure 1.3: The lipid POPC. Figure from commons.wikimedia.org.

The double bond present in the unsaturated acyl chain of POPC introduces a kink in the chain which is permanent (quenched) rather than thermally excited. Lipids such as POPC or dipalmitoyl PC (DOPC), which has two unsaturated chains, are thus prevented from packing tightly together in the same way that saturated lipids can. This biases the competition between attractive Van der Waals interactions and entropy in favor of the latter, with the result that at room temperature DOPC is in the liquid state, whereas a saturated lipid of comparable acyl chain length is in the gel (solid) state. This fact is manifested

in the kitchen, where butter composed of saturated fats is solid, but olive oil, which is composed of unsaturated fats, is liquid [6]. Bilayers made of unsaturated molecules must be cooled to temperatures below the freezing point of water before forming a solid phase [7]. Thus we will sometimes refer to saturated lipids as “high melting temperature” lipids and to unsaturated lipids as “low melting temperature” lipids. This characterization allows us to group together with the unsaturated lipids those lipids which, although not chemically speaking unsaturated, have structures which prevent tight chain packing and thus have low melting temperatures.

In bilayers composed of a single species of saturated lipid, the gel-liquid transition occurs at a single specific temperature. This is no longer the case in bilayers that are composed of mixtures of saturated and unsaturated lipids. At temperatures between the gel-liquid transitions temperatures of the unsaturated and saturated lipids, there is coexistence between a gel phase and a liquid phase in some range of compositions. A limited amount of unsaturated lipids is soluble in the gel phase, beyond which any excess unsaturated lipids (and some saturated ones) form a liquid phase that coexists with the gel phase. This is illustrated in Figure 1.4, which shows a phase diagram obtained by Curatolo et al. [19] for a binary mixture of POPC and DPPC. The phase diagram shows a large region of composi-

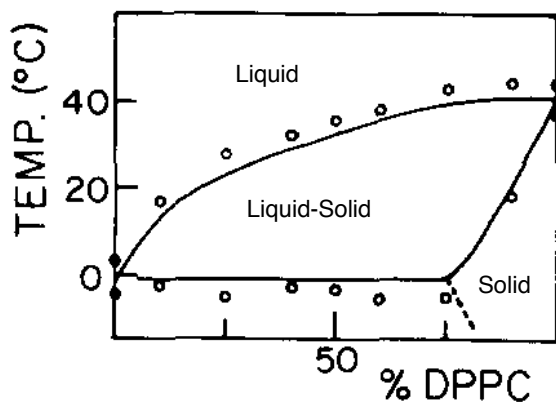


Figure 1.4: Phase diagram of POPC-DPPC binary mixture. Figure taken from [19].

tions and temperature in which a liquid phase rich in POPC coexists with a gel phase rich

in DPPC.

1.2 Cholesterol and the Liquid-Ordered Phase

Lipids with saturated tails, as well as lipids having one saturated and one unsaturated tail, occur in abundance in the cell plasma membrane. In animal cell membranes another major component is cholesterol, which accounts for 20 to 50 percent of the lipid molecules [95]. A molecule of cholesterol is depicted in figure 1.5. The bulk of the cholesterol molecule consists

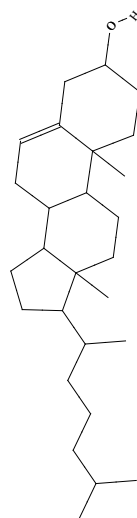


Figure 1.5: A cholesterol molecule.

of a ring structure which is hydrophobic but rigid, unlike the acyl chains of lipids such as DPPC and DOPC. This ring structure packs well with acyl chains of saturated lipids when these are well-ordered. This leads to the “ordering” effect of cholesterol: the addition of cholesterol to a bilayer of saturated lipids increases the orientational order of the acyl chains of the lipids, as has been measured by nuclear magnetic resonance (NMR) [126]. In addition to its sterol ring structure, cholesterol has a short, flexible hydrophobic chain. The only hydrophilic part of the cholesterol molecule is a single hydroxide (OH) group. Compared to phospholipids such as DPPC and DOPC, cholesterol is therefore relatively weakly anchored

to the bilayer-solvent interface, leading to relatively fast “flip-flop” of cholesterol from one leaflet of the bilayer to another [53, 15].

When added to a lipid bilayer in its liquid state, cholesterol may, under some circumstances, give rise to coexistence between two distinct liquid phases: the liquid-disordered (L_d) and the liquid-ordered phases (L_o). Of the two coexisting phases, the liquid-ordered phase has a higher concentration of cholesterol, and the tails of its saturated lipids have a greater degree of orientational order; that is, they are more closely aligned with the direction normal to the bilayer. The conditions under which liquid-liquid coexistence occurs in mixed lipid bilayers are a matter of longstanding controversy due to differing interpretations of key experiments [145]. We briefly describe these experimental findings and state our interpretation of their results, since they are the basis for our phenomenological work described in the next chapter.

The prevailing concept of the liquid-ordered phase, as well as the terms “liquid-ordered” and “liquid-disordered,” come from a theoretical analysis by Ipsen et al. [63] of data from several experiments [121, 151] on the phase behavior of binary mixtures of saturated lipids and cholesterol. Ipsen et al. interpreted these results as indicative of the coexistence of two liquid phases in a range of temperatures above the melting transition of the saturated lipids, and proposed the phase diagram shown in Figure 1.6. In this figure the phases are labeled according to two characteristics: liquid (l) versus solid (s) and ordered (o) versus disordered (d). Liquid (l) and solid (s) refer to the translational degrees of freedom of molecules. In liquid phases, there is no crystalline order in the positions of molecules, which diffuse freely. In the solid phase (which we refer to as the gel phase) the molecules are on average at fixed positions with respect to their neighbors and molecular diffusion is very slow. The terms “ordered” and “disordered” refer to the configurational degrees of freedom of the saturated lipids, that is, to the extent of orientational order of their hydrophobic chains, or equivalently the number of *gauche* bonds. Whereas it was clear that in the liquid-gel transition of pure lipid bilayers, both translational and configurational degrees of freedom undergo a simultaneous change, Ipsen et al. suggested that the addition of cholesterol effectively decoupled these degrees of freedom, giving rise to a liquid-ordered phase having the molecular mobility characteristic of liquid phases [124], but also a degree

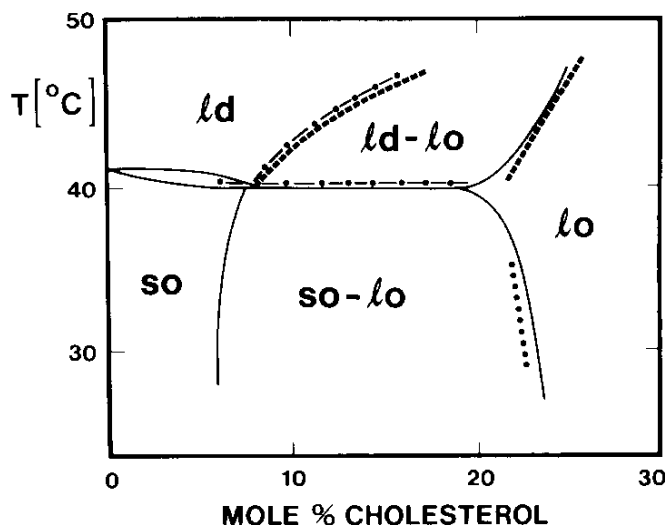


Figure 1.6: Phase diagram proposed by Ipsen et al. [63] for mixtures of saturated PC lipids and cholesterol. Figure taken from [63]. The different lines come from several different experiments and have been scaled to allow qualitative comparison.

of orientational order similar to that of the gel phase [151, 152]. Following the paper of Ipsen et al., it became a consensus among many researchers that binary mixtures of saturated lipids and cholesterol can show liquid-liquid phase separation; the phase diagram published by Vist and Davis [152] has been especially influential in encouraging this view. Vist and Davis studied the binary mixture of cholesterol and saturated DPPC using calorimetry as well as nuclear magnetic resonance (NMR). They inferred the presence of two coexisting phases from the broadening of the NMR spectrum of deuterated DPPC molecules, which indicates that these lipids diffuse between distinct environments on the rapid NMR timescale of $10 \mu\text{s}$ [152].

With the availability of fluorescent-labeled lipids it became possible to visualize phase separation in lipid vesicles directly on the micron scale. In this type of experiment, the fluorescent-labeled lipid is present in different amounts in the two coexisting phases, giving regions of those phases different fluorescence intensities. When this method was brought to bear on binary mixtures of cholesterol and saturated lipids at temperatures above the gel-

liquid transition of the latter, coexistence of two liquid phases was not observed [110, 144]. Thus observations of model membranes under fluorescence microscopy appear to disagree with results obtained for the same systems by other methods such as nuclear magnetic resonance (NMR) as to whether these binary mixtures exhibit coexisting liquid phases. This apparent disagreement is largely due to a difference in interpretation of experiments in terms of the concept of thermodynamic phases. The experiments taken to indicate liquid-liquid phase separation in saturated-cholesterol binary systems are also those which probe length scales much smaller than those visible to fluorescence microscopy. For example, the broadening of the NMR spectra of deuterated lipids in saturated lipid/cholesterol binary mixtures indicates lateral inhomogeneities on the order of 25 nm [152] (for comparison, note that a typical lipid takes up an area of roughly 0.5 nm^2). In contrast, macroscopic phase separation leads to a superposition of the distinct spectra associated with the liquid-ordered and -disordered phases, as observed by Veatch et al. [147], rather than a single broadened spectrum, except in the vicinity of a critical point where the two phases become indistinguishable. There is broad agreement that experiments such as those of Vist and Davis indicate compositional inhomogeneities on the nanometer scale; the question is only whether these inhomogeneities should be considered as phase coexistence or instead simply as lateral structure or fluctuations within a single liquid phase. Because of the connection that has been drawn between liquid-liquid phase separation and the biological phenomenon of lipid rafts [122], this question is relevant to that of the finite size of lipid rafts. In this work we will take the view that phase coexistence is a purely macroscopic phenomenon, and that the experimental results of Vist and Davis [152] suggest the existence of nanoscale inhomogeneities within a single phase, rather than phase separation, in saturated lipid/cholesterol mixed bilayers. The contrary view, in which these inhomogeneities are considered to be domains of coexisting phases, is incompatible with a number of basic thermodynamic notions. For example, the interpretation of thermodynamic behavior in terms of a phase diagram with well-defined tie-lines relies on the fact that interfaces between coexisting phases contribute negligibly to the free energy of a mixture. This is not the case for the “interfaces” surrounding nanoscale inhomogeneities. Most importantly, equilibrium thermodynamics provides a clear distinction between a single phase and two phases in coexistence. This distinction is

lost if we treat nanometer-sized inhomogeneities as coexisting domains; regions of the phase diagram which one researcher may consider to be in a single phase will be considered by another to yield two coexisting phases with very small domains.

In contrast to the situation occurring with saturated lipid/cholesterol binary mixtures, liquid-liquid immiscibility is readily observed by fluorescence microscopy in model membranes which are ternary mixtures of saturated lipids, unsaturated lipids, and cholesterol [28, 43, 144]. Several of these mixtures have been studied systematically, resulting in phase diagrams describing the conditions under which coexistence of two or more phases may occur [21, 143, 147, 20]; a complete list of such phase diagrams is given in [89]. From these studies a general understanding has emerged of which mixtures are capable of displaying *macroscopic* liquid-liquid phase separation: namely, those which are mixtures of high melting temperature lipids (saturated lipids), low melting temperature lipids (such as unsaturated lipids), and cholesterol. Of particular interest has been the ternary mixture of DiphyPC/DPPC/cholesterol studied by Veatch et al. [143], where the role of the low melting temperature lipid is played by diphytanoyl PC (DiphyPC), which has hydrophobic tails that are branched rather than kinked as in unsaturated lipids. At temperatures above the gel-liquid transition temperature of DPPC, Veatch et al. observed liquid-liquid immiscibility in the ternary mixture but not in any of the corresponding binary mixtures, suggesting a phase diagram of the type shown schematically in Figure 1.7. Such a phase diagram is said to have a “closed-loop miscibility gap,” and highlights the necessity of all three components of the mixture in order to observe liquid-liquid immiscibility. This unusual phase behavior has led several researchers to propose phenomenological models in which simple intermolecular interactions give rise to phase diagrams such as the one shown in Figure 1.7.

1.3 The Lipid Raft Hypothesis

Today, the liquid-ordered phase is considered by many to be closely related to nanometer-scale domains of saturated lipids and cholesterol called “lipid rafts,” which are believed to play a number of important roles in living cell membranes [131, 132]. However, the idea of microdomains within the cell membrane predates the discovery of the liquid-ordered phase, and goes back at least to the early 1980’s [67]. The more specific notion of “lipid

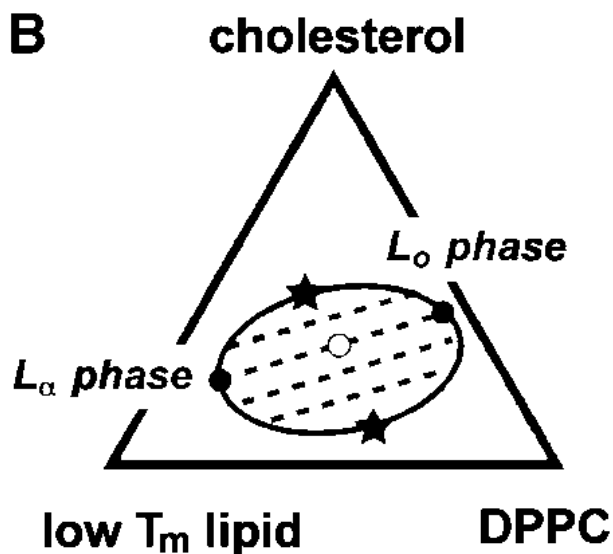


Figure 1.7: Phase diagram of a ternary mixture with closed-loop miscibility gap. Figure taken from [143].

rafts” composed of saturated sphingolipids and cholesterol in the outer leaflet of the cell membrane, as well as the term itself, was proposed by Simons and collaborators [133, 131] to explain the sorting of lipids in epithelial cells lining body cavities. These cells are polarized into distinct “apical” and “basolateral” surfaces. Proteins anchored to the cell membrane by glycosylphosphatidylinositol (GPI) lipid chains were found to be expressed primarily in the apical cell membrane, which itself is rich in saturated sphingolipids. This fact led to the hypothesis [133] that sphingolipid-rich microdomains or “rafts” formed in the Golgi complex act as sorting platforms for directed transport of lipids and proteins to the apical membrane. An important development in the field was the discovery [14] that GPI-anchored proteins, together with sphingolipids, were found in a fraction of the cell membrane which resisted dissolution by the detergent Triton X-100. Following this, the presence of a protein in the “detergent-resistant fraction” of the cell membrane came to be considered as grounds for claiming that the protein partitioned preferentially into lipid rafts. Under this functional biochemical definition, a large number of biological processes became implicated with lipid

rafts, going beyond mere protein and lipid sorting [133, 131] to including viral infection [40] and signal transduction [132, 90]. The study of lipid rafts grew rapidly during the first decade of the twenty-first century, producing hundreds of articles, numerous reviews [122, 13, 132, 33, 98, 134, 55, 64, 129, 83], and at least two books [90, 44]. Several authors have expressed skepticism [130] toward the functional definition of lipid rafts in terms of detergent resistance assays, and consequently toward much of the research implicating rafts with biological processes. Skeptics cite, among other things, evidence that Triton X-100 can itself lead to the formation of phase-separated domains [57] or perhaps to the coalescence of previously existing smaller domains [50]. Although there is mounting evidence for lateral inhomogeneity in cell membranes from a number of independent experimental methods [55, 64, 83], it should be kept in mind that connections drawn between lipid rafts and specific biological processes are still largely based on the presence of proteins in the detergent resistant fraction, or even on the dependence of processes on levels of cholesterol [130].

The lipid raft concept has evolved considerably since the idea was proposed by Simons and collaborators [83]. The physical basis for the formation of sphingolipid-rich rafts was initially thought to be the ability of the head groups of these lipids to form networks of hydrogen bonds [133, 131]. The current emphasis on the interactions of lipid acyl chains and on the effect of cholesterol derives from the confluence of lipid raft research and the previously mentioned studies of liquid-liquid phase coexistence in model membranes containing cholesterol. Lipid rafts have come to be seen [122] as liquid-ordered domains coexisting with a majority liquid-disordered phase. Differences in opinion regarding the status of “nanodomains” notwithstanding, liquid domains within model liquid membranes are well-defined objects which have been studied in the hopes of shedding light on the physical basis of lipid raft formation. The connection between rafts and liquid-liquid coexistence has raised a number of questions, the most important being the size of lipid rafts. If they exist at all [130], lipid rafts must be too small to be visible by optical microscopy; currently they are believed to be tens or hundreds of nanometers in size [112]. Such a small size presents an obstacle to viewing rafts as phase-separated liquid-ordered domains, which would tend to merge into larger domains due to the influence of line tension (the two-dimensional equivalent of surface tension). A number of mechanisms have been proposed to explain the finite

size of lipid rafts. These will be discussed in the concluding chapter; here we note only that the case for associating lipid rafts with liquid phase domains has been greatly strengthened by the observation of liquid-liquid phase separation [8, 146] in “blebs,” lipid vesicles derived directly from cell plasma membranes.

1.4 Problems Addressed in this Thesis

In this thesis, we will discuss a number of theoretical and phenomenological approaches to the study of liquid-liquid phase separation and compositional fluctuations in lipid bilayers composed of mixtures of lipids and cholesterol. Some of this work has been from our own research, namely:

- A phenomenological theory [117] of the ternary mixture of diphyPC/DPPC/cholesterol described in section 2.1.
- The use of this model to examine the effects on phase behavior of lipid cross-linking [118].
- A phenomenological model of a phase-separating bilayer with coupled leaflets [116], presented in section 3.2.
- The analysis in section 3.6 of the fluctuations of domain boundaries in such bilayers.
- The microscopic calculation (see section 3.7) of the the interleaflet coupling on the basis of the model of Elliott et al. [36].
- The treatment in section 4.2 of the effect of electric charges on the phase diagram of the ternary mixture described in section 2.1.
- The analysis (in collaboration with David Allender) of compositional fluctuations in charged mixtures (sections 4.3 and 4.4).

Chapter 2

LIQUID-LIQUID PHASE SEPARATION IN MODEL MEMBRANES

During the past ten years, several research groups made observations of large-scale (that is, micron scale) liquid-liquid phase separation in model lipid bilayer vesicles [28, 21, 145]. In several cases, researchers have mapped out phase diagrams [89] that summarize the conditions under which a mixed lipid bilayer will separate into regions of two or more different phases. The model systems under consideration in these experiments, although far simpler than the cell plasma membrane, are still sufficiently complex to give rise to a rich phase behavior which demands theoretical explanation. This chapter describes phenomenological and theoretical models that attempt to explain the existence of liquid-liquid coexistence. We present our phenomenological model [117] of the ternary mixture of DPPC/DiphyPC/cholesterol, whose unusual phase behavior was mapped out by Veatch et al. [143]. This is followed by an application of this model [118], which gives a possible mechanism for the experimentally observed phenomenon of crosslinking-induced phase separation. This has biological relevance due to the important role played by molecular cross-linking in cellular signaling processes, particularly in immune responses [132]. The chapter ends with a review of several microscopic theories of lipid bilayers. The microscopic model of Elliott et al. [36] describing ternary mixtures of saturated lipids, unsaturated lipids, and cholesterol will be discussed at some length, since it will be used in Chapter 3 to investigate the magnitude and nature of the coupling between the two leaflets of a mixed bilayer.

2.1 Phenomenological Modeling of Liquid-Liquid Phase Separation

As a first approach to understanding the thermodynamic behavior of a mixed lipid bilayer, it is natural to seek a simple phenomenological expression for the appropriate thermodynamic potential describing that system, namely the Helmholtz free energy per molecule $f(s, u, c, T)$ as a function of the mole fractions of saturated lipids (s), unsaturated lipids (u), and

cholesterol (c), as well as the temperature T ; in point of fact there are only two independent mole fractions and we may eliminate one: $u = 1 - s - c$. The expression for the free energy is designed so that the phase diagram calculated from it reproduces as closely as possible the phase behavior known from experiment. The limitations of this approach are clear: with sufficiently many adjustable parameters, one may always find a free energy function whose phase diagram matches the experimental one arbitrarily well. For this reason the phenomenological approach is only useful if the free energy function is simple, containing only a few terms that must furthermore be consistent with, and motivated by, whatever knowledge we already have of the system. The purpose of a phenomenological theory of this kind is to provide a simple guide to thinking about the thermodynamics of a complex system. We should not expect a phenomenological theory of a lipid mixture to enjoy the same quantitative success as, for example, the phenomenological Ginzburg-Landau theory of superconductivity [23], which is guided by a symmetry of the system as well as the existence of a small parameter.

The absence of liquid-liquid immiscibility in binary mixtures seems at first sight to rule out phenomenological models relying solely on pairwise binary interactions. If phase separation is driven by a repulsion between two components of a mixture, then one expects to observe immiscibility in the corresponding binary mixture. In fact, it is possible for a free energy function involving only binary interactions to reproduce a closed-loop miscibility gap [115]; however, this requires unreasonably large attractive intermolecular interactions. By including a ternary interaction proportional to $u \cdot s \cdot c$ as well as binary interactions one may easily produce phase diagrams with closed-loop miscibility gaps [120, 62]. Due to statistical correlations, such a term is always present in the free energy, even when the Hamiltonian contains only binary interactions. However, it is physically unclear why the coefficient of this term should be large enough to lead to a closed-loop miscibility gap. McConnell [93] proposed a simple model which explains the closed-loop miscibility gap by positing a reversible chemical reaction in which cholesterol and saturated lipids together form “condensed complexes” that interact repulsively with unsaturated lipids. The system is treated as a four-component mixture of saturated and unsaturated lipids, cholesterol, and condensed complexes. The interactions between these components are pairwise. For the

purposes of illustrating how McConnell’s theory predicts a closed-loop miscibility gap, we make a few simplifying assumptions. We include only a single pairwise interaction, namely the repulsion between condensed complexes (with mole fraction z) and unsaturated lipids (with mole fraction u). We also assume that cholesterol and saturated lipids bind in pairs, and that their tendency to do so is so strong that complex formation proceeds completely. Then the mole fraction z of complexes is equal to the minimum of the *initial* mole fractions of saturated lipids, s_0 , and cholesterol, c_0 , which occur before complex formation begins. The phenomenological free energy of the system at a given temperature T can be written in units of $k_B T$ as follows:

$$f(s, u, c, z) \equiv \frac{F}{k_B T \cdot N} = s \ln s + u \ln u + c \ln c + z \ln z + Jzu, \quad (2.1)$$

The first four terms represent the entropy of mixing of the four components of the mixture; this is nearly always the starting point of any phenomenological free energy. The term Jzu represents the pairwise repulsion between condensed complexes and unsaturated lipids. The fact that complex formation proceeds to completion implies that

$$z = \min(s_0, c_0) \quad (2.2)$$

$$s \ln s + c \ln c + z \ln z = |c_0 - s_0| \ln |c_0 - s_0| + \min(c_0, s_0) \ln [\min(c_0, s_0)] \quad (2.3)$$

The scaled free energy f is now defined in terms of the initial mole fractions u_0 and s_0 , since $c_0 = 1 - u_0 - s_0$. The resulting phase diagram is shown for $J = 4$ in Figure 2.1, taken from [91]. McConnell’s theory can therefore explain the topology of the phase diagram determined by Veatch et al. without resorting to the arbitrary use of higher-order interactions, but rather by assuming that cholesterol and saturated lipids form complexes which interact with unsaturated lipids via a repulsive binary interaction. McConnell and coworkers [119, 68] had previously used the concept of condensed complexes to explain certain features of the phase diagram of phospholipid-cholesterol monolayers. Although the concept of condensed complexes has proven useful in understanding how a closed-loop miscibility gap might arise from pairwise interactions, the evidence from molecular dynamics simulations for the existence of these complexes is mixed [107, 158, 108]. Furthermore, the explanation of the closed-loop miscibility gap based on the concept of condensed complexes hinges

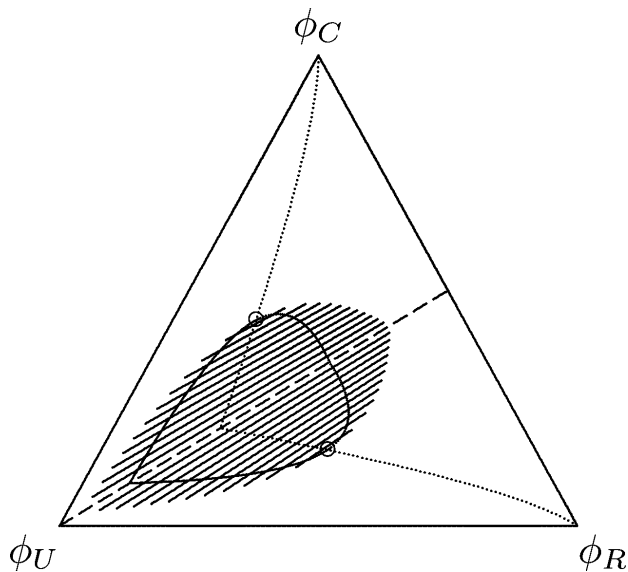


Figure 2.1: Phase diagram calculated from McConnell’s condensed complex theory [93], with $J = 4$. Figure taken from [91]. The mole fractions ϕ_C , ϕ_U , and ϕ_R , are respectively those of cholesterol, unsaturated lipids, and saturated “reactive” lipids. The numerous parallel lines are tie-lines. The dotted lines show the evolution of the two critical points as the parameter J is varied.

on the repulsion between the complexes and the unsaturated lipids, which remains unexplained. It is thus desirable to have a phenomenological model for the DPPC/diphytanoyl PC/cholesterol mixture in which the interactions are based on known facts concerning the molecular components. In particular, it is clear that a theory concerning the coexistence of the liquid-ordered and liquid-disordered phases should make some reference to the configurational order of the lipids, rather than using fixed interaction constants such as J in equation 2.1. Our phenomenological model [117] was motivated by this observation, and is built upon the following assumptions, generally supported by our experimental knowledge of lipid mixtures:

1. The interactions between molecules will in general depend on their internal degrees of freedom. In particular we assume that the interactions involving saturated lipids will depend on an order parameter, δ , representing the extent of orientational order

in the acyl chains (tails) of the saturated lipids. The free energy will depend on δ as well as on the mole fractions u , s , and c . For other theories of lipid mixtures including similar order parameters see [72, 71, 1].

2. Saturated lipids that are highly ordered pack closely together. This packing is favorable for the Van der Waals interaction, but is disrupted by unsaturated (or more generally, low melting temperature) lipids, which have disordered tails. We therefore choose the repulsion between saturated and unsaturated (low melting temperature) lipids to be proportional to δ .
3. In a fluid bilayer, cholesterol increases the extent of order in the tails of saturated lipids. This “condensing effect” of cholesterol has been known in the context of lipid monolayers since 1925 [76] and is also well-documented in fluid lipid bilayers [126].

These three conceptual ingredients are implemented in the following expression for the free energy per unit molecule, describing liquid phases in a ternary mixture of saturated lipids, low-melting-temperature lipids such as diphytanoyl PC (which, in an abuse of terminology, we refer to as an unsaturated lipid), and cholesterol

$$\begin{aligned}
 f_{\text{liq}}(c, s, \delta) &= c \ln c + s \ln s + u \ln u \\
 &+ J_{ss}s^2 [k_1(\delta - 1)^2 + (\delta - 1)^4] \\
 &+ J_{us}us\delta - J_{cs}cs(\delta - k_2\delta^2),
 \end{aligned} \tag{2.4}$$

where $u = 1 - s - c$. The first line is simply the entropy of mixing. The second line represents the δ -dependent interactions among the saturated lipids. The normalization of the order parameter δ is chosen such that $\delta = 1$ for a system of pure saturated lipids. The interactions of the saturated lipids with the other components of the mixture are described by the terms in the third line. The repulsion between saturated and unsaturated lipids is proportional to the extent of order δ of the saturated lipids. The interaction between saturated lipids and cholesterol is also proportional to δ , but is attractive, so that the presence of cholesterol favors higher order in the saturated lipids. The term in δ^2 is necessary to ensure that the

free energy remains finite in the limit where s vanishes, in which case f would otherwise become unbounded from below as a function of δ .

The free energy function 2.4 depends not only on the mole fractions of the components of the mixture, but also on an internal order parameter δ of the saturated lipids, which is neither conserved in the course of experiments (as is the average composition) nor controlled experimentally. Therefore the value of δ occurring in equilibrium will be such that f is minimized as a function of δ . This determines the equilibrium value δ_{eq} as a function of the mole fractions s and c :

$$\left[\frac{\partial f(s, c, \delta)}{\partial \delta} \right]_{\delta=\delta_{eq}} = 0 \quad (2.5)$$

The equation above reduces f_{iq} to a function of the mole fractions only, so that the phase diagram can be calculated as described in Appendix B. A phase diagram derived from the free energy function 2.4 is shown in Figure 2.2. This phenomenological phase diagram

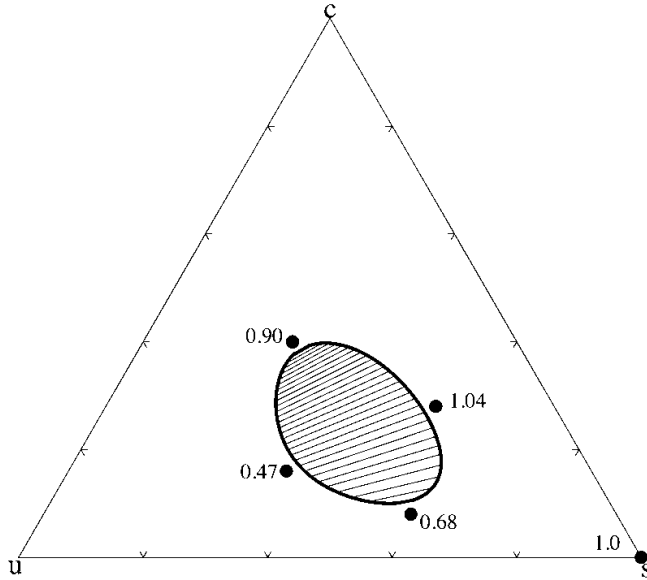


Figure 2.2: Phase diagram calculated from the free energy 2.4, with parameters $J_{ss} = 1.0$, $k_1 = 1.0$, $J_{us} = 1.8$, $J_{cs} = 2.4$, and $k_2 = 0.21$. Values of the order parameter δ are shown at points marked by dots. The closely spaced lines are tie-lines connecting coexisting phases.

shows the result of the basic assumptions listed above. The repulsion between saturated and

unsaturated lipids depends on the order parameter δ , which in the absence of cholesterol is not great enough to trigger phase-separation in the binary lipid mixture. However, the addition of cholesterol orders the saturated lipids, increasing this repulsive interaction. At sufficiently high levels of cholesterol, this repulsion is strong enough to cause phase separation between a phase poor in saturated lipids and cholesterol and a phase rich in these components. Furthermore, the saturated lipids in the saturated-rich phase are highly ordered, as can be seen from the values of δ shown at compositions marked by dots in the figure.

The role of the δ -dependent interactions can be made clear if one makes the approximation that $\delta \approx 1$, so that the term in $(\delta - 1)^4$ in equation 2.4 can be ignored, allowing us to solve for δ_{eq} explicitly. The resulting free energy $f(s, c, \delta_{eq}(s, c))$ contains the term

$$\frac{J_{us}J_{cs}(1 - 2k_2)}{2J_{ss}k_1s + 2J_{cs}k_2c}ucs, \quad (2.6)$$

representing a ternary interaction proportional to J_{us} , the repulsion between saturated and unsaturated lipids, and to J_{cs} , the tendency of cholesterol to order the saturated lipids. The term given in Equation (2.6) neatly encapsulates the conceptual ingredients of this phenomenological theory. It also shows that the ternary interactions suggested by the closed-loop miscibility gap of the DPPC/DiphyPC/cholesterol phase diagram are easily understood on the basis of intermolecular interactions depending on the internal degrees of freedom of molecules. McConnell's model involving condensed complexes can be viewed in a similar light. His free energy depends not only on the initial mole fractions u_0 , s_0 , and c_0 , but also on a parameter that is not controlled externally, namely the fraction of saturated lipids that undergo complexation with cholesterol. This fraction is clearly increased by the presence of cholesterol; moreover, the posited repulsion between unsaturated lipids and complexes amounts to an s - u repulsion which depends on this fraction. In a final analysis, therefore, both phenomenological models described here provide intuitive justifications for including a ternary interaction term in the free energy when it is written as a function of mole fractions only.

In Appendix D we give another phenomenological theory of a ternary mixture of saturated lipids, unsaturated (low melting temperature) lipids, and cholesterol. The theory

has essentially the same content as the one given above, but is simpler and easier to use in calculations.

We have applied the phenomenological model described above to investigate the changes in phase behavior that occur in ternary lipid-cholesterol mixtures when some fraction of the saturated lipids is chemically cross-linked into complexes of p molecules each [118]. This scenario is motivated by experiments on ternary model membranes that showed that chemical cross-linking of lipids can trigger liquid-liquid phase separation in previously uniform mixtures [54, 84], and by the important role played by cross-linking of *proteins* in lipid raft-mediated signaling events [132]. The phenomenological free energy of equation (2.4) is easily extended to include complexes of p saturated lipids each. It is convenient to keep track of the quantity of these complexes by defining z to be the mole fraction of *individual saturated lipids occurring in complexes*, and s to be the the mole fraction of *individual saturated lipids not occurring in complexes*. Our phenomenological free energy for the four-component system including complexes is simply

$$f = \frac{z}{p} \ln z + f_{\text{liq}}(s + z, c, \delta), \quad (2.7)$$

where f_{liq} is the free energy of the ternary mixture given in equation (2.4). The first term is the entropy of mixing of the saturated lipids occurring in complexes. It is reduced by a factor of p as in the Flory-Huggins theory of polymer mixtures [22] to account for the fact that the positions of lipids in a given complex are not independent of each other. The second term is the free energy of the ternary system of saturated lipids, unsaturated lipids, and cholesterol. Its dependence on $s + z$, the mole fraction of saturated lipids regardless of whether they are in complexes, reflects our assumption that lipids in complexes have the same intermolecular interactions as those not in complexes. This assumption amounts to a further mean-field approximation, since in reality two lipids that are cross-linked close together always interact with each other, regardless of the average composition of the mixture. Therefore the dependence of f on $s + z$ should be reasonable if cross-linked lipids are kept far apart compared to the correlation length(s) of the mixture.

A composition of the quaternary mixture of saturated and unsaturated lipids, cholesterol, and complexes of saturated lipids is defined in terms of three independent mole fractions.

The phase diagram of this mixture should therefore be visualized in a three-dimensional tetrahedron or simplex instead of the Gibbs triangle used for ternary systems. Each vertex of the tetrahedron represents a pure phase of one of the components, and the composition (u, s, c, z) is represented by the center of mass of four points with masses u , s , c , and z , located at the respective vertices. The equations of phase coexistence can be solved using methods similar to those described in Appendix B, and the resulting tie-lines displayed in the interior of the ‘‘Gibbs tetrahedron.’’ The region of two-phase coexistence is a three-dimensional solid, making it difficult to portray. The left panel of Figure 2.3 shows, for $p = 5$, some of the tie-lines of the quaternary mixture, namely those for which either the liquid-order or liquid-disordered phases has $z = 0.05$. These tie-lines show the boundary of the two-phase region within the plane $z = 0.05$. This boundary is labeled $z = 0.05$ in the right panel of Figure 2.3, which shows a Gibbs triangle in which one corner represents all saturated lipids, regardless of whether they are in complexes or not. Also shown are the boundaries for $z = 0.03$ and $z = 0$, which is simply the two-phase region of the original ternary system, shown in Figure 2.2.

The right panel of Figure 2.3 shows that cross-linking even a small fraction of the saturated lipids has a significant effect on the phase-behavior of the ternary mixture of saturated lipids, unsaturated lipids, and cholesterol. A bilayer with composition lying inside the solid curve ($z = 0.05$) but outside of the dotted curve ($z = 0$) would be uniform without any cross-linking, but would phase-separate upon cross-linking enough saturated lipids so that the mole-percent of cross-linked saturated lipids is $z = 0.05$. Such cross-linking-triggered liquid-liquid phase separation has been observed experimentally [54] in ternary model membranes in which the saturated ganglioside lipid GM₁ is cross-linked into pentamers ($p = 5$) using cholera toxin. Interestingly, according to Figure 2.3 our model predicts that the effect of cross-linking should be much greater for initial compositions in the liquid-disordered, rather than liquid-ordered, phase. If we modify the phenomenological model so that the unsaturated lipids, rather than the saturated ones, are cross-linked, then the opposite case arises: the tendency to trigger phase-separation is much more significant in the unsaturated-poor liquid-ordered phase [118]. Phase separation triggered by cross-linking of unsaturated lipids has also been observed [84].

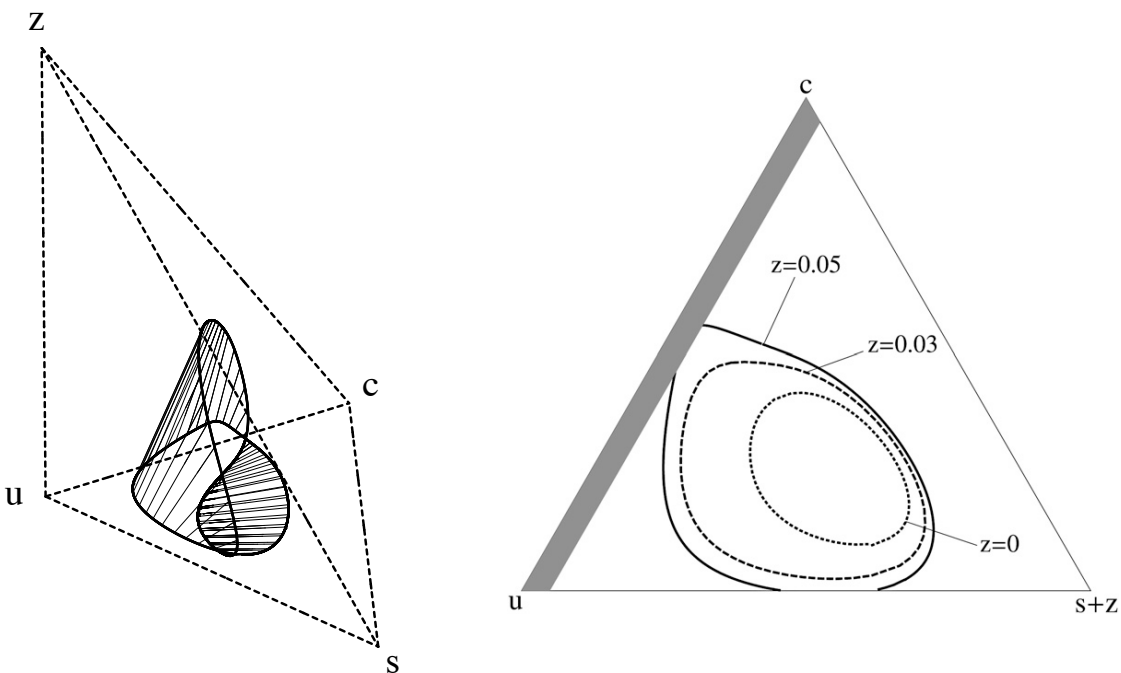


Figure 2.3: Partial phase diagrams calculated from equation (2.7). Left: Partial phase diagram showing tie-lines in which either the liquid-ordered or the liquid-disordered phase contains 5 percent complexed saturated lipids. Right: Boundaries of the two-phase region with various fixed amounts of cross-linked saturated lipids (z). The gray region represents compositions where $s + z \leq 0.05$.

In general, phase separation is driven by intermolecular interactions and opposed by entropy of mixing. Any membrane component that, by nature of its interactions, tends to promote phase separation, will be capable to some degree of triggering phase separation when it is cross-linked. This applies not only to the saturated and unsaturated lipids that were cross-linked in the experiments discussed immediately above, but also to any proteins that might partition preferentially into either the liquid-ordered or -disordered phases. The mechanism of reduction of mixing entropy described above is therefore of biological interest in the context of cell signaling processes known to involve lipid rafts, such as the immune response of T cells [132].

2.2 *Microscopic Models of Lipid Bilayers*

Whereas phenomenological modeling can serve as a guide to studying the thermodynamics of a complex system such as a mixed lipid/cholesterol bilayer, it can not reveal the connection between the known fundamental interactions and the macroscopic phase behavior of interest. For this purpose we must have a description of the system at a molecular level. The most common approaches to modeling lipid bilayers at this level have been Monte Carlo (MC) [74] and molecular dynamics (MD) [46] simulations. Atomistic molecular dynamics, in which Newton's equations of motion are solved in suitably parameterized interatomic force fields, has been a popular approach to studying the structure and dynamics of lipid/cholesterol membranes on the nanometer scale [107, 109, 11]. Unfortunately, atomistic MD simulations are computationally intensive and thus are only able to study length scales of tens of nanometers and time scales of fractions of a microsecond [99], making macroscopic phase behavior and other large-scale phenomena inaccessible. This limitation has led to the development of so-called coarse-grained models of lipid membranes [96, 149], including lipid/cholesterol mixed membranes [99, 123]. A major success has been the simulation by Risselada and Marrink [123] of liquid-liquid immiscibility in a coarse-grained model of a ternary mixed membrane containing saturated lipids, unsaturated lipids, and cholesterol.

A different approach to modeling lipid membranes at the molecular level has been to construct microscopic models of the interactions between lipids which can be solved either analytically or numerically to obtain thermodynamic quantities. These models are usually but not always [100] developed and solved under a mean-field approximation. They offer two important advantages over more detailed simulation methods. First, their simplicity highlights only the most important interactions governing the behavior of lipid membranes, leaving out molecular details which are irrelevant to the phenomena of interest. Second, using these methods it is a simple matter to extract thermodynamic quantities such as the free energy difference between two states; although this is possible in molecular dynamics [46] and Monte Carlo [74] simulations, it is in many cases prohibitively difficult, requiring simulations to be repeated many times.

Molecular mean-field theories describe intermolecular interactions by assuming that a

given molecule experiences an average potential given by a mean field representing its surroundings. The value of this field is determined from the probability distribution of the configurations of the “central molecule” itself in a self-consistent manner. A number of such models have been proposed to describe various aspects of lipid bilayers. We merely list them here; their influence on the model of Elliott et al. [35, 36] will be seen in the next section. Of particular note is the pioneering work of Marčelja [87, 88], who adapted the Maier-Saupe theory of the nematic state of liquid crystals [24] to describe the gel-liquid phase transition in bilayers of saturated lipids. While Marčelja’s model thus describes in a mean-field manner the interactions giving rise to the gel-liquid transition, another model developed by Ben-Shaul and collaborators [136, 41, 42] describes in a detailed manner the dense packing of lipid tails in the interior of the bilayer via an incompressibility constraint, as well as including a realistic treatment of the configurations of the tails, based on Flory’s Rotational Isomeric State Model [45]. Other molecular mean-field models of lipid bilayers were developed by Gruen [52], by Dill and Stigter [29], and by Leermakers and Scheutjens [79]. This type of model has been brought to bear on an impressive array of problems related to lipid membranes and other aggregates, including lipid-protein interactions [42, 31], curvature elasticity of membranes [137], the effects of cholesterol [34, 78], mixtures of lipids with different chain lengths [85], non-bilayer morphologies [97, 82], and membrane fusion [77].

2.3 *The Model of Elliott, Szleifer, and Schick*

In this section we describe the main features of the molecular mean-field theory developed by Elliott et al. to describe lipid bilayers composed of saturated lipids, unsaturated lipids, and cholesterol. For more details on this model, the reader is directed to [34, 35, 36]. The theory combines features of two earlier models. As in the theory of Ben-Shaul [136], it treats the configurations of the lipid tails realistically using the Rotational Isomeric State Model [45], and describes the packing of these tails in the bilayer interior using an incompressibility constraint. It also displays a phase transition between gel and liquid phases driven by a bond orientation-dependent intermolecular interaction as in the work of Marčelja [87, 88]. Most notably, however, the theory of Elliott et al. displays phase separation between phases

with properties similar to those of the liquid-ordered and liquid-disordered phases observed in ternary model membranes [36]. Therein lies our primary interest in this model, since we have used it to calculate the magnitude of the interaction which couples the states of the two leaflets in liquid-liquid phase separated membranes; see section 3.7.

The microscopic model of Elliott et al. describes a bilayer composed of saturated lipids, unsaturated lipids, and cholesterol. More specifically, it describes the interactions among the acyl chains of the lipids as well as the hydrophobic part of the cholesterol molecule. For each of these molecular species, a large set of molecular configurations is enumerated based on the realistic Rotational Isomeric State Model [45, 34]. A given “configuration” includes the orientation of the whole molecule as well as the *trans* or *gauche* state of its carbon-carbon bonds; the internal energy difference between these states is taken into account explicitly. The model accounts for the interactions between molecules in a mean-field way. The probability of a given chain configuration is determined by its coupling to two mean fields: the lateral pressure field $\pi(z)$ and the field $\xi(z)$, which gives the density of carbon-carbon bonds, weighted by the extent to which these bonds are aligned with the bilayer normal. We now describe the physical role of each of these fields.

The field $\pi(z)$ gives the lateral pressure at a depth z into the bilayer, and serves to enforce the constraint of incompressibility of the bilayer interior, as in the work of Ben-Shaul and collaborators [136]. The incompressibility of the bilayer interior is a simple result of two kinds of interactions which would be difficult to account for individually: the short-range steric repulsions between molecules, which prevent them from overlapping, and the weak but long-range attractive Van der Waals interactions. Together these interactions cause the molecules forming the bilayer interior to condense into a densely packed liquid having a constant, uniform, density. The constraint of constant density is imposed via a Lagrange multiplier, which is precisely the lateral pressure profile $\pi(z)$. There is some evidence from experiment to justify the assumption that the bilayer interior has constant density, and is therefore incompressible, under experimentally relevant conditions: Ebel et al. [32] measured the pressure dependence of the gel-liquid transition temperature in DPPC lipid bilayer vesicles, and found that that it was shifted by less than a degree Celsius as the hydrostatic pressure was increased by a factor of roughly 40. A significant change in

volume of the bilayer during the gel-liquid transition would have coupled to the hydrostatic pressure, leading to a large pressure dependence of the gel-liquid transition temperature [58]. Thus, although the lipids are more densely packed in the gel phase than in the liquid phase, and therefore occupy less area, they also form a thicker bilayer; these effects result in nearly the same volume per molecule in both phases.

The field $\xi(z)$ measures the “density of bond order” at a given depth z into the bilayer. It counts the number of carbon-carbon bonds at that location, weighting them by the extent to which they are aligned with the bilayer normal. Molecular configurations experience an interaction proportional to this field: the greater $\xi(z)$ is, the more it tends to align the bonds of these configurations along the bilayer normal. It is this orientation-dependent interaction which leads to the gel-liquid transition, as in the work of Marčelja [87, 88].

Note that in the model of Elliott et al., only the configurations of the hydrophobic components of molecules are treated in detail. The interactions between the lipid head groups, or between the lipids and the solvent, are treated phenomenologically using an effective surface tension term proportional to the area of the bilayer. This takes into account the effective attraction between head groups due to the fact that if these are widely separated, the hydrophobic interior of the bilayer will be exposed to the solvent. Thus the effective “surface tension” used by Elliott et al. [34] is approximately equal to the surface tension between oil and water.

The complete Helmholtz free energy per molecule in the model of Elliott et al. is summarized as follows:

$$\begin{aligned}
 f \equiv \frac{\beta F}{N} = & \quad f_{\text{ideal}} && \text{Ideal gas contribution} \\
 & + f_{\text{internal}} && \text{Internal energy and entropy of configurations} \\
 & + f_{\text{bond}} && \text{Attractive bond interaction} \\
 & + f_{\text{Lagrange}} && \text{Lagrange multiplier for incompressibility} \\
 & + f_{\text{surface}} && \text{Surface interaction}
 \end{aligned} \tag{2.8}$$

This free energy defines a functional of the probability distribution of molecular configurations. The equilibrium distribution is determined by minimizing f . By minimizing the free

energy with respect to areal density as well, we may calculate the Helmholtz free energy of the tensionless state of the mixed bilayer as a function of the mole fractions of each of the constituents of the mixture. This in turn produces a phase diagram as explained in Appendix B. A phase diagram calculated for $T = 290$ K by Uline et al. [141] from the model of Elliott, Szleifer, and Schick is shown in Figure 3.10. It shows a region of saturated-lipid-rich gel phase as well as coexistence between two liquid phases. In section 3.7 we use the model of Elliott et al. to calculate the magnitude of the interaction that couples the states of the two leaflets in phase-separated bilayers. This interleaflet coupling is the subject of the next chapter.

Chapter 3

THE INTERLEAFLET COUPLING

The phenomenological models described in the previous chapter miss an important aspect of the cell plasma membrane: its compositional asymmetry [26, 142, 70]. Whereas the outer (extracellular) leaflet of the plasma membrane is rich in lipids with PC head groups as well as the saturated sphingolipids believed to be involved in the formation of lipid rafts, the inner leaflet is rich in lipids with unsaturated tails and contains essentially all of the lipids with charged head groups. This asymmetry is facilitated by the slow rate of interleaflet translocation or “flip-flop” of lipids [127], but ultimately must be actively maintained by the cell, which uses specialized proteins known as “flippases,” “floppases,” and “scramblases” [27] to translocate certain lipids across the plasma membrane. Since this process costs energy, the lipid asymmetry of the plasma membrane is evidently of importance to cell function. This asymmetry raises an important question regarding the lipid raft hypothesis [26]: since the compositions of the inner and outer leaflets are such that rafts are thought to reside only in the outer leaflet, how does a lipid raft function as a platform for transmembrane signaling? A related question concerns the phenomenon of liquid-liquid phase separation in model membranes containing cholesterol: are liquid domains entities that exist within a single leaflet of the bilayer, or are the leaflets coupled in some way? In Section 3.1 we discuss experimental evidence of an interaction that couples the states of the two leaflets of a bilayer undergoing liquid-liquid phase separation. In Section 3.2 we review phenomenological models of the phase behavior of bilayers with coupled leaflets, including our own [116]. The interleaflet coupling is the free energy penalty per unit area of “mismatch” in which the apposing leaflets have different compositions characteristic of the two liquid phases. We give two thermodynamic definitions of the interleaflet coupling, which we call γ in this work: In Section 3.3 it is defined in the canonical ensemble of fixed particle numbers, while in Section 3.4 it is defined in the grand canonical ensemble, that is, under

conditions of fixed chemical potentials. This discussion is followed by a review of several mechanisms that have been proposed to explain the origin of the interleaflet coupling. In Section 3.6 we give an analysis of domain boundary fluctuations in coupled phase-separated lipid bilayers that clarifies the interpretation of the interleaflet coupling γ as well as the way in which this quantity should be extracted from coarse-grained molecular dynamics simulations such as those of Risselada and Marrink [123]. Finally we describe our molecular mean-field calculation of the interleaflet coupling in a phase-separated ternary mixture of saturated lipids, unsaturated lipids, and cholesterol, using the model developed by Elliott et al. [36].

3.1 Interleaflet Coupling in Liquid-Liquid Phase-Separated Vesicles

The lipid asymmetry of the cell plasma membrane raises important questions related to the lipid raft hypothesis [26] and the related phenomenon of liquid-liquid phase separation in model lipid bilayers containing cholesterol [18]. Artificial model membranes with compositions meant to reflect that of the extracellular monolayer of the plasma membrane have been found to phase-separate into liquid-ordered and liquid-disordered phases [28]. In contrast, model membranes with compositions mimicking that of the cytoplasmic leaflet of the plasma membrane do not show such liquid-liquid phase separation [156]. If the molecular interactions responsible for the existence of rafts are the same as those driving liquid-liquid phase separation in model systems, it follows that in order for lipid rafts to regulate or influence transmembrane signaling processes [132], a lipid raft in the extracellular leaflet of the plasma membrane must somehow induce a change in the cytoplasmic leaflet. This coupling could be performed by a transmembrane protein that partitions preferentially into the raft; however, experiments on protein-free model membranes exhibiting liquid-liquid phase separation indicate a strong inter-leaflet coupling which could provide a mechanism for raft-based transmembrane signaling. The earliest evidence for such a coupling was the fact that liquid domains in phase-separated vesicles [9, 145] were seen to be in registry in both leaflets [17]. In the absence of any inter-leaflet coupling, phase separation would occur independently in each leaflet, whereas a sufficiently weak coupling might still allow fluctuations out of domain registry visible on the micron scale. The fact that such “overhang”

fluctuations are never observed in symmetric model membranes undergoing liquid-liquid phase separation suggested a strong coupling between the states of the two leaflets [17]. We show in section 3.6 that the spatial extent of such fluctuations will be below optical resolution even with a very small interleaflet coupling. Recently, experimentalists have obtained direct evidence of inter-leaflet coupling using supported [69, 49, 155] and unsupported [18] asymmetric membranes. Collins and Keller [18] have shown that this coupling has important effects on the phase behavior of model membranes with asymmetric composition; whether these are uniform or display liquid-liquid phase coexistence depends on the compositions of both of the leaflets.

3.2 Phenomenological Modeling

The experiment of Collins and Keller [18] showed that the interleaflet coupling has important effects on the liquid-liquid phase behavior of lipid bilayers with asymmetric compositions. In this section we discuss theoretical and phenomenological treatments of the phase behavior of coupled bilayers, including our own [116].

The phase behavior of a bilayer can be modeled phenomenologically using a free energy depending jointly on two order parameters, one for each leaflet. Terms in the free energy involving products of these order parameters couple the states of the leaflets. Several studies have used this approach to model the effect of interleaflet coupling on the gel-liquid transition [159, 61]. Here we are interested in the coupling between compositional order parameters in the two leaflets of a mixed bilayer. Several authors have modeled the phase behavior of two leaves whose compositional order parameters are coupled indirectly, via composition-dependent spontaneous curvatures [80, 138, 86]. Hansen et al. [56] were the first to consider a direct intermolecular coupling between the compositional degrees of freedom of the two leaflets. However, they were interested in various spatially modulated phases rather than in determining the miscibility phase behavior of asymmetric bilayers, and their model assumed equal average compositions of the two leaflets. Allender and Schick [1] proposed a model in which two leaflets are separately capable of undergoing phase separation, generally at different temperatures, and considered the phase behavior of this system when the coupling between the leaflets is small. They predicted, among other things, that more

than two liquid phases could coexist in an asymmetric coupled bilayer. We have calculated [116] the miscibility phase diagram of a closely related model, without the assumption of small coupling. This work is the subject of the remainder of this section. Wagner et al. [153] independently published a very similar analysis.

The compositional state of each leaflet of the bilayer is represented by a single order parameter: x for the inner leaflet and y for the outer one. We assume that these order parameters are linear combinations of mole fractions of molecules in their respective leaflets, and that the composition of the liquid-ordered phase corresponds to a positive value of the order parameter, whereas the composition of the liquid-disordered phase corresponds to a negative value of the order parameter. We consider the following phenomenological free energy per molecule for the coupled leaflets (see also [18]):

$$\begin{aligned} f(T, x, y) &= c_i(T)x^2 + x^4 \\ &+ c_o(T)y^2 + y^4 \\ &- \alpha xy \end{aligned} \tag{3.1}$$

The first two lines represent the interactions between molecules within each of the leaflets. The sign of the coefficient $c_i(T)$ determines whether or not phase separation will occur in the inner leaflet in the absence of any coupling to the outer one, and similarly for $c_o(T)$ in the outer leaflet. The last term in (3.1) is an energetic coupling between the compositional states of the inner and outer leaflets. If $\alpha > 0$, then it is energetically favorable for the two leaflets to have similar compositions, as is the case in model lipid membranes capable of undergoing liquid-liquid phase separation.

In the following, it will be convenient to express both the compositional order parameters and the coupling α in dimensionless form. Phase diagrams will be given with order parameters x and y expressed in terms of characteristic values

$$\begin{aligned} \hat{X} &= (|c_i(T)|/2)^{1/2} \\ \hat{Y} &= (|c_o(T)|/2)^{1/2}, \end{aligned}$$

while the magnitude of the interleaflet coupling is given by

$$\beta \equiv \frac{\alpha}{2|c_o|}$$

Because x and y are taken to be linear combinations of mole fractions, the phase diagram of coupled leaves having free energy (3.1) is obtained in the same way as if x and y were themselves mole fractions, via the double-tangent construction. Two distinct cases are of interest: either both c_i and c_o are negative, or only one of these quantities is negative. We first consider two leaflets which both have an intrinsic tendency to phase-separate. The temperature is then such that both $c_i(T)$ and $c_o(T)$ are negative; we choose them to have equal magnitudes. Figure 3.1 shows a phase diagram for this situation, where the coupling between the leaflets is relatively weak ($\beta = 0.5$). The system can exist in four

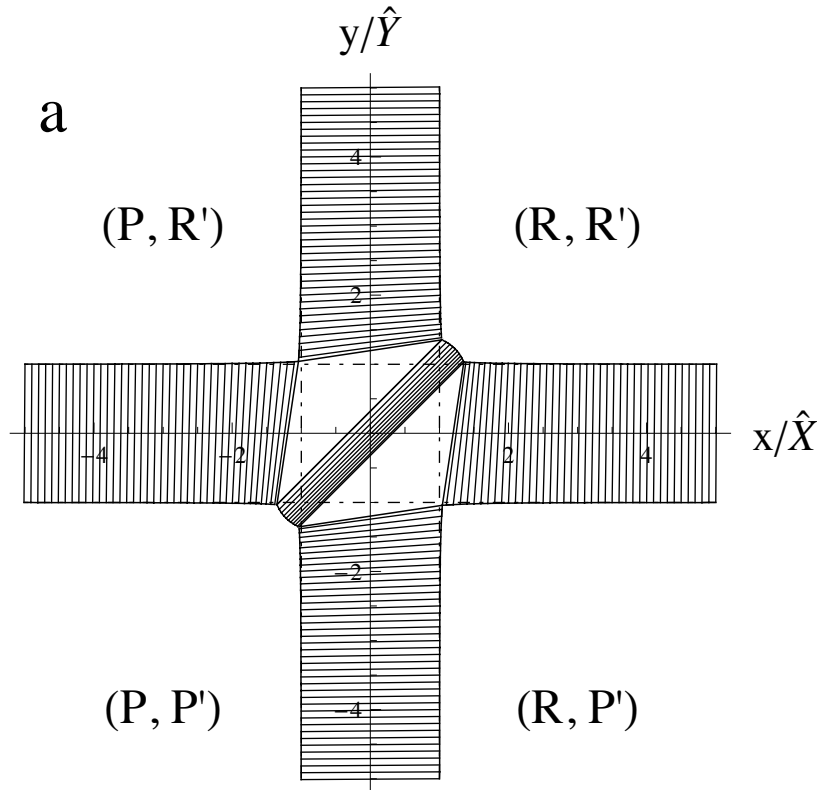


Figure 3.1: Phase diagram of weakly coupled leaves with both c_i and c_o negative, and of equal magnitude. The value of the dimensionless interleaflet coupling is $\beta = 0.5$. The order parameters x and y are plotted in units of \hat{X} and \hat{Y} .

possible phases, corresponding to a choice of positive or negative order parameter in each leaflet. These phases are labeled in Figure 3.1 based on whether each leaflet is rich (R) or

poor (P) in ordered lipids and cholesterol. There are four regions of two-phase coexistence between phases which differ in composition primarily in one leaflet or the other. Without any interleaflet coupling these regions would intersect in the middle of the phase diagram, forming a square region of four-phase coexistence, shown with a dash-dotted line in the figure. The small coupling has an important qualitative effect on the phase behavior; it leads to a new region of coexistence between symmetric phases, as well as two triangular regions of three-phase coexistence. The symmetric coexisting phases are simply the liquid-ordered and liquid-disordered phases observed in experimental studies of liquid-liquid immiscibility in symmetric model membranes. Coexistence between three liquid phases requires membranes of asymmetric average composition, and was observed via fluorescence microscopy by Collins and Keller [18]. Another thermodynamic consequence of interleaflet coupling is illustrated in figure 3.2, which gives the phase diagram for the same system but with a larger coupling ($\beta = 3.0$). Consider the three symmetrically composed bilayers represented by points AA, BB, and CC. Of these, only the composition AA lies in the region of the phase diagram where a single phase is stable. Compositions BB and CC lead to two-phase coexistence, but BB lies deeper in the two-phase region and thus has a stronger tendency to phase-separate. The result of combining one leaflet from each of AA and BB is AB, which does not phase-separate. However, the asymmetric bilayer AC, although similarly constructed out of leaflets from the symmetric one-phase and two-phase regions, does undergo phase-separation. Thus, the phase behavior of an asymmetric bilayer whose outer leaf has a tendency to phase-separate, but whose inner leaf does not, depends on the strength of the outer leaf's tendency to phase separate. This behavior was also observed by Collins and Keller [18].

We have just considered a bilayer in which the lipids composing both leaflets are such that they are both capable of undergoing phase separation in the absence of interleaflet coupling (both c_i and c_o are negative). A different situation occurs in the cell plasma membrane, since the saturated sphingolipids believed to be responsible for the formation of lipid rafts reside mostly in the outer (extracellular) leaflet [142, 70]. Experimentally, model membranes with symmetric compositions meant to mimic the composition of the outer leaflet of the cell plasma membrane show liquid-liquid phase separation [28], whereas

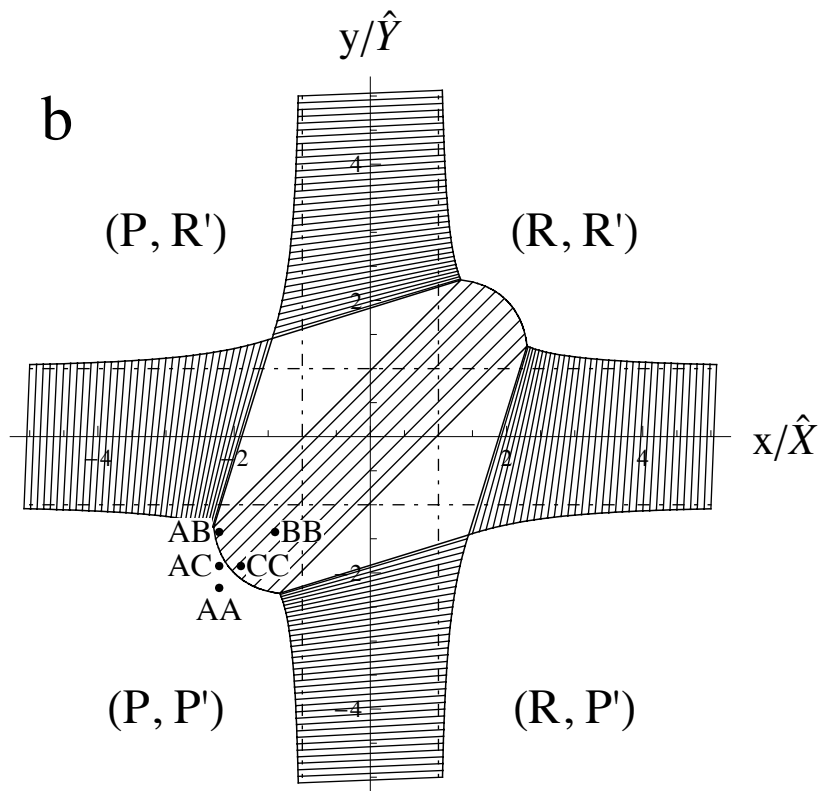


Figure 3.2: Phase diagram of strongly coupled leaves with both c_i and c_o negative, and of equal magnitude. The value of the dimensionless interleaflet coupling is $\beta = 3.0$. The order parameters x and y are plotted in units of \hat{X} and \hat{Y} .

membranes with compositions designed to reflect that of the inner (cytoplasmic) leaflet do not display such phase separation [156]. Therefore it is of interest to consider, in our phenomenological model, the case in which $c_o(T) < 0$ but $c_i(T) > 0$, meaning that only the outer leaflet has an intrinsic tendency to phase-separate. Here we will assume that c_i and c_o have the same absolute value. Figure 3.3 shows the phase diagram of such a bilayer when the coupling is weak ($\beta = 0.75$). The tie-lines in the coexistence region are nearly vertical, meaning that the coexisting phases differ primarily in the composition of their outer leaflets. However, the coupling clearly induces a difference in the inner-leaflet compositions of the coexisting phases as well, as can be seen by the tilting of the tie-lines, especially for x near zero. The figure also shows as a dashed line the spinodal, which gives the boundary of

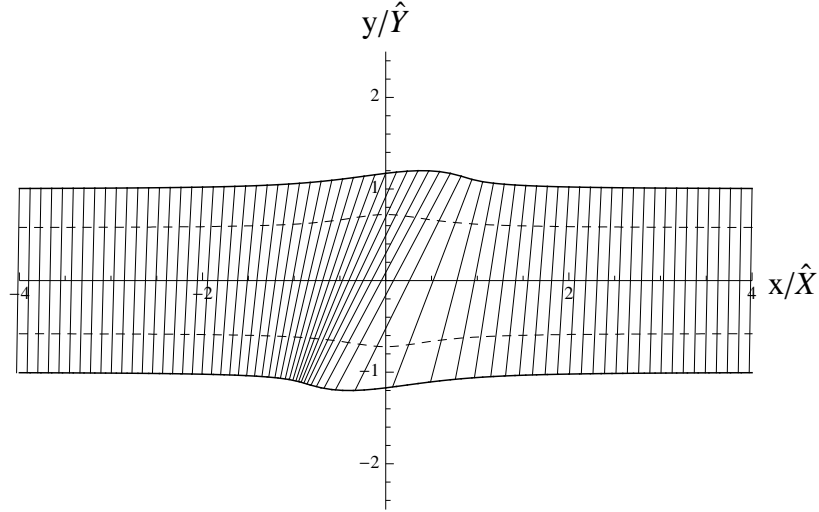


Figure 3.3: Phase diagram of weakly coupled leaves with $c_o = -c_i < 0$. The value of the dimensionless interleaflet coupling is $\beta = 0.75$. The order parameters x and y are plotted in units of \hat{X} and \hat{Y} . The spinodal line is shown dashed.

the region of local stability. Average compositions lying within the two-phase region (the binodal) but outside the spinodal are metastable, that is, globally unstable but locally stable with respect to small changes in composition. Mathematically, the spinodal line is given by the vanishing of the determinant of the matrix of second derivatives of the free energy:

$$\det \begin{pmatrix} \frac{\partial^2 f}{\partial x^2} & \frac{\partial^2 f}{\partial x \partial y} \\ \frac{\partial^2 f}{\partial x \partial y} & \frac{\partial^2 f}{\partial y^2} \end{pmatrix} = 0 \quad (3.2)$$

As the dimensionless interleaflet coupling β is increased, the effect on the inner leaflet of the phase separation driven by the outer leaflet becomes more important. Additionally, near $x = 0$ the spinodal line begins to move toward the boundary of the two-phase region. As the coupling is further increased, miscibility critical points appear at the two locations where the spinodal line and binodal lines meet, as shown in Figure 3.4, in which the dimensionless coupling has been increased to $\beta = 4.0$. These critical points occur at the ends of two new regions of two-phase coexistence. Interestingly, in these regions the coexisting phases differ primarily in their inner-leaflet compositions, even though the phase separation of the whole system is driven by interactions in the outer leaflet. Three-phase coexistence regions

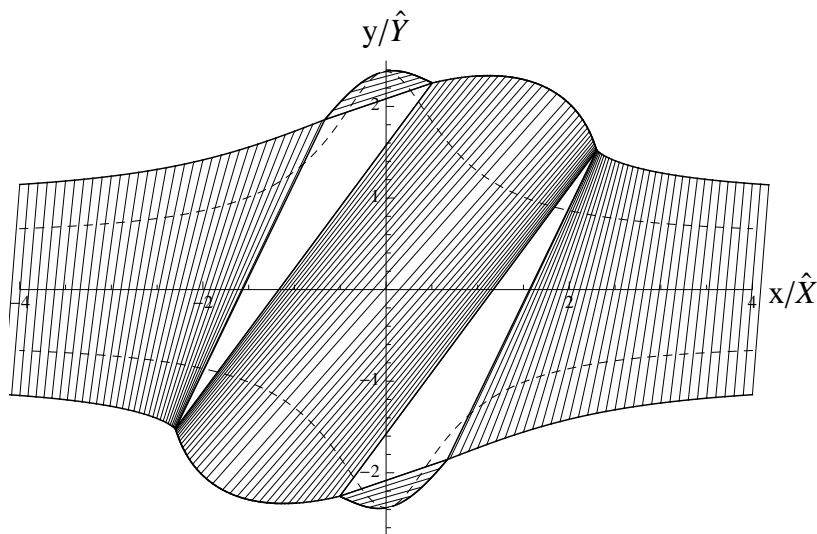


Figure 3.4: Phase diagram of strongly coupled leaves with $c_o = -c_i < 0$. The value of the dimensionless interleaflet coupling is $\beta = 4.0$. The order parameters x and y are plotted in units of \hat{X} and \hat{Y} . The spinodal line is shown dashed.

also appear at high interleaflet coupling, as in the previous case where both c_i and c_o were negative. Thus, if the temperature and the composition of a bilayer are such that only one of its leaflets has an intrinsic tendency to phase separate, the regime of strong coupling is marked by a qualitative change in phase behavior, characterized by the possibility of three-phase coexistence.

3.3 Thermodynamic Definition of Interleaflet Coupling: Canonical Ensemble

At a theoretical level, it is important to define the interleaflet coupling energy in a precise manner. In this section we define it as the free energy difference γ , per unit area, between the initial and final states of a process depicted in Figure 3.5. The initial state (1) consists of two equal areas A of the symmetric coexisting phases L_o and L_d . Because these phases have different areas per molecule, there are different numbers of molecules in the two halves: N_1 in the L_d - L_d bilayer and N_2 in the L_o - L_o bilayer. The final state (2) is reached in two steps. First, the top leaflet is flipped, so that L_o is across from L_d in both halves of the bilayer, which still each have area A . Secondly, the area of this asymmetric bilayer

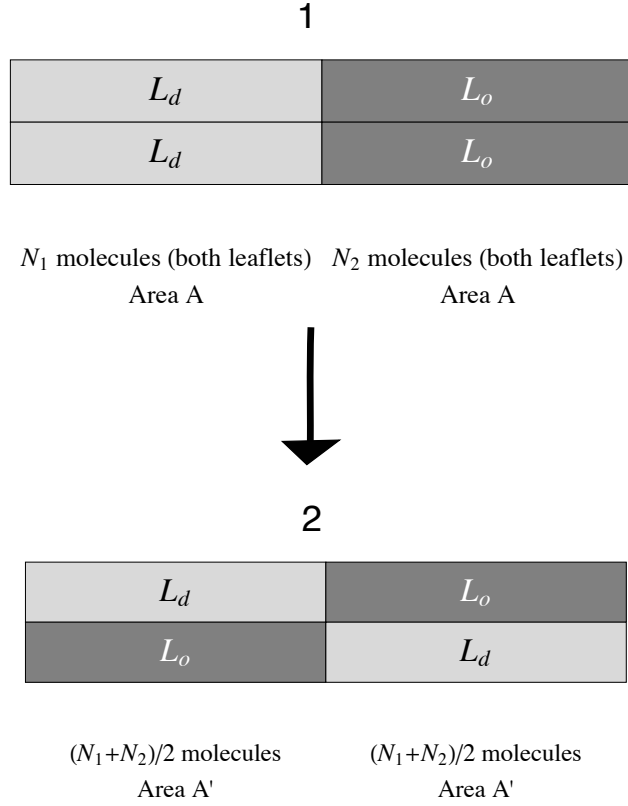


Figure 3.5: Mismatch process used to define interleaflet coupling energy γ .

is allowed to equilibrate at zero surface tension. The asymmetric bilayer then has a new area $2 \cdot A'$. Since we are not interested in the linear interface between the left and right halves of the bilayer shown at the bottom of Figure 3.5, we may flip one half and consider both asymmetric halves to have the L_d composition on top. The relevant thermodynamic potential is the Helmholtz free energy, since the initial and final states have the same number of each species of molecule. We define the interleaflet coupling energy in terms of the Helmholtz free energy difference between the final and initial states. However, this free energy difference is extensive, that is, proportional to A or equivalently to A' . For this reason we define the overlap energy or coupling γ to be

$$\gamma \equiv \frac{F_2 - F_1}{2A'} \quad (3.3)$$

The quantity γ is the free energy cost of creating a unit area of asymmetric membrane at the expense of two areas of the symmetric phases, equal to each other but not necessarily to the area of the new asymmetric region.

The interleaflet coupling energy γ is an intensive quantity, so we may write it in terms of other intensive quantities, such as the Helmholtz free energies per molecule in the three phases (the two symmetric phases as well as the asymmetric one).

$$f_{L_d, L_d} \equiv \frac{F_{L_d, L_d}}{N_1} \quad (3.4)$$

$$f_{L_o, L_o} \equiv \frac{F_{L_o, L_o}}{N_2} \quad (3.5)$$

$$f_{L_d, L_o} \equiv \frac{\beta F_{L_d, L_o}}{N_1 + N_2} = \frac{\beta F_2}{N_1 + N_2} \quad (3.6)$$

The other intensive quantities characterizing the phases are the areas per molecule:

$$a_{L_d, L_d} \equiv \frac{A}{N_1} \quad (3.7)$$

$$a_{L_o, L_o} \equiv \frac{A}{N_2} \quad (3.8)$$

$$a_{L_d, L_o} \equiv \frac{2A'}{N_1 + N_2} \quad (3.9)$$

Note that the denominator in an area per molecule a is the total number of molecules in both leaflets of the bilayer.

We now have everything we need to write F_1 and F_2 in terms of known intensive quantities.

$$\begin{aligned} F_1 &= N_1 f_{L_d, L_d} + N_2 f_{L_o, L_o} \\ &= (A/a_{L_d, L_d}) f_{L_d, L_d} + (A/a_{L_o, L_o}) f_{L_o, L_o} \\ &= A \cdot \left(\frac{f_{L_d, L_d}}{a_{L_d, L_d}} + \frac{f_{L_o, L_o}}{a_{L_o, L_o}} \right) \end{aligned} \quad (3.10)$$

$$F_2 = (N_1 + N_2) f_{L_d, L_o} = 2A' \cdot \frac{f_{L_d, L_o}}{a_{L_d, L_o}} \quad (3.11)$$

This allows us to calculate γ :

$$\gamma = \frac{f_{L_d, L_o}}{a_{L_d, L_o}} - \frac{1}{2} \cdot \frac{A}{A'} \cdot \left(\frac{f_{L_d, L_d}}{a_{L_d, L_d}} + \frac{f_{L_o, L_o}}{a_{L_o, L_o}} \right) \quad (3.12)$$

This expression agrees with that of May [91] only when the factor A/A' is unity. May seems to assume implicitly that the areal densities of the leaflets participating in the mismatch process do not change during that process. This assumption may seem reasonable on the grounds that the areal density of a leaflet is primarily determined by intermolecular interaction within that leaflet. We will see in section 3.7 that although the ratio A/A' is very close to unity, its deviation from unity can easily throw off a numerical estimate of γ in a tensionless bilayer.

We note that $A/2A'$ can be written in terms of intensive quantities:

$$\frac{A}{2A'} = \frac{N_1 \cdot a_{L_d, L_d}}{(N_1 + N_2) \cdot a_{L_d, L_o}} = \eta \cdot \frac{a_{L_d, L_d}}{a_{L_d, L_o}}, \quad (3.13)$$

where η characterizes the difference in areal densities between the symmetric L_o - L_o and L_d - L_d phases:

$$\eta \equiv \frac{a_{L_o, L_o}}{a_{L_o, L_o} + a_{L_d, L_d}} \quad (3.14)$$

3.4 Thermodynamic Definition of Interleaflet Coupling: Grand Canonical Ensemble

In the previous section the interleaflet coupling γ was defined in terms of the free energy change per unit area during a process occurring with constant numbers of molecules of each species. It was assumed that a fluctuation away from interleaflet domain registry gives rise to an asymmetric mismatch region whose leaflets have the same compositions as the two symmetric coexisting phases. In this section we give an alternative definition of the interleaflet coupling by describing a mismatch process occurring at fixed chemical potentials. This, in turn, results in another definition of the interleaflet coupling, the grand canonical coupling γ_{gc} .

If compositionally symmetric regions of liquid-ordered and liquid-disordered phases are in coexistence, then the chemical potentials of all molecular species are necessarily the same in both phases. Thus it is reasonable to view a mismatch region at the interface of the phases as being in contact with a particle reservoir which maintains these chemical potentials. The cost per unit area of mismatch fluctuations will then be given by the

change in the appropriate thermodynamic potential between the final (asymmetric) and initial (symmetric) states. This potential is the Legendre transform of the Helmholtz free energy F with respect to particle numbers N_i . But the two-dimensional version of the thermodynamic Euler relation gives

$$F - \sum_i \mu_i N_i = U - TS - \sum_i \mu_i N_i = \alpha A, \quad (3.15)$$

where α is the surface tension. Thus the two-dimensional version of the grand potential is equal to the surface tension times the area. This is analogous to the familiar situation in three dimensions, where the grand potential is $p \cdot V$. We define the grand canonical interleaflet coupling γ_{gc} to be the difference in grand potential per unit area between the asymmetric final state (L_d - L_o) and the initial state composed of symmetric regions (L_d - L_d and L_o - L_o).

$$\gamma_{\text{gc}} \equiv \alpha_{L_d, L_o} - \frac{1}{2}(\alpha_{L_d, L_d} + \alpha_{L_o, L_o}) \quad (3.16)$$

However, we assume that the bilayer is tensionless, so that in the coexisting symmetric phases the surface tension is zero. Thus the grand canonical interleaflet coupling has the particularly simple form

$$\gamma_{\text{gc}} \equiv \alpha_{L_d, L_o} \quad (3.17)$$

We emphasize the difference between this definition of the interleaflet coupling and the one defined in the canonical ensemble in the previous section. In the grand canonical ensemble, the asymmetric mismatch state is taken to have the same chemical potentials as the two coexisting symmetric states. One manifestation of the interleaflet coupling is that the chemical potential of, for example, an inner-leaflet saturated lipid depends on the composition of the outer leaflet. Thus, in order to impose on the asymmetric bilayer the same chemical potentials occurring in the coexisting phases, we must slightly change its composition (the areal densities of each molecular species) compared to those of the symmetric phases. In section 3.7 we will show how the grand canonical interleaflet coupling can be estimated with the same computer program we use to calculate the canonical interleaflet coupling.

3.5 *The Nature and Magnitude of the Interleaflet Coupling*

We have seen that experiments on mixed model membranes indicate the existence of an interleaflet coupling between the compositional states of the two leaflets, and that this coupling has significant consequences for the phase behavior of mixed membranes. Little is known with certainty about the molecular mechanism of the interleaflet coupling or its magnitude as defined in section 3.3. In this section we discuss a number of possible mechanisms [17, 91] for the interleaflet coupling and review the previous work that has been done to estimate its magnitude.

Collins [17] defined the interleaflet coupling as an effective surface tension acting at the bilayer midplane in “mismatch” regions where one leaflet is liquid-ordered and the other is liquid-disordered. He also gave [17] the following interesting heuristic estimate of its magnitude. We make two assumptions: First, that whatever the mechanism of the interleaflet coupling may be, it is driven by the same interactions responsible for phase separation between liquid-ordered and -disordered phases. Second, we assume that the line tension τ between these phases is the result of this same surface tension acting over an area given by the thickness of the hydrophobic region times the length of the interface between the phases. These assumptions relate the interleaflet coupling energy per unit area, which we call γ , to the line tension τ at a liquid-liquid interface, which has been measured [139, 59], and to the hydrophobic thickness h of the bilayer:

$$\gamma \approx \frac{\tau}{h} \tag{3.18}$$

Using $\tau = 5$ pN and $h = 2.5$ nm, Collins obtained [17] the estimate $\gamma \approx 0.5 k_B T/\text{nm}^2$.

The possible mechanisms of the interleaflet coupling were recently reviewed by May [91]. In one scenario, domain registry in phase-separated symmetric bilayers is caused by the rapid interleaflet translocation or “flip-flop” of cholesterol. Whereas the time scale of phospholipid flip-flop is quite slow, often of minutes or hours [127], cholesterol flip-flops quite rapidly, probably on millisecond time scales [53, 15]. It therefore seems possible that during a mismatch fluctuation, the cholesterol-rich liquid-ordered phase signals its presence to the opposite leaflet via cholesterol flip-flop. A closely related mechanism is considered by May

[91], in which the flip-flop rate of a cholesterol molecule residing in the liquid-disordered phase depends greatly on the the phase of the opposite leaflet, leading to a decrease in entropy if the molecule is prevented from flip-flopping by an apposing liquid-ordered leaflet. However, as pointed out by Collins [17], the rapid equilibration of cholesterol’s chemical potential cannot carry any information across the bilayer; by definition, both coexisting phases have the same chemical potential for cholesterol. In the absence of any other form of interleaflet coupling, there is no reason for a cholesterol molecule in one leaflet to “want” to be in the other. Put in other terms, both leaflets can be considered to be in equilibrium with a single particle bath which determines their chemical potentials. This equilibrium does not couple them any more than does their being in equilibrium with the same thermal reservoir.

May and collaborators [4, 154, 91] have determined the electrostatic contribution to the interleaflet coupling by calculating the electrostatic free energy of an asymmetrically charged lipid bilayer in an aqueous salt solution. However, they find that the resulting coupling is not only much smaller than the order of magnitude expected from coarse-grained MD simulation [123], but is also negative, favoring mismatch regions where leaflets are in different phases. The negative sign of the electrostatic contribution to the coupling is intuitively clear. If one of the constituents of a mixture is charged, or if two are oppositely charged, this causes a repulsion between like molecules, whether within a leaflet or between different leaflets. Finally, it is clear that electric charges can not be of primary importance in the interleaflet coupling, which is observed in mixtures of neutral lipids. We will examine more closely the effect of charges on miscibility in Chapter 4.

Another possible interleaflet coupling mechanism considered by May [91] is bilayer interdigitation, that is, the existence of a region near the bilayer midplane where the densities of molecules from the two leaflets overlap. There are several different contributions that could be thought of as resulting from interdigitation, including changes in the internal energies and entropies of molecules as well as direct intermolecular interactions of the kind considered in the model of Elliott et al. [36]. May argues that the lipids in the L_d leaflet lose internal (configurational) entropy when the opposite leaflet is in the L_o phase, since they cannot easily cross the bilayer midplane into the densely-packed L_o leaflet. In contrast, the

L_d phase is more loosely packed, and more easily accommodates interdigitation. He makes a rough estimate of the resulting interleaflet coupling using calculations by Szleifer et al. [136], by comparing the free energy of a lipid in a monolayer to that of a lipid in a bilayer, whose configurations are limited by the apposed leaflet. The result is $\gamma \approx 0.3 k_B T / \text{nm}^2$, which is of the same order of magnitude as Collins' heuristic estimate [17], as well as the value extracted from coarse-grained MD simulations by Risselada and Marrink [123], as discussed in the next section.

A number of other possible mechanisms for interleaflet coupling have not received close attention in the context of liquid-liquid phase separation. An estimate of the curvature-mediated coupling [80, 138, 86] mentioned in Section 3.2 awaits a detailed molecular calculation of the composition-dependence of the spontaneous curvature of asymmetric bilayers containing cholesterol. Van der Waals interactions, which undoubtedly play an important role in the gel-liquid transitions [100], may also be relevant in liquid-liquid phase separation and could contribute to the interleaflet coupling. Finally we mention one interaction that is sometimes assumed to contribute to the interleaflet coupling, and furthermore to cause a negative coupling: the elastic energy of deformation which occurs at the boundary between the liquid-ordered and -disordered phases. It is clear that the abrupt change in bilayer thickness at the boundary between symmetric L_o - L_o and L_d - L_d phases comes at an energetic cost, both due to elastic deformation and to contact between hydrophobic lipid tails and water. Considering only the energy of this interface, it seems that this energy cost would be minimized if instead the bilayer were asymmetric: an L_d - L_o bilayer would then coexist with an L_o - L_d bilayer of equal thickness. It is important to recognize, firstly, that this situation does not occur in experiment, and secondly, that this argument does not describe a contribution to the interleaflet coupling (which is an energy per unit area), but rather a contribution to the line tension. The elastic contribution to the line tension was calculated by Kuzmin et al. [73], who erroneously claim that all other contributions to the line tension are negligible; were this the case, the system would do better to avoid phase-separating in the first place.

3.6 Fluctuations of Phase Boundaries in Coupled Leaflets

The absence of optically visible mismatch fluctuations in liquid-liquid phase-separated vesicles [17] seems to indicate that the interleaflet coupling is in some sense “large.” Because the interleaflet coupling γ is a free energy penalty per unit area, it is natural to assume that the magnitude of γ should tell us directly the characteristic area of mismatch fluctuations. Thus, Risselada and Marrink extracted from their coarse-grained simulation [123] an estimate of $\gamma \approx 0.15 k_B T / \text{nm}^2$, and argued from $\gamma \cdot 20 \text{ nm}^2 \approx 3 k_B T$ that mismatch fluctuations larger than roughly 20 nm^2 should be suppressed, explaining the experimental absence of visible mismatch fluctuations. In this section we describe the fluctuations of phase boundaries of two coupled leaflets, showing that mismatch of domains is characterized by a characteristic length rather than a characteristic area. This length turns out to depend only weakly on the coupling energy γ , which implies that the characteristic thickness of mismatch regions will be below optical resolution even when γ is greatly reduced.

We consider a fluid lipid bilayer that has phase-separated into macroscopic regions of the liquid-ordered and -disordered phases; this situation is shown in figure 3.6, as viewed from above. Since the bilayer has two leaflets, there are two boundaries. As these boundaries fluctuate, their deviations from the x axis are parameterized by $z_1(x)$ and $z_2(x)$. Our goal is to characterize the fluctuations of the phase boundary, whose average position is taken to lie along the x axis. We assume that these functions are single-valued, meaning that the interfaces don’t curve back on themselves. A microstate of this system is given by functions $z_1(x)$ and $z_2(x)$, defined on a finite interval $[0, L]$. The Hamiltonian includes two types of energy contribution. First, there is a line tension τ acting within each leaflet. It is the energy per unit arc-length of interface between the phases, and gives rise to the following terms of the Hamiltonian

$$H_{\text{line}} [z_1, z_2] = \tau \int_0^L \left[\sqrt{1 + (dz_1/dx)^2} + \sqrt{1 + (dz_2/dx)^2} \right] dx \quad (3.19)$$

We now assume that the fluctuations are small enough to justify the linearization $\sqrt{1 + (dz/dx)^2} \approx 1 + (1/2) \cdot (dz/dx)^2$. The contribution of the line tension to the Hamiltonian becomes, ig-

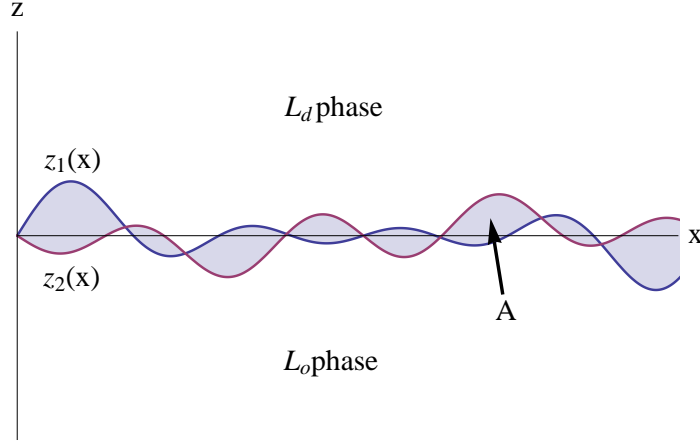


Figure 3.6: Fluctuating phase boundaries in a bilayer with coupled leaflets, seen from above. The mismatch area is A .

noring an additive constant,

$$H_{\text{line}}[z_1, z_2] = \frac{\tau}{2} \cdot \int_0^L \left[\left(\frac{dz_1}{dx} \right)^2 + \left(\frac{dz_2}{dx} \right)^2 \right] dx \quad (3.20)$$

The interleaflet coupling γ gives rise to another contribution to the Hamiltonian, proportional to the area A enclosed between the curves $z_1(x)$ and $z_2(x)$. That area is shaded and labeled in figure 3.6. The contribution of this interaction to the Hamiltonian is

$$H_{\text{area}}[z_1, z_2] = \gamma \cdot A = \gamma \cdot \int_0^L |z_1(x) - z_2(x)| dx \quad (3.21)$$

Note that the area A is the integral of the *absolute value* of the difference between z_1 and z_2 . The total Hamiltonian functional which we will work with is

$$H[z_1, z_2] = \int_0^L \left[\frac{\tau}{2} \cdot \left(\frac{dz_1}{dx} \right)^2 + \frac{\tau}{2} \cdot \left(\frac{dz_2}{dx} \right)^2 + \gamma \cdot |z_1(x) - z_2(x)| \right] dx \quad (3.22)$$

Ultimately, we would like to calculate statistical properties of the system interacting with this Hamiltonian. This will be possible if we can calculate the following partition function.

$$Z(\tau, \gamma) = \int \mathcal{D}z_1 \mathcal{D}z_2 \exp(-\beta H[z_1, z_2]) \quad (3.23)$$

Without the last term in equation (3.22), this path integral would be Gaussian and would lead to equations [38] similar to those used by Honerkamp-Smith et al. [59] to analyze

Classical quantity	Quantum quantity
Spatial coordinate x	Time coordinate t
Line tension τ	Mass m
Microstate $z_1(x), z_2(x)$	Paths of two particles $z_1(t), z_2(t)$
Energy of a microstate in units of $k_B T$	Action of a path in units of \hbar
Partition function	Propagator
Free energy density in limit $L \rightarrow \infty$	Ground state energy

Table 3.1: Statistical mechanics/quantum mechanics correspondence

domain boundary fluctuations and thus to extract the line tension of liquid-liquid domain boundaries.

If the space coordinate x is relabeled as time t , then equation (3.23) becomes the imaginary-time path integral of two quantum particles in one dimension with positions z_1 and z_2 interacting with each other via a potential $\gamma|z_1 - z_2|$. Such a correspondence between a two-dimensional statistical mechanics problem and a one-dimensional quantum mechanics problem is quite general and of frequent use in polymer physics [51] as well as in other problems involving domain boundaries in two-dimensional systems [25]. In our situation the correspondence is summarized in Table 3.6. We are interested in the separation between the two interfaces, so in the quantum mechanical problem we will work in the center of mass frame. The time-independent Schrödinger equation for the separation z between the particles is

$$-\frac{\hbar^2}{2\mu} \cdot \frac{\partial^2}{\partial z^2} \psi(z) + \gamma|z| = E\psi(z), \quad (3.24)$$

where $\mu = m/2$ is the reduced mass. Note that the γ in the Schrödinger equation and the γ in the classical problem have different units because of the correspondence between the distance x in the classical problem and the time t in the quantum problem. This equation can be solved analytically in terms of Airy functions [113]. The characteristic spatial extent

of the wavefunction is

$$l_{\text{quant}} = \left[\frac{\hbar^2}{2\mu\gamma} \right]^{1/3} \quad (3.25)$$

In the classical statistical mechanics problem this corresponds to the following characteristic distance between the fluctuating interfaces:

$$l = \left[\frac{(k_B T)^2}{\tau\gamma} \right]^{1/3} \quad (3.26)$$

The average separation between the interfaces increases with temperature and decreases with γ and τ . If we take values of $\gamma = 0.1 k_B T \cdot \text{nm}^{-2}$ and $\tau = 1 pN$, we get $l \approx 3.5 \text{ nm}$. The fact that the domain interfaces in the two leaflets stay within roughly a distance l of each other is the reason why mismatch fluctuations are never observed in fluorescence microscopy. Furthermore, changing the value of the coupling energy γ hardly affects this result; if γ is reduced by a factor of ten, the characteristic separation l between the interfaces increases by roughly a factor of two, and the mismatch region remains invisible to the optical microscope.

The ground state energy of the quantum system is [113]

$$E_{\text{quant}} \approx \left[\frac{3\pi}{8} \right]^{2/3} \cdot \left[\frac{\hbar^2 \gamma^2}{2\mu} \right]^{1/3} \quad (3.27)$$

The equation above immediately gives us the free energy per unit length of the classical system:

$$\lim_{L \rightarrow \infty} \frac{F}{L} \approx \left[\frac{3\pi}{8} \right]^{2/3} \cdot \left[\frac{(k_B T)^2 \gamma^2}{\tau} \right]^{1/3} \quad (3.28)$$

With this free energy, we can calculate the average overlap area by taking the derivative of F with respect to γ :

$$\begin{aligned} \langle A \rangle &= \frac{\int \mathcal{D}z_1 \mathcal{D}z_2 \left[\int_0^L |z_1(x) - z_2(x)| dx \right] \exp(-\beta H[z_1, z_2])}{\int \mathcal{D}z_1 \mathcal{D}z_2 \exp(-\beta H[z_1, z_2])} \\ &= -k_B T \frac{\partial}{\partial \gamma} \ln Z = \frac{\partial F}{\partial \gamma} \end{aligned} \quad (3.29)$$

Therefore the average mismatch area per unit interface length is

$$\frac{\langle A \rangle}{L} = \frac{2}{3} \cdot \left[\frac{3\pi}{8} \right]^{2/3} \cdot \left[\frac{(k_B T)^2}{\gamma\tau} \right]^{1/3}, \quad (3.30)$$

or in other words

$$\langle A \rangle = 0.74 \cdot l \cdot L. \quad (3.31)$$

The mismatch area is therefore extensive, being proportional to L , the “projected length” of the interface along the x direction. This result invalidates the method by which Risselada and Marrink [123] extracted a value of γ from a coarse-grained MD simulation. They simulated a phase-separated system with projected interface length $L \approx 40$ nm, and generated a histogram representing the probability distribution of values of the total mismatch area A . Their results are shown in Figure 3.7, where the probability of obtaining a mismatch area A is plotted logarithmically. Risselada and Marrink estimated γ by fitting $-\beta \ln P(A)$ to a straight line in the regime of large mismatch area A . That is, they assumed that the temperature and γ alone determine the probability distribution of mismatch areas via $P(A) \approx \exp(-\beta\gamma A)$. However, this neglects the fact that the mismatch area is an extensive quantity. If, hypothetically, Risselada and Marrink had run a simulation at extremely large interface length L , they would have obtained extremely large areas A and would thus have extracted a much smaller value of γ .

In order to determine the correct method of estimating γ from simulation data such as those of Risselada and Marrink, we must derive not only the average mismatch area $\langle A \rangle$ but also the full probability distribution of areas $P(A)$. Formally this can be written in terms of the path integral.

$$P(a) = \frac{\int \mathcal{D}z_1 \mathcal{D}z_2 \delta(A[z_1, z_2] - a) \exp(-\beta H[z_1, z_2])}{\int \mathcal{D}z_1 \mathcal{D}z_2 \exp(-\beta H[z_1, z_2])} \quad (3.32)$$

Now the delta function can be written as

$$\delta(A - a) = \frac{1}{2\pi} \cdot \int_{-\infty}^{\infty} \exp[-i\beta\tilde{\gamma}(A - a)] d\beta\tilde{\gamma}, \quad (3.33)$$

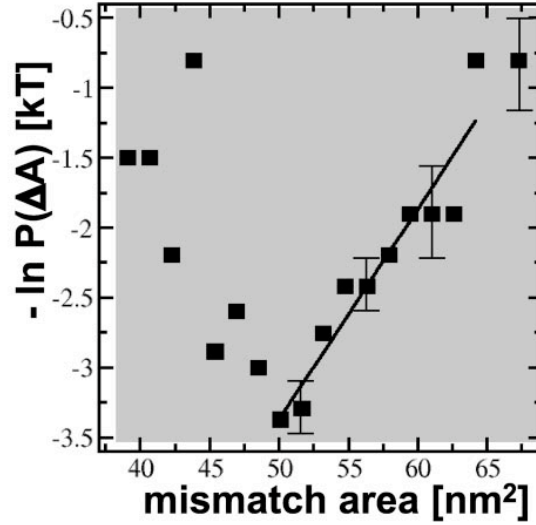


Figure 3.7: Histogram giving the probability distribution of mismatch areas A , from Risselada et al. [123].

with the result

$$\begin{aligned}
P(a) &= \frac{1}{2\pi} \cdot \frac{\int_{-\infty}^{\infty} d\beta\tilde{\gamma} \exp(i\beta\tilde{\gamma}a) \int \mathcal{D}z_1 \mathcal{D}z_2 \exp(-i\beta\tilde{\gamma}A[z_1, z_2]) \exp(-\beta H[z_1, z_2])}{\int \mathcal{D}z_1 \mathcal{D}z_2 \exp(-\beta H[z_1, z_2])} \\
&= \frac{1}{2\pi} \cdot \int_{-\infty}^{\infty} d\beta\tilde{\gamma} \exp(i\beta\tilde{\gamma}a) \frac{Z(\tau, \gamma + i\tilde{\gamma})}{Z(\tau, \gamma)} \\
&= \frac{1}{2\pi} \cdot Z(\tau, \gamma)^{-1} \cdot \int_{-\infty}^{\infty} d\beta\tilde{\gamma} \exp(i\beta\tilde{\gamma}a) \exp[-\beta F(\tau, \gamma + i\tilde{\gamma})] \\
&= \frac{1}{2\pi} \cdot Z(\tau, \gamma)^{-1} \cdot \int_{-\infty}^{\infty} d\beta\tilde{\gamma} \exp(i\beta\tilde{\gamma}a) \exp \left[-\beta L \cdot \left[\frac{3\pi}{8} \right]^{2/3} \cdot \left[\frac{(k_B T)^2 (\gamma + i\tilde{\gamma})^2}{\tau} \right]^{1/3} \right]
\end{aligned}$$

From the fact that the argument of the exponential is dimensionless, we see that there is a characteristic value γ_0 of γ :

$$\gamma_0 = \frac{8}{3\pi} \cdot \left[\frac{k_B T \cdot \tau}{L^3} \right]^{1/2}. \quad (3.34)$$

The integral can be made dimensionless in terms of the quantities

$$g \equiv \frac{\gamma}{\gamma_0}$$

$$\tilde{g} \equiv \frac{\tilde{\gamma}}{\gamma_0}$$

$$\tilde{a} \equiv \beta\gamma_0 a$$

$$P(a) = \frac{1}{2\pi} \cdot Z(\tau, \gamma)^{-1} \beta\gamma_0 \int_{-\infty}^{\infty} d\tilde{g} \exp \left[i\tilde{g}\tilde{a} - (g + i\tilde{g})^{2/3} \right] \quad (3.35)$$

$$= \frac{1}{2\pi} \beta\gamma_0 \exp(\tilde{g}^{2/3}) \int_{-\infty}^{\infty} d\tilde{g} \exp \left[i\tilde{g}\tilde{a} - (g + i\tilde{g})^{2/3} \right] \quad (3.36)$$

This integral can be calculated numerically. Figure 3.8 shows, for several values of the scaled coupling energy g , a plot of the probability distribution of the scaled area \tilde{a} , defined by:

$$\tilde{P}(\tilde{a}) = k_B T \gamma_0^{-1} P(k_B T \gamma_0^{-1} \tilde{a}) \quad (3.37)$$

Interestingly, there is an interval of small values of the mismatch area where the probability

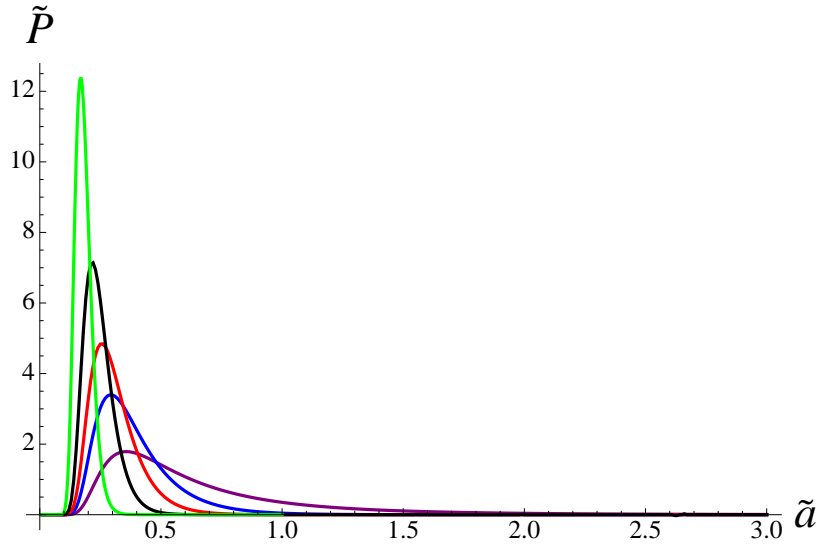


Figure 3.8: Probability distribution of scaled mismatch area \tilde{a} , calculated numerically with the following values of the scaled coupling energy g , which can be read from right to left in the figure as: 1 (purple), 5 (blue), 10 (red), 20 (black), and 50 (green).

is almost identically zero. This effect is of entropic origin, since there are very few configurations with small mismatch areas. It is not the same effect as the short-range entropic

repulsion between the interfaces which Risselada and Marrink [123] inferred from their observation that the interfaces tended to stay a fixed distance (roughly 2 nm) apart, since such an effect is not present in our model. It is possible that this 2 nm “preferred” separation between the interfaces is instead due to a minimization of stretching energy; the change in bilayer thickness between the liquid-ordered and -disordered phases is spread out over this distance to avoid a large elastic contribution to the line tension [73] between the phases.

From the probability distribution given by equation (3.37) we may make a comparison with the data of Risselada and Marrink [123]. For this purpose we must first determine a value of the characteristic scale γ_0 . The simulation of Risselada and Marrink was done at $T = 295 K$ and $L = 40 \text{ nm}$. They also measured different line tensions $\tau = 2.5 \text{ pN}$ and $\tau = 4.5 \text{ pN}$ in the interfaces belonging to the two leaflets. This distinction is possible because of the observed constant 2 nm offset between the interfaces in the leaflets, due to which one interface was always across from a liquid-disordered leaflet, while the other interface was always across from a liquid-ordered leaflet. Taking $\tau = 3 \text{ pN}$, which is roughly the average of the two line tensions of Risselada and Marrink, we have $\gamma_0 = 0.003 k_B T / \text{nm}^2$. With this scale, we plot in Figure 3.9 the probability distribution of mismatch areas predicted by our model. Also shown in the figure is a normalized approximate fit to the data of Risselada and Marrink, given by

$$P(A) \approx 0.075 \cdot \exp \left[-(0.15 k_B T \cdot \text{nm}^{-2}) \cdot |A - 50 \text{ nm}^2| / k_B T \right], \quad (3.38)$$

The green curve with $g = 50$ has approximately the same slope as the empirical fit in the regime of large mismatch areas, and we may use it to estimate $\gamma \approx g \cdot \gamma_0 = 0.15 k_B T / \text{nm}^2$. Choosing $g = 70$ (shown in red), so as to more closely match the average mismatch area, leads to $\gamma \approx 0.2 k_B T / \text{nm}^2$. Thus, although we have shown that the means by which Risselada and Marrink estimated γ was incorrect, it seems that they fortuitously obtained a value which we cannot dispute. Furthermore, this value is of the same order of magnitude as the heuristic estimate made by Collins [17].

We note that other interesting quantities can be calculated using the correspondence summarized in Table 3.6. For example, one may ask what is the correlation length of the fluctuating interfaces along the x direction (see Figure 3.6). That is, if the interfaces were

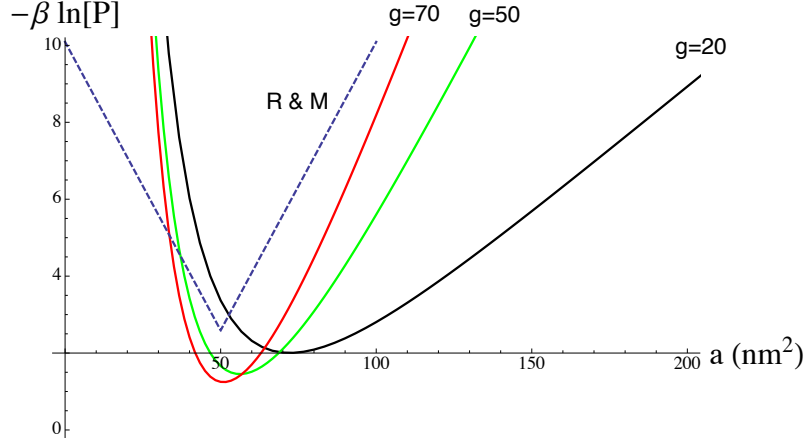


Figure 3.9: Logarithm of probability distribution of mismatch areas scaled by $k_B T$, as predicted by equation (3.37). Values of the scaled coupling energy g are: 20 (black), 50 (green), and 70 (red). Also shown is a suitably normalized approximate fit, given by equation (3.38), to the data of Risselada and Marrink [123].

somehow fixed at one end, how long would they need to be in order to recover the equilibrium probability distribution of separations $|z_1(x) - z_2(x)|$, characterized by the ground state of the quantum problem? Equivalently, how long does an interface need to be in order to be considered a “bulk” interface described by the results just derived in the limit $L \rightarrow \infty$? This correlation length corresponds roughly to the lifetime of the first excited state of the quantum mechanics problem,

$$\Delta t \approx \frac{\hbar}{\Delta E}, \quad (3.39)$$

where ΔE is the difference in energy between the first excited state and the ground state (see [113]):

$$\begin{aligned} \Delta E &\approx \left[\left(\frac{9\pi}{8} \right)^{2/3} - \left(\frac{3\pi}{8} \right)^{2/3} \right] \cdot \left[\frac{\hbar^2 \gamma^2}{2\mu} \right]^{1/3}, \\ \Delta t &\approx 0.83 \cdot \left[\frac{2\mu \hbar}{\gamma^2} \right]^{1/3} \end{aligned} \quad (3.40)$$

The corresponding classical quantity is the correlation length

$$\xi = 0.83 \cdot \left[\frac{k_B T \cdot \tau}{\gamma^2} \right]^{1/3} \quad (3.41)$$

Note that this length scale is *a priori* different from the typical distance between the interfaces, given by equation (3.26). If we take reasonable values of $\gamma = 0.1 k_B T \cdot \text{nm}^{-2}$ and $\tau = 1 pN$, we get $\xi \approx 3 \text{ nm}$.

3.7 Microscopic Calculation of Interleaflet Coupling

We have performed calculations of the interleaflet coupling γ , as defined in the canonical ensemble in Section 3.3, using the model of Elliott et al. [36] described in Section 2.3. For this purpose we modified a computer program developed by Szleifer and collaborators [141] that implements this model. The modifications allow the program to calculate the Helmholtz free energy of compositionally asymmetric bilayers, as required for the computation of γ .

Figure 3.10 shows the phase diagram calculated by Uline et al. [141] for a ternary mixture of saturated lipids, unsaturated lipids and cholesterol at a temperature of 290 K. More specifically, the saturated lipids have two chains of 16 carbons each (C16:0) as in DPPC and the unsaturated lipids have two chains, each of 18 carbons and with a double bond near the middle of the chain (C18:1) as in DOPC. This phase diagram shows the main features of the phase behavior of ternary mixtures such as the DOPC/DPPC/cholesterol mixture, including a gel phase at compositions near the pure saturated one, as well as coexisting liquid-ordered and liquid-disordered phases. Note that the region of liquid-liquid coexistence in the model of Elliott et al. extends all the way to the binary mixture of unsaturated lipids and cholesterol. This is in qualitative agreement with the phase diagram reported for the DOPC/DPPC/cholesterol mixture by Davis et al. [20] as well as that given by de Almeida et al. [21] for a similar mixture where the saturated lipid is palmitoyl sphingomyelin (PSM). However, it disagrees with the phase diagram published for the DOPC/DPPC/cholesterol by Veatch et al. [147] in which the region of liquid-liquid coexistence ends in a critical point rather than extending toward the edge of the phase diagram representing the binary unsaturated lipid/cholesterol mixture. The origin of the discrepancy between the phase diagram of Veatch et al. and that of de Almeida et al. for the same mixture is the same as was discussed in section 1.2 in the context of the binary mixture of DPPC and cholesterol, namely that de Almeida et al. [21] consider evidence of nanoscopic inhomogeneities as indicative of phase coexistence, whereas Veatch et al. [147] do not. We

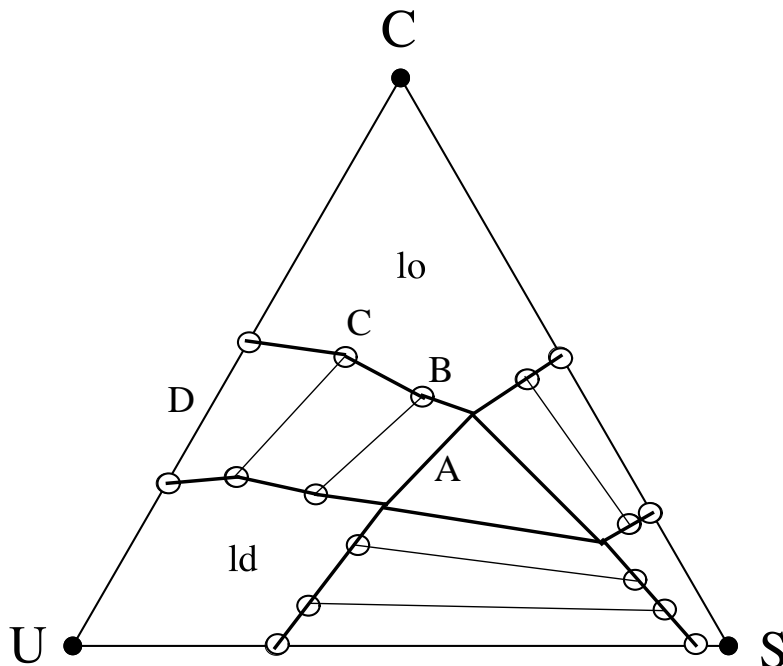


Figure 3.10: Ternary phase diagram calculated by Uline et al. [141] from the model of Elliott et al. [36]. The temperature is 290 K.

argued in section 1.2 in favor of a more conservative definition of phase coexistence as a purely macroscopic phenomenon. Thus it seems that the phase diagram shown in Figure 3.10, which was calculated on the basis of this definition, does not completely reflect the phase behavior of the DOPC/DPPC/cholesterol mixture. However, we believe that the model of Elliott et al. nevertheless describes the essential interactions of this mixture well, as indicated by the fact that it reproduces three phases with properties close to [34, 36] those of the experimentally observed gel, liquid-disordered, and liquid-ordered phases.

We have used the model of Elliott et al. to calculate the interleaflet coupling γ using the following definition derived in the canonical ensemble in Section 3.3:

$$\gamma = \frac{f_{L_d, L_o}}{a_{L_d, L_o}} - \frac{1}{2} \cdot \frac{A}{A'} \cdot \left(\frac{f_{L_d, L_d}}{a_{L_d, L_d}} + \frac{f_{L_o, L_o}}{a_{L_o, L_o}} \right) \quad (3.42)$$

The subscripts of quantities such as free energies per molecule (f) and areas per molecule (a) indicate the compositions of both leaflets (inner, outer). The ratio of areas $A/2A'$ can

be expressed in terms of intensive quantities as follows

$$\frac{A}{2A'} = \eta \cdot \frac{a_{L_d, L_d}}{a_{L_d, L_o}}, \quad (3.43)$$

where η is, for a given area of the bilayer, the fraction of its molecules residing in the inner leaflet. Equation (3.42) allows us to calculate the interleaflet coupling γ by determining the free energies and areas per molecule of the symmetric coexisting phases (L_d - L_d and L_o - L_o) as well as the asymmetric composition resulting from a mismatch of phases between the two leaflets (L_d - L_o). We calculated these quantities using the modified computer program of Uline et al. [141]; the resulting values of γ are shown in Table 3.2. The tie-lines of liquid-liquid coexistence used to determine the mole fractions of the symmetric and asymmetric bilayers are labeled A, B, C, and D in Figure 3.10. The calculated interleaflet couplings are of order $0.01 - 0.03 k_B T / \text{nm}^2$ and decrease with increasing concentration of cholesterol. These values are roughly a factor of ten smaller than the value estimated by Risselada and Marrink [123] on the basis of coarse-grained MD simulations, as well as the heuristic estimate of Collins [17]. Although this discrepancy may indicate that the essential mechanism of the interleaflet coupling is missing from the model of Elliott et al., it is by no means obvious that this is the case. The estimate of Collins (see section 3.5) involves a number of strong assumptions about the nature of the interleaflet coupling as well as the line tension between the coexisting phases, and it is likely that the value obtained by Risselada and Marrink is subject to large errors due to the small free energy differences involved. As of yet, no experimental observation has placed limits on the magnitude of γ which might distinguish between our values of γ and those of Risselada and Marrink. As shown in section 3.6, the characteristic width of the fluctuating mismatch region depends only weakly on γ , so a value as small as $0.01 k_B T / \text{nm}^2$ still would not lead to fluctuations visible to the optical microscope.

3.8 Calculation of Grand Canonical Interleaflet Coupling

Because our calculated values of the canonical interleaflet coupling γ are a factor of ten smaller than previous estimates, we have also estimated the grand canonical interleaflet

Tie-line	γ ($k_B T/\text{nm}^2$)
A	0.032
B	0.025
C	0.016
D	0.013

Table 3.2: Calculated values of the canonical interleaflet coupling γ , for four tie-lines labeled in Figure 3.10.

coupling γ_{gc} defined in section 3.4 as an independent estimate of the magnitude of the interleaflet coupling. As explained in section 3.4, the grand canonical interleaflet coupling is equal to the surface tension α (or equivalently, the grand potential per unit area) of the asymmetric bilayer whose leaflets have compositions close to those of the symmetric liquid-ordered and -disordered phases, subject to the constraint that the chemical potentials of all molecular species are equal to those in the coexisting symmetric phases. The computer program of Uline et al. [141] calculates Helmholtz free energies of bilayers of specified composition, rather than at specified chemical potentials. The grand canonical interleaflet coupling can nevertheless be calculated starting from a bilayer whose state is close to that of the desired one. Specifically, we consider an asymmetric bilayer (which we call our “guess”) whose leaflets have exactly the compositions of the two coexisting symmetric phases. Because of the interleaflet coupling, the chemical potentials of molecules in this bilayer are shifted by a small amount $\delta\mu_i$ compared to those occurring in coexistence:

$$\delta\mu_i \equiv \mu_{i,\text{guess}} - \mu_{i,\text{coex}} \quad (3.44)$$

The grand canonical interleaflet coupling can now be estimated as follows:

$$\begin{aligned} \gamma_{\text{gc}} &\equiv \alpha(\mu_{i,\text{coex}}) \approx \alpha(\mu_{i,\text{guess}}) - \sum_i \left(\frac{\partial \alpha}{\partial \mu_i} \right) \cdot \delta\mu_i \\ &= \alpha(\mu_{i,\text{guess}}) + \sum_i \rho_i \cdot \delta\mu_i \end{aligned} \quad (3.45)$$

Here ρ_i is the areal density of component i and we have used $\partial\alpha/\partial\mu_i = -\rho_i$, which can be seen from the fact that the grand potential is the Legendre transform of the Helmholtz free energy with respect to particle numbers. Equation (3.45) allows us to estimate γ_{gc} starting from an asymmetric membrane with compositions given by the coexisting phases (our “initial guess”). The chemical potential shifts $\delta\mu_i$ are calculated numerically by evaluating the free energy at different mole fractions; equations relating derivatives of the Helmholtz free energy to chemical potentials are given in Appendix A. The areal densities ρ_i as well as the surface tension of the “initial guess” state can be calculated from the dependence of the Helmholtz free energy on molecular area a .

We have performed the calculation of γ_{gc} described above at $T = 290$ K for a tie-line with compositions close to those of the tie-line labeled A in Figure 3.10, namely $s = 0.21$ and $c = 0.27$ in the L_d phase and $s = 0.3$ and $c = 0.48$ in the L_o phase. We obtained the result $\gamma_{\text{gc}} = 0.013 k_B T/\text{nm}^2$, which is of the same order of magnitude as our calculated values of the canonical interleaflet coupling γ . This confirms that the model of Elliott et al. [36] predicts an interleaflet coupling with order of magnitude $0.01 k_B T/\text{nm}^2$ rather than $\approx 0.1 k_B T/\text{nm}^2$ as obtained by Risselada and Marrink [123].

Chapter 4

**ELECTROSTATIC EFFECTS AND THE INNER LEAFLET OF THE
PLASMA MEMBRANE**

4.1 Phase Behavior of Charged Mixtures

Motivated both by the biological fact that the inner leaflet of the plasma membrane contains significant quantities of lipids with charged head groups [142, 70] and by experiments performed on model lipid bilayers including charged lipids [150], we discuss in this section the influence of electric charges on the miscibility phase behavior of mixtures, both with and without screening induced by salt in the aqueous solvent. It is intuitively clear that the electrostatic energy due to the presence of electric charges or dipoles favors mixing rather than phase separation. In a mixture of molecules of opposite charge, for example, macroscopic phase separation is equivalent to large-scale separation of charge, which costs a great deal of energy. In the absence of any screening mechanism, this energy cost precludes the possibility of macroscopic phase separation. This can be seen by calculating the electrostatic energy of a two-dimensional binary mixture of oppositely charged molecules. For the sake of simplicity we suppose that the mixture is incompressible and that two constituents are completely immiscible, forming regions of areal charge density σ_0 and $-\sigma_0$. If the characteristic size of these regions is L , then by dimensional considerations the electrostatic contribution to the areal energy density must be of order

$$\frac{F_{\text{el}}}{L^2} \propto \frac{\sigma_0^2 \cdot L}{\epsilon_0} \quad (4.1)$$

An important consequence is that in the absence of screening the electrostatic free energy is not extensive, since its density diverges as $L \rightarrow \infty$. This result implies that macroscopic phase separation is impossible. Instead, the mixture develops domains of a finite size determined by the competition between short-range intermolecular interactions favoring immiscibility and electrostatic interactions favoring mixing. If the two components of the mixture are highly immiscible, they will make contact only along well-defined linear

boundaries, and we can model the contribution of short-range molecular interactions using a “line tension” τ . The length of interface contained in an area L^2 is proportional to L regardless of the morphology of the domains, so the short-range interactions make a contribution of order τ/L to the free energy density. Balancing this free energy density against the electrostatic contribution of equation (4.1), we obtain the characteristic size of domains in the absence of screening [135, 102]:

$$L_0 = \frac{\sqrt{\tau\epsilon}}{\sigma_0} \quad (4.2)$$

Finite domains also occur in mixtures of molecules with opposite dipole moments rather than electric charges [3]. A common theme in physics is that the competition between short-range attractions and long-range repulsions leads to structures of a finite characteristic size [148]. This competition leads, for example, to finite domains in ferromagnets [48] and in monolayers of polar lipids [92], and to structured phases of two-dimensional electron systems [66].

In the cellular cytoplasm electrostatic interactions are not long-range but rather are heavily screened by high concentrations of salt ions, which introduce a new length scale into the problem: the Debye screening length κ^{-1} which characterizes the exponential decay of the electrostatic potential. In the case of the cellular cytoplasm, concentrations of salt ions are relatively high and $\kappa^{-1} \approx 1$ nm. A finite screening length occurs even in pure water due to the presence of hydrogen and hydroxide ions. However, electrostatic interactions still prevent macroscopic phase separation as long as the salt concentration is small enough so that the length scale L_0 defined in equation (4.2) is much smaller than the Debye screening length. Interestingly, the transition from finite domains of characteristic size L_0 to macroscopic phase separation is of first order. As shown by Solis et al. [135], the characteristic domain size jumps from a finite value of order L_0 to infinity when the Debye screening length reaches a threshold of order L_0 .

In this discussion we have only dealt with the regime of strong segregation, that is, the case where the intermolecular interactions favoring phase separation are so strong that the constituents of the mixture segregate completely, whether into finite or macroscopic regions. Electrostatic interactions have similar effects in the opposite limit [3], when the

compositional order parameter only varies slightly between different regions, as is the case near a miscibility critical point.

4.2 *Electrostatic Effect on Phase Behavior in Model Membranes*

In the previous section we discussed the influence of electrostatic interactions on the phase behavior of mixtures involving charged molecules. These interactions may also influence the gel-liquid phase transition of a bilayer composed of a single lipid component, due to the fact that the gel and liquid phases have different thicknesses and areal densities. The influence of the electrostatic free energy on the gel-liquid phase temperature has been calculated by Jähnig [65] and observed experimentally by Träuble et al. [140]; see also [58]. Because the liquid-ordered and liquid-disordered phases also differ in thickness and areal density, the influence of electrostatic interactions via this mechanism should also be seen in the phase diagram of lipid mixtures in which one of the components is charged. In order to estimate this influence, we use a simplified version of the phenomenological model [117] of ternary model membranes discussed in Section 2.1. This simplified model is set out in Appendix D. It describes a mixture of unsaturated lipids and cholesterol as well as saturated lipids which can exist in one of two configurational states, the ordered state (with mole fraction s_o) and the disordered state (with mole fraction s_d). The physical assumptions of the model are as described in Section 2.1: there is a repulsion between unsaturated lipids and saturated lipids, which is greater for ordered saturated lipids than for disordered ones. Also as in the previous model, cholesterol tends to order the saturated lipids via an attractive interaction with ordered saturated lipids. Like the model described in Section 2.1, this model yields a phase diagram with a closed-loop miscibility gap shown in black in Figure 4.1.

We now consider the effect on this phase diagram of electrostatic interactions. If some of the lipids are charged, leading to an areal charge density σ on each of the surfaces of the bilayer, there is an electrostatic contribution to the free energy per molecule that can be calculated easily from the linearized Poisson-Boltzmann equation:

$$\frac{F_{el}}{k_B T N} = \frac{3}{4} \cdot \frac{\sigma^2 a}{k_B T \epsilon_W \kappa}, \quad (4.3)$$

where a is the area per molecule, which is the total area divided by the total number of

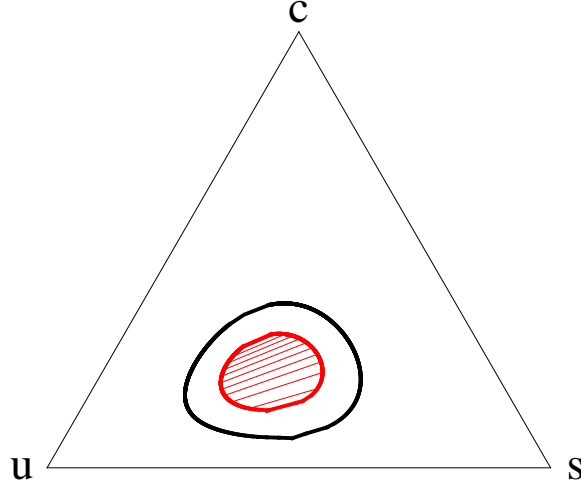


Figure 4.1: Phase diagram of ternary mixture with charged unsaturated lipids. The border of the two-phase region in the absence of charges is shown in black, while the smaller region of coexistence in the presence of charged unsaturated lipids is shown in red for $J_{el} = 0.1$. The other parameters of the model are $J_d = 1.6$, $J_o = 2.2$, $J_{sc} = 4.5$, $a_o/a_u = 2/3$, and $a_d/a_u = a_c/a_u = 1$ (see Appendix D).

molecules in both leaflets. We assume that the head groups of the unsaturated lipids are charged, as in the experiment of Vequi-Suplicy et al. [150]. In this case the charge density is determined by the mole fraction of unsaturated lipids, each of which has q elementary charges:

$$\sigma(s, c) = qe \frac{1}{2} \cdot \frac{N_u}{A} = qe \frac{1}{2} \cdot \frac{N_u}{N} \cdot \frac{1}{a} = qe \frac{1}{2} (1 - s - c) \cdot \frac{1}{a} \quad (4.4)$$

The factor of $1/2$ is due to the fact that σ is the charge density of only one monolayer. We must now relate the area per lipid, a , to the composition of the membrane. The simplest way of doing this is to interpolate linearly between the different species, assuming that each has its own natural area per molecule:

$$\begin{aligned} a(s, c) &= (1 - s - c) \cdot a_u + s_d \cdot a_d + s_o \cdot a_o + c \cdot a_c \\ &= a_u \left[(1 - s - c) + s_d \left(\frac{a_d}{a_u} \right) + s_o \left(\frac{a_o}{a_u} \right) + c \left(\frac{a_c}{a_u} \right) \right] \end{aligned} \quad (4.5)$$

The preferred molecular areas of each species are a_o , a_d , a_u , and a_c for ordered saturated lipids, disordered saturated lipids, unsaturated lipids, and cholesterol, respectively. Now

that equations (4.4) and (4.5) give σ and a in terms of the mole fractions, we can substitute these expressions into equation (4.3) to obtain the electrostatic free energy in terms of the compositions:

$$\frac{F_{el}}{k_B T N} = J_{el} \cdot \frac{(1 - s - c)^2}{(1 - s - c) + s_d \left(\frac{a_d}{a_u}\right) + s_o \left(\frac{a_o}{a_u}\right) + c \left(\frac{a_c}{a_u}\right)}, \quad (4.6)$$

where

$$J_{el} = \frac{3}{16} \cdot \frac{q^2 e^2}{k_B T \epsilon_W \kappa a_u} = \frac{3}{16} q^2 \frac{4\pi l_B}{\kappa a_u}, \quad (4.7)$$

and l_B is the Bjerrum length. Equation (4.6) represents a repulsion between unsaturated lipids of like charge, which favors mixing of these molecules with the other molecular species. The strength of this interaction depends via its denominator on the ratios of the cross-sectional areas a_d , a_o , a_u , and a_c of disordered saturated lipids, ordered saturated lipids, unsaturated lipids, and cholesterol. The quantity J_{el} gives a dimensionless measure of the importance of electrostatic interactions in determining the phase diagram of the mixture. In Figure 4.1 the two-phase region of a mixture with charged unsaturated lipids is shown for the dimensionless electrostatic coupling $J_{el} = 0.1$. We have also chosen the values $a_o/a_u = 2/3$, and $a_d/a_u = a_c/a_u = 1$. That is, for simplicity the “pure disordered” and “pure cholesterol” molecular areas are taken to be the same as the molecular area of the pure unsaturated lipid membrane, whereas the ordered membrane is taken to be thicker by a factor of $3/2$ than the pure unsaturated lipid membrane. We see that even for a small value of the dimensionless electrostatic coupling J_{el} , there is a significant decrease in the area of composition space taken up by the two-phase coexistence region. In this model of the liquid-liquid phase behavior of ternary mixed model membranes, electric charges on the unsaturated lipids are extremely efficient at opposing the tendency to phase-separate. Furthermore, we expect the dimensionless coupling parameter J_{el} to be much larger in conditions under which experiments have been done on such charged mixtures [150]. For water at room temperature the Bjerrum length l_B is about 0.7 nm. We take a_u to be about a half a square nanometer. At physiological salt concentrations, κ^{-1} is of order one nanometer, but in experiments on model membranes (which are more relevant here), it will be much larger. Using $\kappa^{-1} \approx 1$ nm and $q = 1$ yields $J_{el} \approx 3.3$. According to this model, even

at physiological salt concentrations, and certainly in experiments performed without added salt, the electrostatic repulsion between charged lipids should abolish macroscopic phase separation. That macroscopic liquid-liquid phase separation has been observed in model membranes with charged lipids [150] is surprising. It may indicate that the simple theory described above should be modified to take into account the charge regulation [16, 81] of the lipid head groups, that is, the ability of the charged head groups to recapture their counterions and become neutral if this leads to a sufficient reduction of the electrostatic repulsive energy.

4.3 Effect of Charges on Concentration Fluctuations

As noted in connection with the interleaflet coupling in Chapter 3, the lipid composition of the inner leaflet of the cell plasma membrane does not lend itself to liquid-liquid phase separation. The experiment of Wang and Silvius [156] showed that model bilayers with compositions reflecting that of the inner leaflet do not undergo macroscopic phase-separation. Therefore the discussion in the previous two sections of the effect of electric charge on phase separation is not directly relevant to the lateral organization of the inner leaflet, except insofar as it is coupled to the outer leaflet, which may itself contain raft domains of ordered saturated lipids and cholesterol. For this reason we have investigated the possibility that the presence of charged lipids in the inner leaflet might influence, rather than the average compositions of liquid phases and their possible coexistence, the spatial *fluctuations* of composition in a single liquid phase whose average composition is uniform. We ask whether the same electrostatic effects that lead to finite domain sizes in mixtures undergoing phase-separation could also give rise to a characteristic length scale in the spectrum of compositional fluctuations of charged lipids at temperatures for which macroscopic phase separation does not occur. A cell might exploit such fluctuations to organize processes laterally on this length scale. In this section we calculate the spectrum of compositional fluctuations in a simple model of a charged two-dimensional binary mixture surrounded by solvent. A more detailed analysis, including the electrostatic effect of the finite thickness of the bilayer, shows that such effects do not change our qualitative results.

We consider a two-dimensional binary mixture described by a compositional order pa-

parameter ϕ , the difference between the mole fractions of its components. We assume that the temperature is such that a single phase of uniform average composition is stable. Since we are interested in spatial fluctuations of the composition, we consider the free energy as a functional of an order parameter field $\phi(x, y)$ which varies in space. Here the x and y directions span the surface of the bilayer, while the z direction is normal to it. We choose the following functional to describe the intermolecular interactions not including electrostatics:

$$\frac{F_0[\phi(x, y)]}{N} = A^{-1} \cdot \int [a\phi^2(x, y) + b(\nabla\phi(x, y))^2] dx dy, \quad (4.8)$$

where A is the area of the charged mixture. The first term describes the effect of mixing entropy as well as short-range intermolecular interactions. Since we assume the temperature to be higher than the miscibility critical temperature, $a > 0$. The second term represents an energetic penalty for spatial variations of the order parameter. Such a term exists (with $b > 0$) as long as there are short-range repulsions between different molecular species, even when these are not strong enough to lead to phase separation. This free energy functional is conveniently expressed in terms of the Fourier modes of the order parameter

$$\phi(x) = \sum_q \phi_q \exp(iqx), \quad (4.9)$$

as

$$\frac{F_0[\phi_q]}{N} = \sum_q (a + bq^2) |\phi_q|^2, \quad (4.10)$$

where since $\phi(x)$ is real $\phi_q^* = \phi_{-q}$. The free energy contribution of the electrostatic interactions between molecules can be added by defining the charge density

$$\sigma(x) = pe \cdot \frac{N}{A} \equiv \sigma_0 \cdot \phi(x) \quad (4.11)$$

where $\sigma_0 = peN/A$ is defined to be the maximum charge density, that is, the charge density of the mixture when $\phi = 1$. Because of the linearity of the linearized Poisson-Boltzmann (Debye-Hückel) equation

$$\nabla^2 V = \kappa^2 V \quad (4.12)$$

the potential V_q due to each Fourier mode $\sigma_0 \cdot \phi_q \exp(iqx)$ of the charge density can be calculated separately. The solution to equation (4.12) satisfying the appropriate boundary

conditions is

$$V = V_q \cdot \exp(iqx), \quad \text{where} \quad (4.13)$$

$$V_q = \frac{\sigma_0 \phi_q}{2\epsilon_W} \cdot \frac{\exp(-\kappa'|z|)}{\kappa'} \quad (4.14)$$

$$\kappa'^2 = \kappa^2 + q^2 \quad (4.15)$$

The total potential is then

$$V = \sum_q V_q \exp(iqx) \quad (4.16)$$

The total electrostatic free energy includes the electrostatic energy of the surface charge and the ions in solution, as well as the entropy of the ions:

$$\begin{aligned} F_{\text{el}} = & \frac{1}{2} \int V(x, z=0) \sigma(x) dx dy + \frac{1}{2} \int V(\mathbf{r}) (e\rho_+(\mathbf{r}) - e\rho_-(\mathbf{r})) d^3\mathbf{r} \\ & + k_B T \int [\rho_+(\mathbf{r}) \ln(\rho_+(\mathbf{r})) + \rho_-(\mathbf{r}) \ln(\rho_-(\mathbf{r}))] d^3\mathbf{r}, \end{aligned} \quad (4.17)$$

where $\rho_+(\mathbf{r})$ and $\rho_-(\mathbf{r})$ are number densities of positive and negative ions in solution. We assume that these obey the Boltzmann distribution:

$$\rho_+(\mathbf{r}) = \rho_0 \exp(-\beta eV(\mathbf{r})) \quad (4.18)$$

$$\rho_-(\mathbf{r}) = \rho_0 \exp(\beta eV(\mathbf{r})) \quad (4.19)$$

Here ρ_0 is the bulk ($V=0$) density of both positive and negative ions in the solution. Thus the entropy term is

$$-TS = k_B T \int [\rho_+(\mathbf{r}) \ln(\rho_+(\mathbf{r})) + \rho_-(\mathbf{r}) \ln(\rho_-(\mathbf{r}))] d^3\mathbf{r} \quad (4.20)$$

$$\begin{aligned} & = k_B T \int [\rho_+(\mathbf{r}) \ln(\rho_0) + \rho_-(\mathbf{r}) \ln(\rho_0)] d^3\mathbf{r} \\ & + k_B T \int [-\rho_+(\mathbf{r})\beta eV(\mathbf{r}) + \rho_-(\mathbf{r})\beta eV(\mathbf{r})] d^3\mathbf{r} \end{aligned} \quad (4.21)$$

The first term is constant since the total number of ions does not change. The second term is twice the electrostatic energy of the ions, but of opposite sign. So the total electrostatic energy becomes

$$F_{\text{el}} = \frac{1}{2} \int V(x, z=0) \sigma(x) dx dy - \frac{1}{2} \int V(\mathbf{r}) \rho(\mathbf{r}) d^3\mathbf{r}, \quad (4.22)$$

where $\rho(\mathbf{r})$ is now the total charge (not number) density of ions in solution. Note that taking into account the entropy of the ions introduces the minus sign in the second term.

The second term of equation (4.22) can be written in terms of the potential using the Poisson equation and the Debye-Hückel equation:

$$\rho = -\epsilon_W \nabla^2 V = -\epsilon_W \kappa^2 V \quad (4.23)$$

After a few more steps, the electrostatic contribution to the free energy can be written in the form

$$\frac{F_{\text{el}}}{N} = \alpha \cdot \sum_q |\phi_q|^2 \left[\frac{1}{\kappa'} + \frac{1}{2} \cdot \frac{\kappa^2}{\kappa'^3} \right], \quad (4.24)$$

where the quantity α determines the relative importance of the electrostatic contribution to the free energy:

$$\alpha \equiv \frac{1}{4} \cdot \frac{p^2 e^2}{\epsilon_W} \cdot \frac{N}{A} \quad (4.25)$$

We can then consider the total free energy functional, including the electrostatic contribution:

$$\frac{F}{N} = \sum_q |\phi_q|^2 \underbrace{\left[a + bq^2 + \alpha \left(\frac{1}{\kappa'} + \frac{1}{2} \cdot \frac{\kappa^2}{\kappa'^3} \right) \right]}_{f_q}, \quad (4.26)$$

where again $\kappa'^2 = \kappa^2 + q^2$. The expression in square brackets is f_q , the free energy cost of a compositional fluctuation with wavevector q . It determines, via the equipartition theorem, the strength of these fluctuations in thermal equilibrium:

$$\langle |\phi_q|^2 \rangle \propto \frac{k_B T}{f_q} \quad (4.27)$$

We note first that the electrostatic contribution to equation (4.26), proportional to α , is always positive. This means that compositional fluctuations of all wavenumbers are suppressed by electrostatic interactions. Just as electrostatic interactions favor mixing and thus suppress macroscopic phase separation (which corresponds to a fluctuation with $q = 0$), they also suppress fluctuations of finite spatial extent.

However, it is clear from the fact that f_q depends on q that compositional fluctuations with different wavenumbers will be suppressed to different extents. Thus, one may wonder whether the presence of charged molecules in a mixture leads to a “preferred” size of fluctuations in composition. The simple model just described predicts such a characteristic length as long as the relative strength of the electrostatic interactions is large enough, as given by the dimensionless quantity α/κ^3b . This is illustrated in Figure 4.2, where a dimensionless quantity proportional to f_q^{-1} is plotted as a function of the dimensionless scaled wavenumber q/κ , for $a = b\kappa^2$ and for two values of the dimensionless electrostatic interaction strength α/κ^3b . The quantity plotted gives an indication of the strength of fluctuations of various wavenumbers. It can be seen that for $\alpha/\kappa^3b = 2.5$ (dashed line) f_q^{-1} has a local maximum at nonzero q , indicating that there is a characteristic wavelength of the fluctuations, whereas at a lower value $\alpha/\kappa^3b = 0.5$, the function f_q^{-1} decreases monotonically. It is easy to show

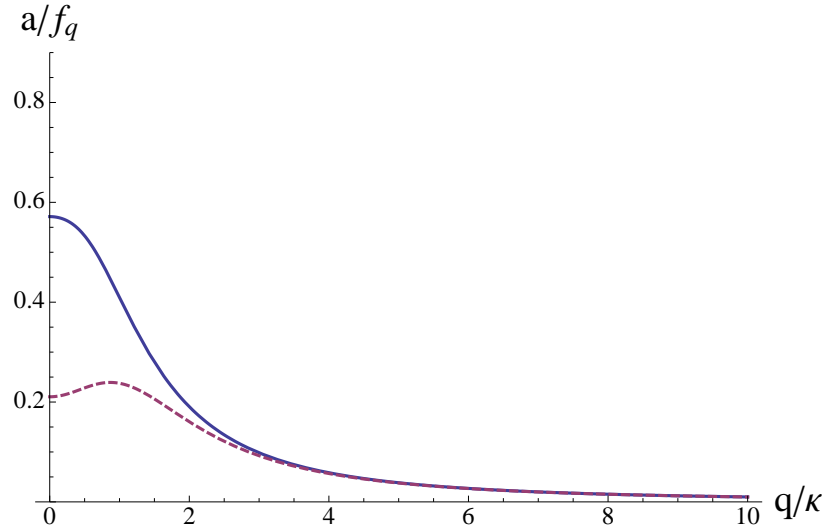


Figure 4.2: Dimensionless strength of composition fluctuations, proportional to the inverse of f_q , as a function of the dimensionless wavenumber, q/κ . Values of the parameters of the free energy are $a\kappa^{-1} = b\kappa = 1$. Values of α are 0.5 (solid) and 2.5 (dashed).

that the condition for the existence of the local maximum in f_q^{-1} is

$$\alpha > \frac{4}{5}\kappa^3b, \quad (4.28)$$

or, using the definition (4.25) of α and the Bjerrum length $l_B = \beta e^2 / 4\pi\epsilon_W$,

$$p^2 \cdot \frac{k_B T l_B}{\kappa^3 b} \cdot \frac{N}{A} > 0.25 \dots \quad (4.29)$$

It is easy to obtain estimates for the quantities involved in this inequality under physiologically relevant conditions, with the exception of the coefficient b introduced in the square-gradient term in equation (4.8). If we assume that each lipid has an elementary charge ($p = 1$) and a cross-sectional area of 0.5 nm^2 , a temperature of 300 K, a Bjerrum length in water of 0.7 nm, and a Debye screening length of $\kappa^{-1} = 1 \text{ nm}$, then the inequality becomes $b < 5.6 k_B T \text{ nm}^2$. Since the coefficient b of the square-gradient term in the free energy functional (4.8) is proportional [125] to the strength of the interactions between neighboring molecules, this inequality tells us that the compositional fluctuations will have a nonzero characteristic length as long as these intermolecular interactions are sufficiently weak. This is promising, since we know that the interactions between lipids in the inner leaflet of the cell plasma membrane are not strong enough to lead to phase separation [156]. However, at present we have no quantitative estimate of the coefficient b .

The analysis presented above of the effect of electrostatic interactions on compositional fluctuations made a number of simplifying assumptions. First, we have described a binary mixture of oppositely charged molecules, whereas the plasma membrane inner leaflet is better described as having a minority component (10–30 percent) of charged lipids [70]. We have also assumed that the short-range interactions between molecules are well described in a continuum approximation by the simple free energy functional given in equation (4.8). Finally, we have neglected the effect of the electrostatic boundary conditions at the interface between the aqueous solvent and the lipid bilayer; this effect does not change the qualitative behavior described above.

The effect of electrically charged lipid head groups on the compositional fluctuations in the inner leaflet of the cell plasma membrane can be more accurately investigated via a lattice Monte Carlo simulation in which both short-range intermolecular interactions and electrostatic interactions (mediated by salt in the solvent) are taken into account explicitly. Such an approach does not involve a continuum approximation of the local composition of the mixture, and so should accurately reflect composition fluctuations on small length

scales of the order of the average distance between charged lipids. As a first step toward performing such simulations, we have calculated the effective electrostatic interaction between two charged lipid head groups at the interface between the bilayer and the aqueous solvent. This interaction, which will be included in the lattice MC simulations, is mediated by the interactions of these charges with the salt ions in the solvent; both the electrostatic energy and the translational entropy of the ions is taken into account. The calculation of the effective electrostatic interaction is summarized in the next section and described in more detail in Appendix C.

4.4 Effective Electrostatic Potential between Charged Lipids

Figure 4.3 shows schematically a lipid bilayer of thickness d immersed in an aqueous solution containing salt. The solution has relative dielectric constant $\epsilon_W = 80$, while that of the interior of the bilayer is $\epsilon_B \approx 2$, close to that of oil. The salt in the solution gives rise to a Debye screening length κ^{-1} . Lipids with charged head groups, which are considered to exist in only one leaflet of the bilayer, are modeled as point charges (each with n negative elementary charges) located at the interface at $z = 0$ between the two dielectrics. In

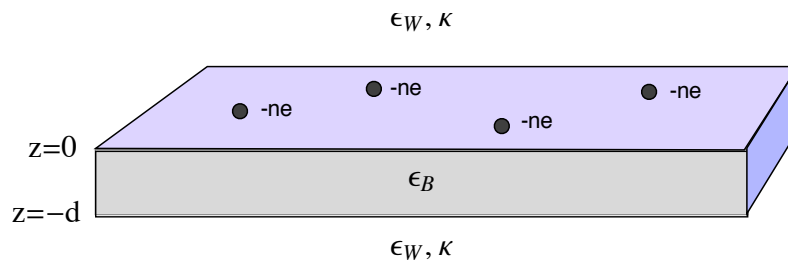


Figure 4.3: Electric charges at the lipid-water interface.

Appendix C we show that in the regime where the Poisson-Boltzmann equation can be linearized, the free energy of the system of charged lipids and the ions in solution can be decomposed into pairwise effective interactions acting between charged lipid head groups. The calculation of this effective potential, which includes the translational entropy of the ions in solution as well as their electrostatic energy, is greatly facilitated by the expressions for the

Green's function of the linearized Poisson-Boltzmann (Debye-Hückel) equation published by Netz [104]. Here we give the result in the limit where $\epsilon_B/\epsilon_W \approx 0$, which is a reasonable approximation given the values of the dielectric constants. Under this approximation, the effective interaction between charged lipid head groups separated by a distance r within the bilayer is

$$U_{\text{eff}}(r) = \frac{(ne)^2}{4\pi\epsilon_W} \cdot \frac{\exp(-\kappa r)}{r} \cdot [2 + \gamma + \exp(2\kappa r)\Gamma(0, 2\kappa r) + \ln(2\kappa r)], \quad (4.30)$$

where $\gamma = 0.577\dots$ is the Euler-Mascheroni constant and $\Gamma(0, x)$ is an incomplete gamma function defined by

$$\Gamma(0, x) = \int_x^\infty \frac{\exp(-t)}{t} dt \quad (4.31)$$

This function decays exponentially for large x . The factor outside the square brackets in equation (4.30) is the ordinary screened Coulomb (Yukawa) potential which acts between two charges $-ne$ far from any dielectric interfaces:

$$U_o(r) = \frac{(ne)^2}{4\pi\epsilon_W} \cdot \frac{\exp(-\kappa r)}{r} \quad (4.32)$$

Figure 4.4 shows as a solid line the effective potential U_{eff} between charges, scaled by $n^2e^2\kappa/4\pi\epsilon_W$ to make it dimensionless. The screened Coulomb potential U_o is also shown as a dashed line for comparison. The proximity of an interface between dielectrics significantly increases the effective repulsion between charged lipid head groups. This is further shown in Figure 4.5, which plots the ratio U_{eff}/U_o , or equivalently the quantity in square brackets in equation (4.30). Clearly the presence of the dielectric interface between the solvent and the lipid bilayer has an important effect in the electrostatic interactions between charged lipid head groups, and should be taken into account in modeling composition fluctuations of the inner leaflet of the cell membrane.

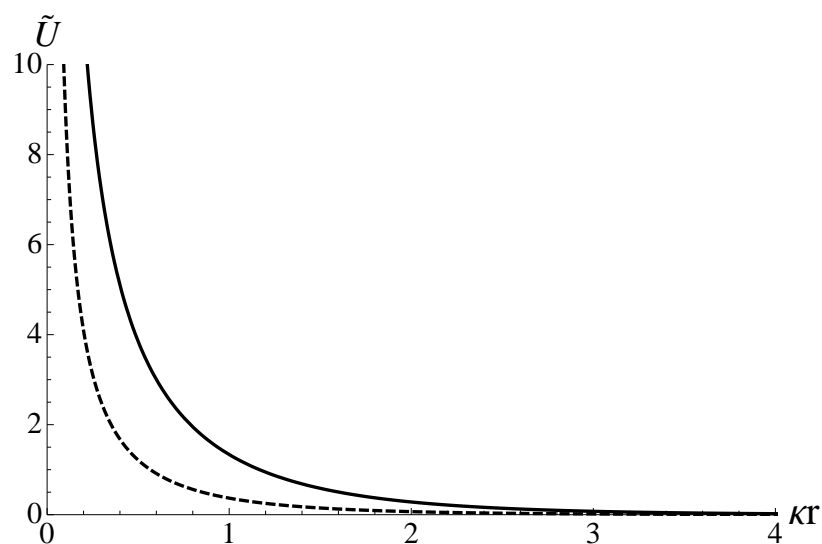


Figure 4.4: Effective electrostatic potential between two charged lipid headgroups. For comparison, the ordinary screened Coulomb interaction of two charges far from any interfaces is shown as a dashed line. Energies are plotted in dimensionless form in terms of the characteristic energy $n^2 e^2 \kappa / 4\pi \epsilon_W$.

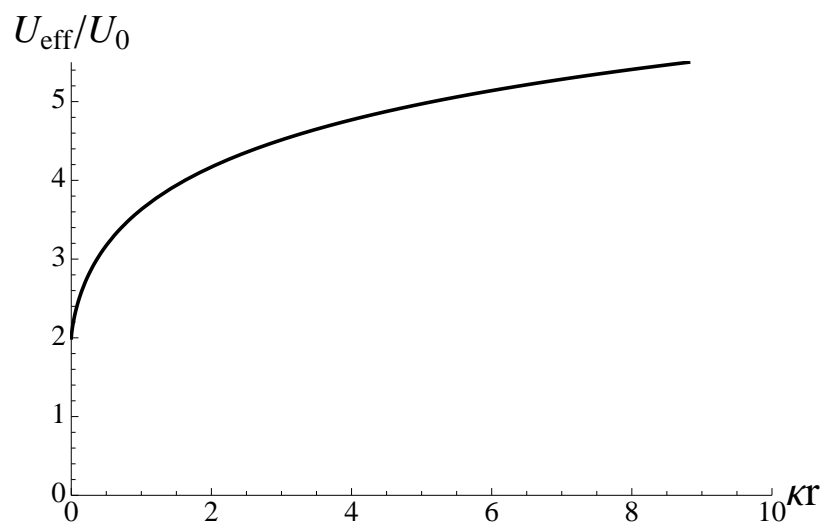


Figure 4.5: Plot of U_{eff}/U_0 , which is the factor by which the electrostatic repulsion between charged lipid head groups is enhanced compared to the screened Coulomb repulsion far from dielectric interfaces.

Chapter 5

QUESTIONS AND FUTURE RESEARCH DIRECTIONS

We conclude this thesis by discussing two questions related to lipid rafts in the cell plasma membrane and to the related phenomenon of liquid-liquid phase separation in model lipid bilayers composed of a mixture of high and low melting temperature lipids as well as cholesterol. Both of these questions can be posed as challenges to the current conception lipid rafts as nanoscale domains of the liquid-ordered phase. Firstly, what prevents these nanometer-scale domains from merging together into larger, eventually macroscopic domains? We list a number of explanations for the finite size of lipid rafts. Secondly, if the existence of lipid rafts is driven by interactions between molecules of the plasma membrane outer leaflet, what effects do the rafts have on the state of the inner leaflet? A complete answer to this question will require systematic study of the phase behavior of bilayers with asymmetric compositions.

5.1 *The Size of Lipid Rafts*

Assuming that the intermolecular interactions responsible for the existence of lipid rafts are the same as those that drive liquid-liquid phase separation in model membranes raises the question of why macroscopic liquid-ordered or liquid-disordered domains are not visible in cell plasma membranes. Here we review a number of mechanisms which have been proposed to explain why lipid rafts are limited to sizes below optical resolution.

The cell membrane is commonly viewed, to first approximation, as a bilayer composed of lipids including cholesterol. However, the cell plasma membrane contains large amounts of protein. For example, proteins occupy roughly 20 percent of the area of the plasma membranes of red blood cells [30]. Yethiraj and Weisshaar [157] suggested that the integral membrane proteins which anchor the cell cytoskeleton to the plasma membrane act as fixed impurities which prevent large-scale phase separation.

A key difference between living cells and model membranes is that the latter are typically studied in thermodynamic equilibrium, while the former are decidedly out of equilibrium. In particular, the lipids composing the cell plasma membrane are continually being recycled through metabolic processes [142] requiring energy input. Thus even if the average lipid composition of the cell membrane lends itself to phase separation, it is plausible that lipid transport and metabolism keep the plasma membrane lipids well-mixed, preventing the formation of large-scale domains. Fan et al. [39] studied the dynamics of a mixture which would phase separate if left to equilibrate, but which is prevented from doing so by a continuous transport process ensuring that the mixture is uniform on large length scales. They argued that, like this system, the cell membrane could have a non-equilibrium steady state characterized by finite-sized liquid domains.

An intriguing possibility is that lipid rafts, rather than being liquid-ordered domains limited to a finite size by some mechanism, are compositional fluctuations of a mixture near a miscibility critical point [60]. Honerkamp-Smith et al. [59] measured the correlation length in a ternary model membrane capable of liquid-liquid phase separation, and used critical scaling to argue that at temperatures a few degrees above the critical temperature, compositional fluctuations with sizes of tens of nanometers could be expected. Surprisingly, critical fluctuations have been observed in giant plasma membrane vesicles or “blebs” extracted directly from cell plasma membranes [146], suggesting the possibility that cells tune the lipid compositions of their plasma membranes in order to exploit these fluctuations.

A number of other mechanisms have been proposed to explain the finite size of lipid rafts, beyond those just mentioned. Kuzmin et al. [73] calculated the contribution of elastic deformation energy to the line tension of the liquid-liquid phase boundary, and found it to be so small that domain coalescence driven by this contribution only would proceed extremely slowly, leading to an effective finite size of domains. However, the most important contribution to the line tension is likely due not to elastic deformation energy, but rather to the same molecular interactions which drive phase separation; this can not be negligibly small if phase coexistence is in fact observed in model membranes. Frolov et al. [47] note that coalescence of small domains, while energetically favored due to the line tension, is entropically disfavored. They argued that a competition between energy and entropy results

in a finite domain size. Recently, Brewster et al. [12] suggested that hybrid lipids, which have one saturated and one unsaturated acyl chain, might stabilize liquid domains of finite size by preferentially partitioning to the domain interface. This mechanism is similar to that of Kuzmin et al. [73] in that it involves a reduction of line tension, which is the driving force of domain coalescence. It is difficult to reconcile these proposed mechanisms with the observation of liquid-liquid phase separation in “blebs” extracted from cell plasma membranes [8, 146]. This observation suggests that the mechanism preventing domain coalescence in cell membranes is not intrinsic to the lipid or protein composition of the membrane, but is rather due to external influences such as the cytoskeleton [157], nonequilibrium transport processes [39], or both.

5.2 The Phase Behavior of Asymmetric Mixed Bilayers

The observation of liquid-liquid phase coexistence in model membranes with compositions reflecting that of the plasma membrane outer leaflet [28] but not in those mimicking the composition of the inner leaflet [156] raised the following question: Can lipid rafts still be viable platforms for transmembrane signaling [132, 26]? That is, can a lipid raft residing in the outer leaflet influence transmembrane signaling processes by including or excluding membrane-bound proteins known to be involved in those processes? A relevant question in the context of model membranes is: under what conditions does an asymmetric bilayer with given compositions in each leaflet undergo phase separation? Collins and Keller [18] have shown experimentally that a bilayer in which one leaflet has an intrinsic tendency toward phase separation, but the other does not, can either phase-separate or not depending on the precise compositions of the leaflets. A complete answer to the question above therefore requires a systematic study of the phase diagram of an asymmetric bilayer. Given the difficulty of preparing bilayers with known asymmetric compositions, or of mapping out the phase diagram of a *symmetric* ternary mixture, it does not seem feasible in the near future for experimentalists to determine a complete phase diagram for an asymmetric bilayer. In contrast, it is a tractable (though difficult) problem to calculate the phase diagram of an asymmetric mixed bilayer on the basis of a model such as that of Elliott et al. [36]. Such a calculation would provide answers to a number of other questions of biological interest. For

example, if molecular interactions in the outer leaflet of an asymmetric bilayer drive phase separation, how great is the difference in inner-leaflet compositions between the two phases? Methods similar to those used to calculate partition coefficients of lipid-anchored proteins [141] in the two liquid phases could be used to determine whether the interleaflet coupling alone is capable of efficiently concentrating raft-associated proteins or exclude non-raft proteins from liquid-ordered domains. Another interesting question that could be addressed using such calculations is: if the relative concentrations of saturated and unsaturated lipids are fixed in both leaflets of an asymmetric bilayer, but cholesterol is allowed to flip-flop rapidly between leaflets, what will be the equilibrium concentrations of cholesterol in each of the leaflets? It is clear that due to cholesterol's different interactions with saturated and unsaturated lipids, it will not partition equally between the leaflets. However, we do not know *a priori* whether the difference in cholesterol concentration between the leaflets should be large.

Theoretical studies of the phase behavior of compositionally asymmetric bilayers must take into account their curvature. In general, a flat, asymmetric bilayer may lower its free energy by curving in one direction or another; this change in free energy may have an important effect on its phase diagram. This spontaneous curvature may even contribute significantly to the interleaflet coupling energy [80, 138, 86]. There has been a great deal of interest in the interplay between the curvature and compositional degrees of freedom of lipid bilayers [111, 128]. The spontaneous curvature of asymmetric mixed membranes can be calculated from the model of Elliott et al. [36] using the approach of Szleifer et al. [137]. This calculation would address a number of important questions: Based on its asymmetric lipid composition, how great is the cell plasma membrane's tendency to curve? Does this have a significant effect on its ability to phase-separate? Could the composition dependence of the spontaneous curvature make a significant contribution to the interleaflet coupling, thus accounting for the discrepancy between our estimate of this quantity and that of Risselada and Marrink? We hope that these questions and others will motivate further research in this area.

BIBLIOGRAPHY

- [1] D.W. Allender and M. Schick. Phase separation in bilayer lipid membranes: Effects on the inner leaf due to coupling to the outer leaf. *Biophys. J.*, 91:2828–2935, 2006.
- [2] D. Andelman. *Handbook of Biological Physics*, volume 1, chapter 12. North-Holland, Amsterdam, 1995.
- [3] D. Andelman, F. Brochard, and J. Joanny. Phase transitions in Langmuir monolayers of polar molecules. *J. Chem. Phys.*, 86:3673–3681, 1987.
- [4] C. L. Baciú and S. May. Stability of charged, mixed lipid bilayers: effect of electrostatic coupling between the monolayers. *J. Phys.: Condens. Matter*, 16:S2455–S2460, 2004.
- [5] C.B. Barber and H. Huhdanpaa. qhull version 2010.1. <http://www.qhull.org>.
- [6] P. Barham. *The Science of Cooking*. Springer, New York, 2000.
- [7] P.G. Barton and F.D. Gunstone. Hydrocarbon chain packing and molecular motion in phospholipid bilayers formed from unsaturated lecithins. *J. Biol. Chem.*, 250:4470–4476, 1975.
- [8] T. Baumgart, A.T. Hammond, P. Sengupta, S. T. Hess, D.A. Holowka, B.A. Baird, and W.W. Webb. Large-scale fluid/fluid phase separation of proteins and lipids in giant plasma membrane vesicles. *PNAS*, 104:3165–3170, 2007.
- [9] T. Baumgart, S.T. Hess, and W.W. Webb. Imaging coexisting fluid domains in biomembrane models coupling curvature and line tension. *Nature*, 425:821–824, 2003.
- [10] A. Ben-Shaul and I. Szleifer. Chain organization and thermodynamics in micelles and bilayers. I. Theory. *J. Chem. Phys.*, 83:3597–3610, 1985.
- [11] M.L. Berkowitz. Detailed molecular dynamics simulations of model biological membranes containing cholesterol. *Biochim. Biophys. Acta*, 1788:86–96, 2009.
- [12] R. Brewster, P.A. Pincus, and S.A. Safran. Hybrid lipids as a biological surface-active component. *Biophys. J.*, 97:1087–1094, 2009.
- [13] D.A. Brown and E. London. Functions of lipid rafts in biological membranes. *Annu. Rev. Cell Dev. Biol.*, 14:111–136, 1998.

- [14] D.A. Brown and J.K. Rose. Sorting of GPI-anchored proteins to glycolipid-enriched membrane subdomains during transport to the apical cell surface. *Cell*, 68:533–544, 1992.
- [15] R.J. Bruckner, S.S. Mansy, A. Ricardo, L. Mahadevan, and J.W. Szostak. Flip-flop induced relaxation of bending energy: Implications for membrane remodeling. *Biophys. J.*, 97:3113–3122, 2009.
- [16] S.L. Carnie and D.Y.C. Chan. Interaction free energy between plates with charge regulation: A linearized model. *J. Colloid and Interface Sci.*, 161:260–264, 1993.
- [17] M.D. Collins. Interleaflet coupling mechanisms in bilayers of lipids and cholesterol. *Biophys. J.*, 94:L32–L34, 2008.
- [18] M.D. Collins and S.L. Keller. Tuning lipid mixtures to induce or suppress domain formation across leaflets of unsupported asymmetric bilayers. *Proc. Natl. Acad. Sci. USA*, 105:124–128, 2008.
- [19] W. Curatolo, B. Sears, and L.J. Neuringer. A calorimetry and deuterium NMR study of mixed model membranes of 1-palmitoyl-2-oleylphosphatidylcholine and saturated phosphatidylcholines. *Biochim. Biophys. Acta*, 817:261–270, 1985.
- [20] J.H. Davis, J.J. Clair, and J. Juhasz. Phase equilibria in DOPC/DPPC-d₆₂/cholesterol mixtures. *Biophys. J.*, 96:521–539, 2009.
- [21] R. de Almeida, A. Fedorov, and M. Prieto. Sphingomyelin/ phosphatidylcholine/ cholesterol phase diagram: Boundaries and composition of lipid rafts. *Biophys. J.*, 85:2406–2416, 2003.
- [22] P.G. de Gennes. *Scaling Concepts in Polymer Physics*. Cornell University Press, Ithaca, NY, 1979.
- [23] P.G. de Gennes. *Superconductivity of Metals and Alloys*. Westview Press, Boulder, CO, 1999.
- [24] P.G. de Gennes and J. Prost. *The Physics of Liquid Crystals*. Oxford University Press, Oxford, 1995.
- [25] M. den Nijs. *Phase Transitions and Critical Phenomena*, volume 12, chapter 2. Academic Press, New York, 1988.
- [26] P. F. Devaux and R. Morris. Transmembrane asymmetry and lateral domains in biological membranes. *Traffic*, 5:241–246, 2004.

- [27] P.F. Devaux, A. Herrmann, N. Ohlwein, and M. M. Kozlov. How lipid flippases can modulate membrane structure. *Biochim. Biophys. Acta*, 1778:1591–1600, 2008.
- [28] C. Dietrich, L.A. Bagatolli, Z.N. Volovyk, N.L. Thompson, M. Levi, K. Jacobson, and E. Gratton. Lipid rafts reconstituted in model membranes. *Biophys. J.*, 80:1417–1428, 2001.
- [29] K.A. Dill and D. Stigter. Lateral interactions among phosphatidylcholine and phosphatidylethanolamine head groups in phospholipid monolayers and bilayers. *Biochem.*, 27:3446–3453, 1988.
- [30] A.D. Dupuy and D.M. Engelman. Protein area occupancy at the center of the red blood cell membrane. *PNAS*, 105:2848–2852, 2008.
- [31] D. Duque, X. Li, K. Katsov, and M. Schick. Molecular theory of hydrophobic mismatch between lipids and peptides. *J. Chem. Phys.*, 116:10478–10484, 2002.
- [32] H. Ebel, P. Grabitz, and T. Heimburg. Enthalpy and volume changes in lipid membranes. I. The proportionality of heat and volume changes in the lipid melting transition and its implication for the elastic constants. *J. Phys. Chem. B*, 105:7353–7360, 2001.
- [33] M. Edidin. The state of lipid rafts: From model membranes to cells. *Annu. Rev. Biophys. Biomol. Struct.*, 32:257–283, 2003.
- [34] R. Elliott. *Phase Separation in Mixed Bilayers containing Saturated and Mono-unsaturated Lipids with Cholesterol as determined from a Microscopic Model*. PhD thesis, University of Washington, Seattle, 2005.
- [35] R. Elliott, K. Katsov, M. Schick, and I. Szleifer. Phase separation of saturated and mono-unsaturated lipids as determined from a microscopic model. *J. Chem. Phys.*, 122:044094, 2005.
- [36] R. Elliott, I. Szleifer, and M. Schick. Phase diagram of a ternary mixture of cholesterol and saturated and unsaturated lipids calculated from a microscopic model. *Phys. Rev. Lett.*, 96:098101, 2006.
- [37] A. Erdélyi, editor. *Tables of Integral Transforms*, volume 2. McGraw-Hill, New York, 1954.
- [38] C. Esposito, A. Tian, S. Melamed, C. Johnson, S. Tee, and T. Baumgart. Flicker spectroscopy of thermal bilayer domain boundary fluctuations. *Biophys. J.*, 93:3169–3181, 2007.

- [39] J. Fan, M. Sammalkorpi, and M. Haataja. Domain formation in the plasma membrane: Role of nonequilibrium lipid transport and membrane proteins. *Phys. Rev. Lett.*, 100:178102, 2008.
- [40] J. Fantini, N. Garmy, R. Mahfoud, and N. Yahi. Lipid rafts: structure, function and role in HIV, Alzheimer’s and prion diseases. *Exp. Rev. Mol. Med.*, 2002.
- [41] D.R. Fattal and A. Ben-Shaul. Mean-field calculations of chain packing and conformational statistics in lipid bilayers: Comparison with experiments and molecular dynamics studies. *Biophys. J.*, 67:983–995, 1994.
- [42] D.R. Fattal and A. Ben-Shaul. Lipid chain packing and lipid-protein interaction in membranes. *Physica A*, 220:192–216, 1995.
- [43] G.W. Feigenson and J.T. Buboltz. Ternary phase diagram of dipalmitoyl-pc/dilauroyl-pc/cholesterol: nanoscopic domain formation driven by cholesterol. *Biophys. J.*, 80:2775–2788, 2001.
- [44] C.J. Fielding, editor. *Lipid Rafts and Caveolae*. Wiley VCH, Weinheim, Germany, 2006.
- [45] P.J. Flory. *Statistical Mechanics of Chain Molecules*. Wiley-Interscience, New York, 1969.
- [46] D. Frenkel and B. Smit. *Understanding Molecular Simulations*. Academic Press, London, 1996.
- [47] V.A.J. Frolov, Y.A. Chizmadzhev, F.S. Cohen, and J. Zimmerberg. “Entropic traps” in the kinetics of phase separation in multicomponent membranes stabilize nanodomains. *Biophys. J.*, 91:189–205, 2006.
- [48] T. Garel and S. Doniach. Phase transitions with spontaneous modulation - the dipolarising ferromagnet. *Phys. Rev. B*, 26:325–329, 1982.
- [49] S. Garge, J. Rühle, K. Lüdtke, R. Jordan, and C.A. Naumann. Domain registration in raft-mimicking lipid mixtures studied using polymer-tethered lipid bilayers. *Biophys. J.*, 92:1263–1270, 2007.
- [50] M. Giocondi, V. Vié, E. Lesniewska, J. Goudonnet, and C. Le Grimellec. In situ imaging of detergent-resistant membranes by atomic force microscopy. *J. Structural Biol.*, 131:38–43, 2000.
- [51] A. Yu. Grosberg and A. R. Khokhlov. *Statistical Physics of Macromolecules*. American Institute of Physics Press, Woodbury, NY, 1994.

- [52] D.W.R. Gruen. A mean-field model of the alkane-saturated lipid bilayer above its phase transition. *Biophys. J.*, 33:149–166, 1981.
- [53] J.A. Hamilton. Fast flip-flop of cholesterol and fatty acids in membranes: implications for membrane transport proteins. *Curr. Opin. Lipidol.*, 14:263–271, 2003.
- [54] A.T. Hammond, F. Heberle, T. Baumgart, D. Holowka, B. Baird, and G.W. Feigenson. Crosslinking a lipid raft component triggers liquid ordered-liquid disordered phase separation in model plasma membranes. *PNAS*, 102:6320–6325, 2005.
- [55] J.F. Hancock. Lipid rafts: contentious only from simplistic standpoints. *Nature Rev. Mol. Cell. Bio.*, 7:456–462, 2006.
- [56] P.L. Hansen, L. Miao, and J.H. Ipsen. Fluid lipid bilayers: Intermonolayer coupling and its thermodynamic manifestations. *Phys. Rev. E*, 58:2311–2324, 1998.
- [57] H. Heerklotz. Triton promotes domain formation in lipid raft mixtures. *Biophys. J.*, 83:2693–2701, 2002.
- [58] T. Heimburg. *Thermal Biophysics of Membranes*. Wiley-VCH Verlag GmbH & Co. KGaA, Weinheim, Germany, 2007.
- [59] A.R. Honerkamp-Smith, P. Cicuta, M.D. Collins, S.L. Veatch, M. den Nijs, M. Schick, and S.L. Keller. Line tensions, correlation lengths, and critical exponents in lipid membranes near critical points. *Biophys. J.*, 95:236–246, 2008.
- [60] A.R. Honerkamp-Smith, S.L. Veatch, and S.L. Keller. An introduction to critical points for biophysicists; observations of compositional heterogeneity in lipid membranes. *Biochim. Biophys. Acta*, 1788:53–63, 2009.
- [61] T. Hønger, K. Mortensen, J.H. Ipsen, J. Lemmich, R. Bauer, and O.G. Mouritsen. Anomalous swelling of multilamellar lipid bilayers in the transition region by renormalization of curvature elasticity. *Phys. Rev. Lett.*, 72:3911–3914, 1994.
- [62] T. Idema, J.M.J. van Leeuwen, and C. Storm. Phase coexistence and line tension in ternary lipid systems. *Phys. Rev. E*, 80:041924, 2009.
- [63] J.H. Ipsen, G. Karlström, O.G. Mouritsen, H. Wennerström, and M.J. Zuckermann. Phase equilibria in the phosphatidylcholine-cholesterol system. *Biochim. Biophys. Acta*, 905:162–172, 1987.
- [64] K. Jacobson, O.G. Mouritsen, and R.G.W. Anderson. Lipid rafts: at a crossroad between cell biology and physics. *Nature Cell Bio.*, 9:7–14, 2007.

- [65] F. Jähnig. Electrostatic free energy and shift of the phase transition for charged lipid membranes. *Biophys. Chem.*, 4:309–318, 1976.
- [66] R. Jamei, S. Kivelson, and B. Spivak. Universal aspects of coulomb-frustrated phase separation. *Phys. Rev. Lett.*, 94:056805, 2005.
- [67] M.J. Karnovsky, A.M. Kleinfeld, R.L. Hoover, and R.D. Klausner. The concept of lipid domains in membranes. *J. Cell Bio.*, 94:1–6, 1982.
- [68] S.L. Keller, A. Radhakrishnan, and H.M. McConnell. Saturated phospholipids with high melting temperatures form complexes with cholesterol in monolayers. *J. Phys. Chem. B*, 104:7522–7527, 2000.
- [69] V. Kiessling, J.M. Crane, and L.K. Tamm. Transbilayer effects of raft-like lipid domains in asymmetric planar bilayers measured by single molecule tracking. *Biophys. J.*, 91:3313–3326, 2006.
- [70] V. Kiessling, C. Wan, and L. K. Tamm. Domain coupling in asymmetric lipid bilayers. *Biochim. Biophys. Acta*, 1788:64–71, 2009.
- [71] S. Komura, H. Shirotori, and P.D. Olmsted. Phase behaviour of three-component lipid mixtures. *J. Phys.L Condens. Matter*, 17:S2951–S2956, 2005.
- [72] S. Komura, H. Shirotori, P.D. Olmsted, and D. Andelman. Lateral phase separation in mixtures of lipids and cholesterol. *Europhys. Lett.*, 67:321–327, 2004.
- [73] P.I. Kuzmin, S. A. Akimov, Yu. A. Chizmadzhev, J. Zimmerberg, and F.S. Cohen. Line tension and interaction energies of membrane rafts calculated from lipid splay and tilt. *Biophys. J.*, 88:1120–1133, 2005.
- [74] D.P. Landau and K. Binder. *A Guide to Monte Carlo Simulations in Statistical Physics*. Cambridge University Press, Cambridge, 2000.
- [75] L.D. Landau, E.M. Lifshitz, and L.P. Pitaevskii. *Electrodynamics of Continuous Media*. Butterworth-Heinemann, New York, 2007.
- [76] J.B. Leathes. Condensing effect of cholesterol on monolayers. *Lancet*, 208:853–856, 1925.
- [77] J-Y. Lee and M. Schick. Dependence of the energies of fusion on the intermembrane separation: optimal and constrained. *J. Chem. Phys.*, 127:075102, 2007.
- [78] F.A.M. Leermakers and A.L. Rabinovich. Interaction of cholesterol-like molecules in polyunsaturated phosphatidylcholine lipid bilayers as revealed by a self-consistent field theory. *Phys. Rev. E*, 76:031904, 2007.

- [79] F.A.M. Leermakers and J.M.H.M. Scheutjens. Statistical thermodynamics of association colloids. I. Lipid bilayer membranes. *J. Chem. Phys.*, 89:3264–3274, 1988.
- [80] S. Leibler and D. Andelman. Ordered and curved meso-structures in membranes and amphiphilic films. *J. Physique*, 48:2013–2018, 1987.
- [81] X. Li and M. Schick. Theory of tunable pH-sensitive vesicles of anionic and cationic lipids or anionic and neutral lipids. *Biophys. J.*, 80:1703–1711, 2001.
- [82] X. Li and M. Schick. Distribution of lipids in nonlamellar phases of their mixtures. *J. Chem. Phys.*, 112:6063–6072, 2002.
- [83] D. Lingwood and K. Simons. Lipid rafts as a membrane-organizing principle. *Science*, 327:46–50, 2010.
- [84] A.P. Liu and D.A. Fletcher. Actin polymerization serves as a membrane domain switch in model lipid bilayers. *Biophys. J.*, 91:4064–4070, 2006.
- [85] G.S. Longo, M. Schick, and I. Szleifer. Stability and liquid-liquid phase separation in mixed saturated lipids bilayers. *Biophys. J.*, 96:3977–3986, 2009.
- [86] F.C. MacKintosh. Mixed fluid bilayers: Effects of confinement. *Phys. Rev. E*, 50:2891–2897, 1994.
- [87] S. Marčelja. Molecular model for phase transition in biological membranes. *Nature*, 241:451–453, 1973.
- [88] S. Marčelja. Chain ordering in liquid crystals II. Structure of bilayer membranes. *Biochim. Biophys. Acta*, 367:165–176, 1974.
- [89] D. Marsh. Cholesterol-induced fluid membrane domains: A compendium of lipid-raft ternary phase diagrams. *Biochim. Biophys. Acta*, 1788:2114–2123, 2009.
- [90] M.P. Mattson, editor. *Membrane Microdomain Signaling: Lipid Rafts in Biology and Medicine*. Humana Press, Totowa, NJ, 2005.
- [91] S. May. Trans-monolayer coupling of fluid domains in lipid bilayers. *Soft Matter*, 5:3148–3156, 2009.
- [92] H. M. McConnell. Structures and transitions in lipid monolayers at the air-water interface. *Annu. Rev. Phys. Chem.*, 42:171–195, 1991.
- [93] H. M. McConnell. Complexes in ternary cholesterol-phospholipid mixtures. *Biophys. J.*, 88:L23–L25, 2005.

- [94] H. M. McConnell and V. T. Moy. Shapes of finite two-dimensional lipid domains. *J. Phys. Chem.*, 92:4520–4525, 1988.
- [95] O.G. Mouritsen. *Life - As A Matter of Fat: The Emerging Science of Lipidomics*. Springer-Verlag, Berlin, 2005.
- [96] M. Müller, K. Katsov, and M. Schick. Biological and synthetic membranes: What can be learned from a coarse-grained description? *Phys. Reports*, 434:113–176, 2006.
- [97] M. Müller and M. Schick. Calculation of the phase behavior of lipids. *Phys. Rev. E*, 57:6973–6978, 1998.
- [98] S. Munro. Lipid rafts: Elusive or illusive? *Cell*, 115:377–388, 2003.
- [99] T. Murtola, E. Falck, M. Karttunen, and I. Vattulainen. Coarse-grained model for phospholipid/cholesterol bilayer employing inverse monte carlo with thermodynamic constraints. *J. Chem. Phys.*, 126:075101, 2007.
- [100] J.F. Nagle. Theory of the main lipid bilayer phase transition. *Ann. Rev. Phys. Chem.*, 31:157–195, 1980.
- [101] J.F. Nagle and H.L. Scott. Biomembrane phase transitions. *Physics Today*, 31:38–47, 1978.
- [102] A. Naydenov, P.A. Pincus, and S.A. Safran. Equilibrium domains on heterogeneously charged surfaces. *Langmuir*, 23:12016–12023, 2007.
- [103] P.C. Nelson. *Biological Physics: Energy, Information, Life*. W.H. Freeman, New York, 2004.
- [104] R.R. Netz. Debye-Hückel theory for slab geometries. *Eur. Phys. J. E*, 3:131–141, 2000.
- [105] R.R. Netz. Theoretical approaches to charged surfaces. *J.Phys.: Condens. Matter*, 16:S2353–S2368, 2004.
- [106] J. O’Rourke. *Computational Geometry in C*. Cambridge University Press, Cambridge, 1998.
- [107] S.A. Pandit, D. Bostick, and M.L. Berkowitz. Lateral organization in lipid-cholesterol mixed bilayers. *Biophys. J.*, 86:1345–1356, 2004.
- [108] S.A. Pandit, G. Khelashvili, E. Jakobsson, A. Grama, and H.L. Scott. Complexation of phosphatidylcholine lipids with cholesterol. *Biophys. J.*, 92:440–447, 2007.

- [109] S.A. Pandit and H.L. Scott. Multiscale simulations of heterogeneous model membranes. *Biochim. Biophys. Acta*, 1788:136–148, 2009.
- [110] T. Parasassi, E. Gratton, W.M. Yu, P. Wilson, and M. Levi. Two-photon fluorescence microscopy of laurdan generalized polarization domains in model and natural membranes. *Biophys. J.*, 72:2413–2429, 1997.
- [111] R. Parthasarathy and J.T. Groves. Curvature and spatial organization in biological membranes. *Soft Matter*, 3:24–33, 2007.
- [112] L.J. Pike. Rafts defined: a report on the Keystone symposium on lipid rafts and cell function. *J. Lipid Res.*, 47:1597–1598, 2006.
- [113] Z.S. Popovic and S. Satpathy. Wedge-shaped potential and Airy-function electron localization in oxide superlattices. *Phys. Rev. Lett.*, 94:176805, 2005.
- [114] W.H. Press, B.P. Flannery, S. A. Teukolsky, and W.T. Vetterling. *Numerical Recipes in C*. Cambridge University Press, Cambridge, 1992.
- [115] I. Prigogine and R. Defay. *Chemical Thermodynamics*. Longmans Green, London, 1954.
- [116] G. G. Putzel and M. Schick. Phase behavior of a model bilayer membrane with coupled leaves. *Biophys. J.*, 94:869–877, 2008.
- [117] G. G. Putzel and M. Schick. Phenomenological model and phase behavior of saturated and unsaturated lipids and cholesterol. *Biophys. J.*, 95:4756–4762, 2008.
- [118] G. G. Putzel and M. Schick. Theory of raft formation by the cross-linking of saturated or unsaturated lipids in model lipid bilayers. *Biophys. J.*, 96:4935–4940, 2009.
- [119] A. Radhakrishnan and H. M. McConnell. Condensed complexes of cholesterol and phospholipids. *Biophys. J.*, 77:1507–1517, 1999.
- [120] A. Radhakrishnan and H. M. McConnell. Condensed complexes in vesicles containing cholesterol and phospholipids. *PNAS*, 102:12662–12666, 2005.
- [121] D.J. Recktenwald and H.M. McConnell. Phase equilibria in binary mixtures of phosphatidylcholine and cholesterol. *Biochemistry*, 20:4505–4510, 1981.
- [122] A. Rietveld and K. Simons. The differential miscibility of lipids as the basis for the formation of functional membrane rafts. *Biochim. Biophys. Acta*, 1376:467–479, 1998.

- [123] H.J. Risselada and S.J. Marrink. The molecular face of lipid rafts in model membranes. *Proc. Natl. Acad. Sci. USA*, 105:17367–17372, 2008.
- [124] J.L.R. Rubenstein, B.A. Smith, and H.M. McConnell. Lateral diffusion in binary mixtures of cholesterol and phosphatidylcholines. *PNAS*, 76:15–18, 1979.
- [125] S.A. Safran. *Statistical Thermodynamics of Surfaces, Interfaces, and Membranes*. Westview Press, Boulder, CO, 2003.
- [126] M.B. Sankaram and T.E. Thompson. Modulation of phospholipid acyl chain order by cholesterol. A solid-state ^2H nuclear magnetic resonance study. *Biochemistry*, 29:10676–10684, 1990.
- [127] N. Sapay, W.F.D. Bennett, and D.P. Tieleman. Thermodynamics of flip-flop and desorption for a systematic series of phosphatidylcholine lipids. *Soft Matter*, 5:3295–3302, 2009.
- [128] S. Semrau and T. Schmidt. Membrane heterogeneity – from lipid domains to curvature effects. *Soft Matter*, 5:3174–3186, 2009.
- [129] P. Sengupta, B. Baird, and D. Holowka. Lipid rafts, fluid/fluid phase separation, and their relevance to plasma membrane structure and function. *Sem. Cell. Dev. Biol.*, 18:583–590, 2007.
- [130] A. S. Shaw. Lipid rafts: now you see them, now you don't. *Nature Immun.*, 7:1139–1142, 2006.
- [131] K. Simons and E. Ikonen. Functional rafts in cell membranes. *Nature*, 387:569–572, 1997.
- [132] K. Simons and D. Toomre. Lipid rafts and signal transduction. *Nature Rev. Mol. Cell Bio.*, 1:31–40, 2000.
- [133] K. Simons and G. van Meer. Lipid sorting in epithelial cells. *Biochemistry*, 27:6197–6202, 1988.
- [134] K. Simons and W.L.C. Vaz. Model systems, lipid rafts, and cell membranes. *Annu. Rev. Biophys. Biomol. Struct.*, 33:269–295, 2004.
- [135] F.J. Solis, S.I. Stupp, and M. Olvera de la Cruz. Charge induced pattern formation on surfaces: Segregation in cylindrical micelles of cationic-anionic peptide-amphiphiles. *J. Chem. Phys.*, 122:054905, 2005.

- [136] I. Szleifer, A. Ben-Shaul, and W.M. Gelbart. Chain packing statistics and thermodynamics of amphiphile monolayers. *J. Phys. Chem.*, 94:5081–5089, 1990.
- [137] I. Szleifer, D. Kramer, A. Ben-Shaul, W. M. Gelbart, and S.A. Safran. Molecular theory of curvature elasticity in surfactant films. *J. Chem. Phys.*, 92:6800–6817, 1990.
- [138] T. Taniguchi, K. Kawasaki, D. Andelman, and T. Kawakatsu. Phase transitions and shapes of two component membranes and vesicles II: Weak segregation limit. *J. Phys. II France*, 4:1333–1362, 1994.
- [139] A. Tian, C. Johnson, W. Wang, and T. Baumgart. Line tension at fluid membrane domain boundaries measured by micropipette aspiration. *Phys. Rev. Lett.*, 98:208102, 2007.
- [140] H. Träuble, M. Teubner, P. Woolley, and H. Eibl. Electrostatic interactions at charged lipid membranes. I. Effects of pH and univalent cations on membrane structure. *Biophys. Chem.*, 4:319–342, 1976.
- [141] M. J. Uline, G.S. Longo, M. Schick, and I. Szleifer. Calculating partition coefficients of chain anchors in liquid-ordered and liquid-disordered phases. *Biophys. J.*, 98:1883–1892, 2010.
- [142] G. van Meer, D.R. Voelker, and G.W. Feigenson. Membrane lipids: where they are and how they behave. *Nature Rev. Mol. Cell Bio.*, 9:112–124, 2008.
- [143] S.L. Veatch, K. Gawrisch, and S.L. Keller. Closed-loop miscibility gap and quantitative tie-lines in ternary membranes containing diphytanoyl PC. *Biophys. J.*, 90:4428–4436, 2006.
- [144] S.L. Veatch and S.L. Keller. Separation of liquid phases in giant vesicles of ternary mixtures of phospholipids and cholesterol. *Biophys. J.*, 85:3074–3083, 2003.
- [145] S.L. Veatch and S.L. Keller. Seeing spots: Complex phase behavior in simple membranes. *Biochim. Biophys. Acta*, 1746:172–185, 2005.
- [146] S.L. Veatch, P. Sengupta, A. Honerkamp-Smith, D. Holowka, and B. Baird. Critical fluctuations in plasma membrane vesicles. *ACS Chem. Bio.*, 3:287–293, 2008.
- [147] S.L. Veatch, O. Soubias, S.L. Keller, and K. Gawrisch. Critical fluctuations in domain-forming lipid mixtures. *PNAS*, 104:17650–17655, 2007.
- [148] E.Y. Vedmedenko. *Competing Interactions and Pattern Formation in Nanoworld*. Wiley-VCH, Weinheim, Germany, 2007.

- [149] M. Venturoli, M. M. Sperotto, M. Kranenburg, and B. Smit. Mesoscopic models of biological membranes. *Phys. Reports*, 437:1–54, 2006.
- [150] C. C. Vequi-Suplicy, K. A. Riske, R. L. Knorr, and R. Dimova. Vesicles with charged domains. *Biochim. Biophys. Acta*, 2010.
- [151] M.R. Vist. Partial phase behavior of perdeuterated dipalmitoyl phosphatidyl choline-cholesterol model membranes. Master’s thesis, University of Guelph, Ontario, Canada, 1984.
- [152] M.R. Vist and J.H. Davis. Phase equilibria of cholesterol/ dipalmitoylphosphatidylcholine mixtures: ^2H nuclear magnetic resonance and differential scanning calorimetry. *Biochemistry*, 29:451–464, 1990.
- [153] A.J. Wagner, S. Loew, and S. May. Influence of monolayer-monolayer coupling on the phase behavior of a fluid lipid bilayer. *Biophys. J.*, 93:4268–4277, 2007.
- [154] A.J. Wagner and S. May. Electrostatic interactions across a charged lipid bilayer. *Eur. Biophys. J.*, 36:293–303, 2007.
- [155] C. Wan, V. Kiessling, and L. K. Tamm. Coupling of cholesterol-rich lipid phases in asymmetric bilayers. *Biochemistry*, 47:2190–2198, 2008.
- [156] T. Wang and J.R. Silvius. Cholesterol does not induce segregation of liquid-ordered domains in bilayers modeling the inner leaflet of the plasma membrane. *Biophys. J.*, 81:2762–2773, 2001.
- [157] A. Yethiraj and J.C. Weisshaar. Why are lipid rafts not observed in vivo? *Biophys. J.*, 93:3113–3119, 2007.
- [158] Z. Zhang, S.Y. Bhide, and M.L. Berkowitz. Molecular dynamics simulations of bilayers containing mixtures of sphingomyelin with cholesterol and phosphatidylcholine with cholesterol. *J. Phys. Chem.*, 111:12888–12897, 2007.
- [159] Z. Zhang, M.J. Zuckermann, and O.G. Mouritsen. Effect of intermonolayer coupling on the phase behavior of lipid bilayers. *Phys. Rev. A*, 46:6707–6713, 1992.

Appendix A

THERMODYNAMICS OF MIXED BILAYERS

In this appendix we derive basic thermodynamics relations for a mixed lipid bilayer composed of saturated lipids, unsaturated lipids, and cholesterol. These tell us, for example, how the derivatives of the Helmholtz free energy per molecule f are related to physical quantities such as chemical potentials and surface tensions.

We consider a lipid bilayer of area A composed of a mixture of saturated lipids, unsaturated lipids, and cholesterol. From the area A and the total number of molecules N we define the area per molecule a :

$$a \equiv \frac{A}{N} \quad (\text{A.1})$$

The bilayer is made up of an “inner” leaflet and an “outer” one. Strictly speaking, in thermodynamic equilibrium the leaflets will have the same composition. We assume that the flip-flop process by which the leaflet compositions become identical is slow enough that we may reasonably speak of an asymmetric bilayer in thermodynamic equilibrium. The total numbers of molecules in the inner and outer leaflets are N_{in} and N_{out} , respectively. The fraction of the total molecules N in the bilayer which reside in the inner leaflet is given by

$$\eta \equiv \frac{N_{\text{in}}}{N} \quad (\text{A.2})$$

We are assuming that the area accessible to lipids in both leaflets is the same (A); physically this corresponds to the assumption that the bilayer is flat rather than curved. The number of saturated lipids, unsaturated lipids, and cholesterol in the inner leaflet are $N_{s,\text{in}}$, $N_{u,\text{in}}$, and $N_{c,\text{in}}$; likewise for the outer leaflet. The composition of the bilayer is completely specified by η as well as the mole fractions

$$\begin{aligned} s_{\text{in}} &\equiv \frac{N_{s,\text{in}}}{N_{\text{in}}} & c_{\text{in}} &\equiv \frac{N_{c,\text{in}}}{N_{\text{in}}} \\ s_{\text{out}} &\equiv \frac{N_{s,\text{out}}}{N_{\text{out}}} & c_{\text{out}} &\equiv \frac{N_{c,\text{out}}}{N_{\text{out}}} \end{aligned}$$

Note that only two mole fractions are needed to describe the composition of each leaflet, since for example $u_{\text{in}} = 1 - s_{\text{in}} - c_{\text{in}}$.

The thermodynamic potential appropriate to a system with fixed composition (number of each molecular species) and temperature is determined by the Helmholtz free energy $F(T, \{N_i\}, A)$. Here the notation $\{N_i\}$ denotes the numbers of each molecular species, with molecules in different leaflets considered to be different species. The Helmholtz free energy determines the equilibrium thermodynamic behavior of the system via the first law of thermodynamics:

$$dF = -SdT + \sum_i \mu_i dN_i + \alpha \cdot dA \quad (\text{A.3})$$

and the second law:

$$dF = 0 \quad (\text{A.4})$$

We have used α to denote the surface tension (the two-dimensional equivalent of pressure) rather than the more traditional γ , since we use the latter for the interleaflet coupling throughout the text. In a spatially homogeneous system, equation A.3 can be integrated to yield the thermodynamic Euler relation

$$F = -ST + \sum_i \mu_i N_i + \alpha \cdot A \quad (\text{A.5})$$

The free energy calculations described in the text make no reference to extensive quantities such as F , but rather to intensive quantities only. We define the Helmholtz free energy per molecule f by

$$f \equiv \frac{F}{N} \quad (\text{A.6})$$

The fundamental thermodynamic relation involving the Helmholtz free energy per molecule can be obtained by substituting into equation A.3 the relations $A = aN$, $N_{s,\text{in}} = \eta s_{\text{in}} N$ and

so on. After simplification, the result has the form $dF = f dN + N df$, where

$$\begin{aligned}
df &= \{(\mu_{s,\text{in}} - \mu_{u,\text{in}})s_{\text{in}} + (\mu_{c,\text{in}} - \mu_{u,\text{in}})c_{\text{in}} \\
&\quad - (\mu_{s,\text{out}} - \mu_{u,\text{out}})s_{\text{out}} - (\mu_{c,\text{out}} - \mu_{u,\text{out}})c_{\text{out}} + (\mu_{u,\text{in}} - \mu_{u,\text{out}})\}d\eta \\
&\quad + (\mu_{s,\text{in}} - \mu_{u,\text{in}})\eta ds_{\text{in}} + (\mu_{c,\text{in}} - \mu_{u,\text{in}})\eta dc_{\text{in}} \\
&\quad + (\mu_{s,\text{out}} - \mu_{u,\text{out}})(1 - \eta)ds_{\text{out}} + (\mu_{c,\text{out}} - \mu_{u,\text{out}})(1 - \eta)dc_{\text{out}} \\
&\quad + \alpha \cdot da
\end{aligned} \tag{A.7}$$

and

$$\begin{aligned}
f &= (\mu_{s,\text{in}} - \mu_{u,\text{in}})\eta s_{\text{in}} + (\mu_{c,\text{in}} - \mu_{u,\text{in}})\eta c_{\text{in}} \\
&\quad + (\mu_{s,\text{out}} - \mu_{u,\text{out}})(1 - \eta)s_{\text{out}} + (\mu_{c,\text{out}} - \mu_{u,\text{out}})(1 - \eta)c_{\text{out}} \\
&\quad + \eta\mu_{u,\text{in}} + (1 - \eta)\mu_{u,\text{out}} + \alpha \cdot a
\end{aligned} \tag{A.8}$$

Here we have assumed that $dT = 0$. From equation A.7 we may read off the derivatives of $f(T, s_{\text{in}}, c_{\text{in}}, s_{\text{out}}, c_{\text{out}}, \eta, a)$ for a given temperature.

$$\begin{aligned}
\frac{\partial f}{\partial s_{\text{in}}} &= \eta(\mu_{s,\text{in}} - \mu_{u,\text{in}}), & \frac{\partial f}{\partial c_{\text{in}}} &= \eta(\mu_{c,\text{in}} - \mu_{u,\text{in}}) \\
\frac{\partial f}{\partial s_{\text{out}}} &= (1 - \eta)(\mu_{s,\text{out}} - \mu_{u,\text{out}}), & \frac{\partial f}{\partial c_{\text{out}}} &= (1 - \eta)(\mu_{c,\text{out}} - \mu_{u,\text{out}}) \\
\frac{\partial f}{\partial \eta} &= (\mu_{s,\text{in}} - \mu_{u,\text{in}})s_{\text{in}} + (\mu_{c,\text{in}} - \mu_{u,\text{in}})c_{\text{in}} \\
&\quad - (\mu_{s,\text{out}} - \mu_{u,\text{out}})s_{\text{out}} - (\mu_{c,\text{out}} - \mu_{u,\text{out}})c_{\text{out}} + (\mu_{u,\text{in}} - \mu_{u,\text{out}}) \\
\frac{\partial f}{\partial a} &= \alpha
\end{aligned} \tag{A.9}$$

Equations A.8 and A.9 allow us to calculate the chemical potentials of all molecular species from numerical derivatives of f with respect to mole fractions and to η .

Appendix B

**CALCULATING PHASE DIAGRAMS FROM
PHENOMENOLOGICAL FREE ENERGIES**

The purpose of this appendix is to provide a practical guide to the problem of calculating the phase diagram of a mixture, beginning with an expression for the free energy as a function of the mole fractions of the components of the mixture. As an illustration we will consider the following free energy of a ternary mixture of saturated (s) lipids, unsaturated ($u = 1 - s - c$) lipids, and cholesterol (c):

$$f(s, c) = s \ln s + u \ln u + c \ln c + Jus + Kusc \quad (\text{B.1})$$

Mathematically, the problem of calculating the tie-lines connecting coexisting phases is straightforward. We define the functions

$$\mu_s(s, c) = \frac{\partial f}{\partial s} \quad (\text{B.2})$$

$$\mu_c(s, c) = \frac{\partial f}{\partial c} \quad (\text{B.3})$$

$$\gamma(s, c) = f(s, c) - s \cdot \mu_s(s, c) - c \cdot \mu_c(s, c), \quad (\text{B.4})$$

It should be noted that the use of the symbols μ and γ here is merely suggestive; these functions are not chemical potentials or surface tensions, as can be seen from Equations (A.9). However, one may show using Equations (A.9) that the equality of μ_s , μ_c , and γ between two states is a necessary condition for their coexistence. There will be coexistence between phases with compositions (s_1, c_1) and (s_2, c_2) if these compositions satisfy the following equations:

$$\mu_s(s_1, c_1) = \mu_s(s_2, c_2) \quad (\text{B.5})$$

$$\mu_c(s_1, c_1) = \mu_c(s_2, c_2) \quad (\text{B.6})$$

$$\gamma(s_1, c_1) = \gamma(s_2, c_2) \quad (\text{B.7})$$

Because there are four unknowns (s_1 , c_1 , s_2 , and c_2) but only three equations, if there is phase coexistence at all there will be a one-dimensional continuum of solutions, so one must impose an additional constraint such as fixing a particular value of c_1 . Usually the equations above must be solved numerically, for example by using the multidimensional Newton iteration [114]. Of course, for any values of s and c there is always a trivial solution where $s_1 = s_2 = s$ and $c_1 = c_2 = c$. This makes it necessary to make an appropriate initial guess for the unknowns. We now describe several methods for making this initial guess, which is the most difficult aspect of the calculation of miscibility phase diagrams.

Reduction to a binary mixture

We begin with a simple case where $J = 3$ and $K = 1$ in equation (B.1), which means that the binary repulsion between u and s is large enough for phase separation to occur in the binary u - s mixture. Then it is easy to obtain the coexisting phases in the binary system by plotting $f(s, 0.001)$ versus s , as shown in Figure B.1. The reason for plotting $f(s, 0.001)$ instead of $f(s, 0)$ is that the entropy term $c \ln c$ in equation (B.1) is undefined at $c = 0$, even though its limit is finite as $c \rightarrow 0$.

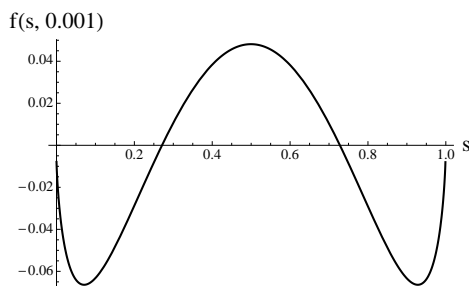


Figure B.1: Free energy of a binary mixture with $J = 3$.

From Figure B.1 one can read off a good guess for a tie-line of a mixture which is nearly binary: $s_1 \approx 0.1$ and $s_2 \approx 0.9$, while $c_1 \approx c_2 \approx 0.001$. By fixing $c_1 = 0.001$ and using a numerical solver we then find an exact tie-line. This tie-line can in turn be used as a good initial guess for a tie-line with a slightly different value of c_1 , for example $c_1 = 0.002$.

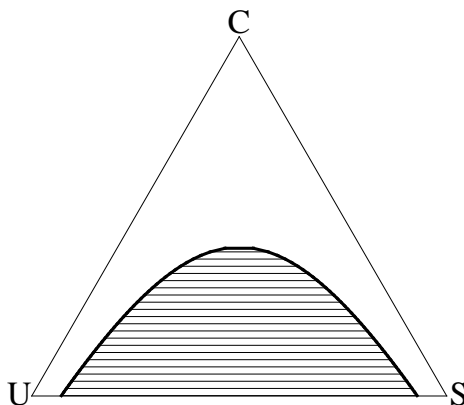


Figure B.2: Ternary phase diagram calculated from equation (B.1) with $J = 3$ and $K = 1$.

Continuing in this way one obtains the phase diagram shown in figure B.2. Thus a miscibility phase diagram for a ternary system can in some cases be determined from an initial guess in a binary subsystem. The tie-lines for the quaternary mixture shown in Figure 2.3 of Chapter 2 were calculated in an analogous fashion by using the known tie-lines of the ternary mixture (with $z = 0$) as initial guesses.

The Spinodal Line

In some cases, phase separation occurs in a ternary system but not in any of its binary subsystems. Then we may not calculate tie-lines using the method described in the previous section, and we need other methods to make initial guesses as to the location of the tie-lines. To illustrate this, we consider the same free energy (B.1) as before, but now with $J = 0$ and $K = 9$. In this case, although there is a very strong ternary interaction, there will be no phase separation in any binary mixtures. One way to see that there will indeed be phase separation in the ternary system, and to get an idea of the location of the tie-lines, is to consider the condition of local stability of the mixture. We define $\sigma(s, c)$ to be the determinant of the matrix of second derivatives (or Hessian) of f

$$\sigma(x, y) \equiv \det \begin{pmatrix} \frac{\partial^2 f}{\partial s^2} & \frac{\partial^2 f}{\partial s \partial c} \\ \frac{\partial^2 f}{\partial s \partial c} & \frac{\partial^2 f}{\partial c^2} \end{pmatrix} \quad (\text{B.8})$$

Compositions for which $\sigma(s, c) < 0$ are locally unstable with respect to phase separation. The locally unstable region of composition space is bounded by a line called the “spinodal.” Although phase separation may occur for average compositions lying outside of the spinodal, the possibility of phase separation at a given temperature is always signaled by the existence of a spinodal. This allows us to use σ as a criterion to tell whether or not phase separation will occur by doing a contour plot of the spinodal, where $\sigma(s, c)$ vanishes. This is shown in figure B.3 for the free energy function (B.1) with $J = 0$ and $K = 9$.

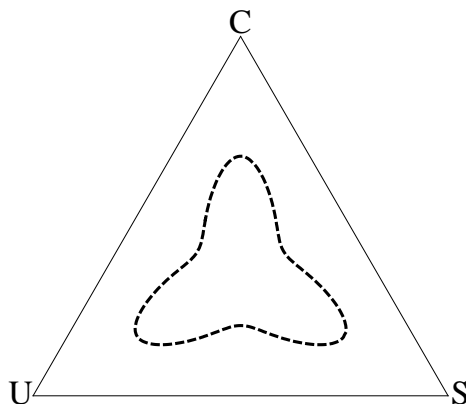


Figure B.3: Spinodal region calculated from equation (B.8) with $J = 0$ and $K = 9$.

In the interior of the dashed spinodal line, the ternary mixture is locally unstable. We might also guess that the outermost points of the spinodal region are critical points, which gives an indication of the directions of the tie-lines. However, there is still a good deal of guesswork involved, so we next describe a method which quickly gives us information about the tie-lines (which end on the binodal).

The Convex Hull Method

Phase separation occurs whenever the graph of the free energy as a function of composition fails to be convex. The process of finding tie-lines is equivalent to replacing the concave regions of the graph with straight lines or planes which are doubly tangent with the graph. Mathematically speaking, this is equivalent to the problem of finding the so-called “convex

hull” of the graph of f . The convex hull of a region in space is the smallest convex set containing that region (a region is convex if the straight line segment connecting any two of its points lies entirely within it). Intuitively, it is the shape taken on by an idealized rubber sheet stretched around the region. Finding the convex hull of a set of points is a common problem in the mathematical field of computational geometry, and efficient algorithms exist to solve it in any number of dimensions [106]. A straightforward, if brute-force, approach to calculating phase diagrams is to take a large set of random points on the graph of f and to use software such as `qhull`[5] to find the convex hull. The result is a convex polyhedron with a large number of faces, such as the one shown in figure B.4. The facets of the convex

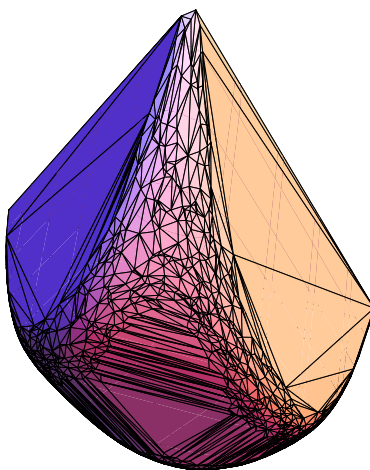


Figure B.4: Convex hull of a large number of random points on the graph of the free energy function (B.1) with $J = 0$ and $K = 9$.

hull can then be projected onto the Gibbs triangle as shown in figure B.5. The facets of the convex hull give us enough information to make a phase diagram of the mixture. Regions of the Gibbs triangle in which a single phase is globally stable are filled with small triangles, since the convex hull did not include any facets connecting these regions to points distant from them. On the other hand, the long, thin facets of the convex hull are good

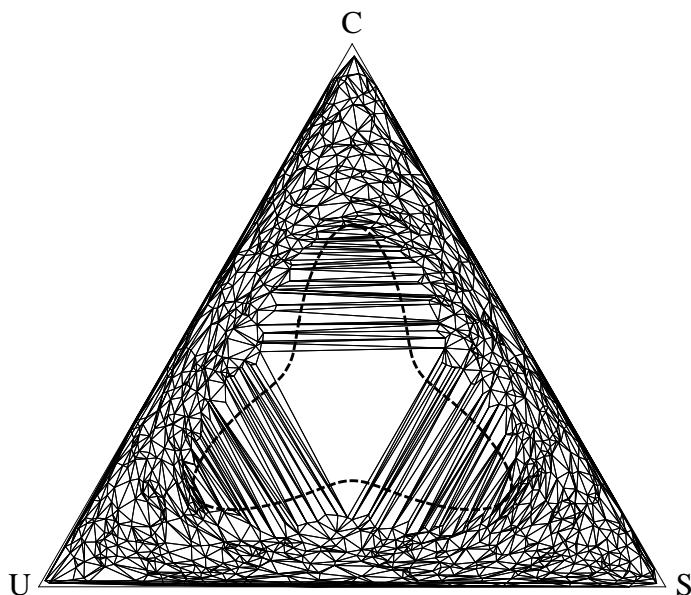


Figure B.5: Projection of the facets of the convex hull in figure B.4 onto the Gibbs triangle, showing tie-lines and a region of three-phase coexistence. The spinodal line from figure B.3 is shown dashed.

approximations of tie-lines and can be used as initial guesses in the method described in the first section of this appendix. The large triangular facet in the middle of the phase diagram is a region of three-phase coexistence.

The method of convex hulls is quite useful when dealing with an expression for the free energy whose phase behavior is not obvious. This is particularly true for systems with internal degrees of freedom such as the ternary mixture described in section 2.1, since in general it is not possible to find an expression for the spinodal line of these systems.

Appendix C

DERIVATION OF EFFECTIVE INTERACTION BETWEEN CHARGED LIPIDS

In this Appendix we calculate the effective electrostatic free energy of a set of charged lipid head groups lying at the interface between a lipid bilayer and an aqueous solvent, as depicted in Figure 4.3. This free energy includes both electrostatic energy and the entropy associated with the salt ions in a solution with Debye screening length κ^{-1} . It will be assumed that for a given set of positions of charged lipids, the ions will rapidly reach their equilibrium distribution, given by the Poisson-Boltzmann equation. Furthermore, we will assume that the electrostatic potential is always small enough to linearize the Poisson-Boltzmann equation. This could limit the validity of this model to situations where the lipids have only one elementary charge each ($n = 1$), since the dimensionless coupling parameter which must be small in order for the Poisson-Boltzmann equation to be valid is proportional to n^3 [105].

The charge density on the surface of the bilayer is

$$\sigma(\mathbf{x}) = \sum_i -ne \cdot \delta(\mathbf{x} - \mathbf{x}_i) \quad (\text{C.1})$$

Throughout this Appendix \mathbf{x} will be used as an in-plane vector at the surface $z = 0$ of the bilayer, while \mathbf{r} will be a three-dimensional position vector. The charge density will generate a potential, as well as a redistribution of salt ions. The electrostatic free energy is

$$F_{\text{el}} = \frac{1}{2} \int V(\mathbf{x}, z = 0) \sigma(\mathbf{x}) d^2 \mathbf{x} + \frac{1}{2} \int V(\mathbf{r}) (e\rho_+(\mathbf{r}) - e\rho_-(\mathbf{r})) d^3 \mathbf{r} \\ + k_B T \int [\rho_+(\mathbf{r}) \ln(\rho_+(\mathbf{r})) + \rho_-(\mathbf{r}) \ln(\rho_-(\mathbf{r}))] d^3 \mathbf{r}, \quad (\text{C.2})$$

where $\rho_+(\mathbf{r})$ and $\rho_-(\mathbf{r})$ are number densities of positive and negative ions in solution. If one substitutes the Poisson-Boltzmann charge distributions into the entropy terms, there is a partial cancellation with the simplified result (see also section 4.3)

$$F_{\text{el}} = \frac{1}{2} \int V(\mathbf{x}, z = 0) \sigma(\mathbf{x}) d^2 \mathbf{x} - \frac{1}{2} \int V(\mathbf{r}) \rho(\mathbf{r}) d^3 \mathbf{r}, \quad (\text{C.3})$$

where $\rho(\mathbf{r})$ is now the total charge (not number) density of ions in solution. Furthermore, since the potential in the solution obeys the Debye-Hückel equation $\nabla^2 V = \kappa^2 V$, we can write the second term in terms of the potential only:

$$F_{\text{el}} = \frac{1}{2} \int V(\mathbf{x}, z=0) \sigma(\mathbf{x}) d^2 \mathbf{x} + \epsilon_W \kappa^2 \frac{1}{2} \int V(\mathbf{r})^2 d^3 \mathbf{r}, \quad (\text{C.4})$$

Because of the linearity of the Debye-Hückel equation, the potential due to all the charged lipids is the sum of the potentials due to single lipids, V_1 .

$$V(\mathbf{r}) = \sum_i V_1(\mathbf{r} - \mathbf{x}_i) \quad (\text{C.5})$$

The single-lipid potential V_1 is the Green's function of the Debye-Hückel equation with appropriate boundary conditions at the interfaces between different dielectrics. It will be given in the next section, allowing us to calculate the electrostatic free energy, since substituting equations (C.1) and (C.5) into (C.4) gives (using labels i and j when there are two sums over particles)

$$\begin{aligned} F_{\text{el}} &= -ne \sum_{i < j} V_1(\mathbf{x}_i - \mathbf{x}_j) + \epsilon_W \kappa^2 \sum_{i < j} \int V_1(\mathbf{r} - \mathbf{x}_i) V_1(\mathbf{r} - \mathbf{x}_j) d^3 \mathbf{r} \\ &+ \frac{1}{2} \epsilon_W \kappa^2 \sum_i \int V_1(\mathbf{r} - \mathbf{x}_i)^2 d^3 \mathbf{r} \end{aligned} \quad (\text{C.6})$$

The first term comes from the first term of equation (C.4). The second and third terms come from the second term of equation (C.4). However, the third term, which occurs because of the cases where $i = j$ in the double sum over particles, is a self-energy which by translational symmetry does not depend on the positions \mathbf{x}_i . We therefore neglect it in the following. From equation (C.6) we can identify the effective interaction between each pair of charged lipids:

$$U_{\text{eff}}(\mathbf{x}_1, \mathbf{x}_2) = -ne \cdot V_1(\mathbf{x}_1 - \mathbf{x}_2) + \epsilon_W \kappa^2 \int V_1(\mathbf{r} - \mathbf{x}_1) V_1(\mathbf{r} - \mathbf{x}_2) d^3 \mathbf{r} \quad (\text{C.7})$$

In order to calculate this effective interaction, we must now find the single-particle potential V_1 .

Single-particle potential V_1

The desired Green's function has been calculated by Netz [104]. It is conveniently expressed in cylindrical coordinates (z, ρ) , assuming that the point source is located at the origin.

$$V_1(\mathbf{r}) = \frac{1}{2\pi} \int_0^\infty p \cdot J_0(p\rho) V_1(z, p) dp \quad (\text{C.8})$$

where J_0 is a Bessel function and $V_1(z, p)$ is a partial Fourier transform of the Green's function. Netz gives different expressions for $V_1(z, p)$ for the cases where z lies above, or below, the dielectric membrane:

$$\begin{aligned} V_1(z, p) &= \exp(-z\sqrt{\kappa^2 + p^2}) \cdot (C + D), & z > 0 \\ &= \exp(z\sqrt{\kappa^2 + p^2}) \cdot L, & z < -d \end{aligned} \quad (\text{C.9})$$

We will not need the expression for the potential when z lies inside the slab. The definitions of C , D , and L are:

$$D = \frac{-ne}{2\epsilon_W \sqrt{\kappa^2 + p^2}} \quad (\text{C.10})$$

$$C = D \cdot \Delta \cdot \left[\frac{1 - \exp(-2d\sqrt{\kappa^2 + p^2})}{1 - \Delta^2 \exp(-2d\sqrt{\kappa^2 + p^2})} \right] \quad (\text{C.11})$$

$$L = \frac{-2ne \cdot \epsilon_{BP} \cdot \exp \left[d(p + \sqrt{\kappa^2 + p^2}) \right]}{(\epsilon_W \sqrt{\kappa^2 + p^2} + \epsilon_{BP})^2 (\exp(2dp) - \Delta^2)} \quad (\text{C.12})$$

$$\Delta = \frac{\epsilon_W \sqrt{\kappa^2 + p^2} - \epsilon_{BP}}{\epsilon_W \sqrt{\kappa^2 + p^2} + \epsilon_{BP}} \quad (\text{C.13})$$

Calculation of effective interaction when $\epsilon_B/\epsilon_W \approx 0$

Using the expressions from equation (C.9) for the partially Fourier-transformed Green's function $V_1(z, p)$, we can put these into equation (C.8) to obtain the real-space Green's function in cylindrical coordinates. In general, the integrals involved will be very difficult or intractable analytically. Here, we look at a special case where $\epsilon_B/\epsilon_W \approx 0$. In that case,

$$\Delta \approx 0$$

$$C \approx D$$

$$L \approx 0$$

The potential due to a single charged lipid, in the region $z > 0$, is then

$$\begin{aligned} V_1(\mathbf{r}) &= \frac{1}{2\pi} \int_0^\infty p \cdot J_0(p\rho) \left[\frac{-ne}{\epsilon_W \sqrt{\kappa^2 + p^2}} \right] \exp(-z\sqrt{\kappa^2 + p^2}) dp \\ &= \frac{-ne}{2\pi\epsilon_W} \cdot \frac{\exp(-\kappa r)}{r} \end{aligned} \quad (\text{C.14})$$

The first term in the effective interaction energy (C.7) is then

$$-ne \cdot V_1(\mathbf{x}_1 - \mathbf{x}_2) = \frac{(-ne)^2}{2\pi\epsilon_W} \cdot \frac{\exp(-\kappa r)}{r}, \quad (\text{C.15})$$

where r is the distance between the two charged lipids. This is exactly twice the ordinary screened Coulomb interaction which we would get if the charges were far from the interface. This is due to the presence of image charges induced by the interface between two dielectrics. One can calculate the image charge of a point charge e to be [75]

$$e' = e \cdot \frac{\epsilon_W - \epsilon_B}{\epsilon_W + \epsilon_B} \quad (\text{C.16})$$

In the limit where $\epsilon_B/\epsilon_W \approx 0$, the image charge has the same value as the original one. Thus the factor of two represents the repulsion of a given lipid from each other lipid, as well as from the image charges of the other lipids.

We must now calculate the second term in the effective interaction energy between charged lipids, namely

$$\epsilon_W \kappa^2 \int V_1(\mathbf{r} - \mathbf{x}_1) V_1(\mathbf{r} - \mathbf{x}_2) d^3 \mathbf{r} = \epsilon_W \kappa^2 \left(\frac{ne}{2\pi\epsilon_W} \right)^2 \int_{z>0} \frac{\exp(-\kappa r_1)}{r_1} \cdot \frac{\exp(-\kappa r_2)}{r_2} d^3 \mathbf{r},$$

where $r_1 = \|\mathbf{r} - \mathbf{x}_1\|$ and $r_2 = \|\mathbf{r} - \mathbf{x}_2\|$. In this integral, the positions of the two lipids are fixed at \mathbf{x}_1 and \mathbf{x}_2 , while \mathbf{r} runs over the half-space $z > 0$. In the end, it will only depend on the distance between the two charged lipids, so we are free to choose our coordinate system such that one charge is at the origin, and the other charge is on the z axis, with a distance ρ between them. It is then possible to simplify the integral by evaluating it in spherical coordinates. The integral above becomes, after extending it to all of space and dividing by two,

$$\begin{aligned} &\frac{1}{2} \cdot \int_0^\infty dr \frac{\exp(-\kappa r)}{r} \cdot 2\pi r \cdot \int_{-1}^1 d \cos \theta \cdot \frac{\exp \left[-\kappa \sqrt{r^2 \sin^2 \theta + (r \cos \theta - \rho)^2} \right]}{\sqrt{r^2 \sin^2 \theta + (r \cos \theta - \rho)^2}} \\ &= \pi \int_0^\infty dr \exp(-\kappa r) \int_{-1}^1 du \frac{\exp \left[-\kappa \sqrt{r^2 + \rho^2 - 2r\rho u} \right]}{\sqrt{r^2 + \rho^2 - 2r\rho u}} \end{aligned} \quad (\text{C.17})$$

This integral can be done analytically. The resulting value of the second term in the effective interaction is

$$\epsilon_W \kappa^2 \int V_1(\mathbf{r} - \mathbf{x}_1) V_1(\mathbf{r} - \mathbf{x}_2) d^3 \mathbf{r} \quad (\text{C.18})$$

$$= \frac{(ne)^2 \kappa}{4\pi\epsilon_W} \cdot \frac{\exp(-\kappa\rho)}{\kappa\rho} \cdot [\gamma + \exp(2\kappa\rho) \cdot \Gamma(0, 2\kappa\rho) + \ln(2\kappa\rho)], \quad (\text{C.19})$$

where $\gamma = 0.577\dots$ is the Euler-Mascheroni constant and $\Gamma(0, x)$ is an incomplete gamma function, defined by

$$\Gamma(0, x) = \int_x^\infty \frac{\exp(-t)}{t} dt \quad (\text{C.20})$$

This function decreases exponentially for large x .

Result

The final result is that in the limit where $\epsilon_B/\epsilon_W \approx 0$, the effective interaction between two charged lipids separated by a distance r in the plane of the bilayer is

$$U_{\text{eff}}(r) = \frac{(ne)^2}{4\pi\epsilon_W} \cdot \frac{\exp(-\kappa r)}{r} \cdot [2 + \gamma + \exp(2\kappa r)\Gamma(0, 2\kappa r) + \ln(2\kappa r)] \quad (\text{C.21})$$

This potential is compared to the ordinary screened Coulomb potential (far from any interfaces) in section 4.4 of the text.

Appendix D

**SIMPLIFIED PHENOMENOLOGICAL MODEL OF TERNARY
MIXTURE OF SATURATED AND UNSATURATED LIPIDS AND
CHOLESTEROL**

In this Appendix we describe a model of a ternary mixture of saturated lipids, unsaturated (low melting temperature) lipids, and cholesterol. The model is similar to the one described in Section 2.1, but simpler and easier to use in calculations. Instead of a continuum of states labeled by values of δ as in the previous model, the saturated lipids have two states, ordered and disordered. The mole fractions of ordered saturated lipids and of disordered saturated lipids are s_o and s_d , respectively. The physics is the same as has been discussed previously [117]: the repulsion between saturated and unsaturated lipids is stronger when the saturated lipids are in their ordered state. Furthermore, there is an attractive term acting between cholesterol and ordered saturated lipids. The free energy per molecule, in units of $k_B T$, is

$$\begin{aligned} f(s_d, s_o, c) &= s_o \ln s_o + s_d \ln s_d + c \ln c + (1 - s_d - s_o - c) \ln(1 - s_d - s_o - c) \\ &+ J_d s_d (1 - s_d - s_o - c) + J_o s_o (1 - s_d - s_o - c) - J_{sc} s_o c \end{aligned} \quad (\text{D.1})$$

Of course, the ordered and disordered saturated lipids are not different species: they can turn into each other. Thus we must set their chemical potentials equal to each other:

$$\frac{\partial f}{\partial s_d} = \frac{\partial f}{\partial s_o} \quad (\text{D.2})$$

We can use this equation to write both s_d and s_o in terms of the total mole fraction $s = s_d + s_o$. The result is

$$s_d(s, c) = \frac{1}{1 + \exp(-\{(J_o - J_d)(1 - s - c) - J_{sc}c\})} \cdot s \quad (\text{D.3})$$

$$s_o(s, c) = \frac{\exp(-\{(J_o - J_d)(1 - s - c) - J_{sc}c\})}{1 + \exp(-\{(J_o - J_d)(1 - s - c) - J_{sc}c\})} \cdot s \quad (\text{D.4})$$

The interpretation of these equations in terms of Boltzmann factors is clear. We can now put these expressions back into the original free energy, obtaining

$$f(s, c) \equiv f(s_d(s, c), s_o(s, c), c) \tag{D.5}$$

This is like taking the equilibrium value of δ in the model described in section 2.1 and substituting it back into the free energy to obtain a free energy as a function of compositions only. However, the current method has the advantage that when the Boltzmann weights above are put into the mixing entropy in equation (D.1), there will be terms that give the internal (configurational) entropy of the saturated lipids. A phase diagram derived from this simplified model is shown in Figure 4.1; compare to Figure 2.2.

VITA

Gregory Garbès Putzel was born in Montreal, Canada in 1982, and grew up in Jericho, Vermont. He graduated from Carnegie Mellon University in 2004 with degrees in mathematics and physics, then enrolled in the physics program at the University of Washington.